A study on PsbS and its role as a pH sensor

Krishnan, M.

Exploring an enigma

A study on PsbS and its role as a pH sensor

Maithili Krishnan

Exploring an enigma

A study on PsbS and its role as a pH sensor

Proefschrift

ter verkrijging van
de graad van Doctor aan de Universiteit Leiden,
op gezag van Rector Magnificus Prof. Mr. C. J. J. M. Stolker,
volgens besluit van het College voor Promoties
te verdedigen on donderdag, 12 September 2019
klokke 15:00 uur

door

Maithili Krishnan

geboren te Bhilai, India
in 1988

Promotor:	Prof. dr. Huub J. M. de Groot
Copromotor:	Dr. Anjali Pandit
Overige leden:	Prof. dr. Hermen S. Overkleeft Prof. dr. Marcellus Ubbink Prof. dr. W. J. de Grip Dr. Tomas Morosinotto *(University of Padova, Italy)* Dr. Emilie Wientjes *(Wageningen University & Research, NL)*

Maithili Krishnan
Exploring an enigma: A study on PsbS and its role as a pH sensor
PhD Thesis, Leiden University

ISBN: 978-94-6332-531-8

Cover and bookmark designed by Maithili Krishnan
(vectors taken from deoci.com and freepik.com)

This research was financed by CW-VIDI grant from the Netherlands Organization of Scientific Research (NWO) under grant nr. 723.012.103

For my parents

Table of Contents

Abbreviations

ATP : Adenosine triphosphate
Arabidopsis-PsbS : PsbS protein from *A. thaliana*
Arg : Arginine, R
Asp : Aspartic acid, D
BeStSel : Beta Structure Selection
β-DM : n-Dodecyl β-D-maltoside
Brij-78 : Polyethylene glycol octadecyl ether
BSA : Bovine serum albumin
CD : Circular dichroism
Chl : Chlorophyll
CMC : Critical micelle concentration
DCCD : N,N'-Dicyclohexylcarbodiimide
DNA : Deoxyribonucleic acid
DHPC : 1,2-Dihexanoyl-sn-Glycero-3-phosphocholine
D_t : Translational diffusion constant
DLS : Dynamic light scattering
DOSY : Diffusion-ordered spectroscopy
EDC : 1-ethyl-3-(3-dimethylaminopropyl)carbodiimidehydrochloride
FC-12 : n-dodecyl phosphocholine
FTIR : Fourier-transform infrared spectroscopy
Glu : Glutamic acid, E
Gly : Glycine, G
HEPES : 4-(2-hydroxyethyl)-1-piperazineethanesulfonic acid
His : Histidine, H
HSQC : Heteronuclear single quantum coherence
Ile : Isoleucine, I
IPTG : Isopropyl β-D-1-thiogalactopyranoside
LB : Luria-Bertani broth
LDS : Lithium dodecyl sulfate
LHCII : Light harvesting complex II
LHCSR : Light harvesting complex stress-related
MAS : Magic angle spinning
MCT : Mercury Cadmium Telluride
NADPH : Nicotinamide adenine dinucleotide phosphate
NG : n- nonyl- β-D- glucopyranoside
Ni-NTA : Nickel-nitrilotriacetic acid
NMR : Nuclear magnetic resonance
NPQ : Non-photochemical quenching

OG	: n-octyl β-D-glucopyranoside
Patens-PsbS	: PsbS protein from P. patens
PCR	: Polymerase chain reactions
Phe	: Phenylalanine, F
pH	: Hydrogen ion concentration (potential of hydrogen)
pD	: Deuterium ions concentration
p.p.m.	: Parts per million
PsbS	: Photosystem II subunit S
PSI / II	: Photosystem I / II
PMMA	: Polymethyl methacrylate
qE	: ΔpH-dependent or energy component
ROS	: Reactive oxygen species
RNA	: Ribonucleic acid
SDS	: Sodium dodecyl sulfate
SEC	: Size exclusion chromatography
Spinach-PsbS	: PsbS protein from *S. oleracea*
Thr	: Threonine, T
Tyr	: Tyrosine, Y
Trp	: Tryptophan, W
UP	: Urea phosophate buffer (8 M urea, 100 mM sodium phosphate, 100 mM Tris)
UV/LS/RI	: Ultraviolet–visible/ Light scattering/ Refractive index
V	: Violaxanthin
VAZ	: Di-epoxy xanthophyll V, xanthophyll A, xanthophyll Z
VDE	: Violaxanthin de-epoxidase
WT	: Wild-type
Z	: Zeaxanthin

Keywords: Photoprotection, membrane proteins, oligomerization, protonation sites

Increasing light conditions
LHC
PsbS
CP
PS II
Stroma
Lumen
COO-
E71
E176
High pH
COOH
Quenched state
Low pH

1

Introduction

Solar energy harnessed by plants and algae has great potential to be converted into biofuels for future generations. Understanding the regulatory mechanism of photosynthesis can increase biomass yield and drive the generation of biofuels to its maximum. PsbS, a membrane protein, is an essential component for NPQ and has been studied extensively in this thesis. PsbS is hypothesized to sense pH and to regulate photosynthesis under light stress conditions. The first objective in this thesis is to produce, purify and refold recombinant PsbS with sufficiently high yields for biochemical studies along with optimizing the detergent conditions for maintaining its stability. The second objective is the spectroscopic characterization of PsbS to understand its role as a pH sensor and its molecular mechanism during photoprotection.

1

By the year 2050, the human population is projected to reach 9.1 billion, bringing with it a major energy-related crisis[1]. The shortage of fuels will be one of the major issues to deal with due to the limited availability of non-renewable resources like coal, oil, and natural gas. For more than a century, scientists are exploring the possibility of biofuels generated from plants and plant products to overcome this crisis. Although direct synthesis of biofuels like hydrogen, isoprene, toluene[2] and longer hydrocarbons can be achieved by photosynthetic microorganisms[3], some inhibitory pathways make it complicated to achieve high efficiency of biofuel production[4]. To improve the production of biofuel, an increase in biomass production or genetic engineering of photosynthetic proteins is necessary, but this requires an in-depth knowledge of the photosynthetic mechanism that improves CO_2 assimilation. Currently, many countries are attempting to develop bio-solar fuels, for example, *BioSolar Cells*, a Dutch research program in the field of photosynthesis aimed at the sustainable production of food and renewable energy[5]. Apart from such programs, the emergence of new technologies and advancements in scientific tools enable us today to unravel many photosynthetic mechanisms[6]. These scientific effort may one day enable us to solve food and energy crisis to free the world from hunger and from exploiting our limited resources like petrol and oil.

1.1 Photosynthesis and photoprotection

Oxygenic photosynthesis is the conversion of solar energy to chemical energy while producing oxygen that takes place in microalgae/cyanobacteria and all land plants. When photons of sun rays hit a leaf surface, they are absorbed by an antenna that transfers excitations to the two photosystems, the oxygen-evolving PSII and the ferredoxin-reducing PSI[7]. Both PSII and PSI are important for light driven charge separation and transport of electrons. The splitting of water takes places in PSII which generates electrons that are used in oxygen evolution. The remaining electrons from the PSII are then transported to PSI via plastoquinones, the cytochrome b_6f complex and plastocyanin. The electron acceptor $NADP^+$ is converted to NADPH, which contributes to carbon fixation of solar energy, the prime objective of photosynthesis[8]. The protons evolved from water oxidation also contribute to drive the ATP synthase to produce ATP, another essential energy source.

One way to measure the efficiency of photosynthesis is through *Solar Energy Storage Efficiency*, which is the percentage of solar energy converted into biomass[8]. This conversion efficiency in direct sunlight is less compared to low irradiance conditions[9] due to the *light-saturation effect*[8], depicted in Figure 1.1. This light-saturation effect is driven by a mechanism called *photoprotection*. Photoprotection against sunlight takes place to prevent damage from toxic ROS that are produced when electrons leak out of

the electron transfer chain or when photosynthetic pigments transfer energy to oxygen to produce singlet oxygen.

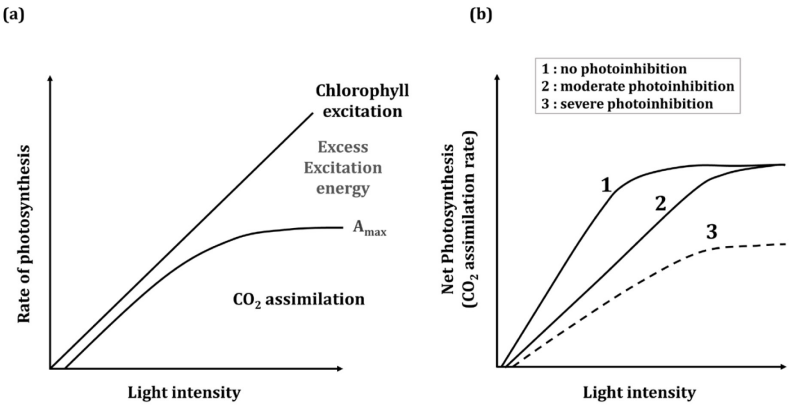

Figure 1.1 (a) Principle of photoprotection showing excess excitation energy that is dissipated as compared to the absorbed light. A_{max}, the maximal light-saturated photosynthetic rate is achieved; (b) Effect of photoinhibition on quantum yield and CO_2 assimilation rate is shown. A_{max} is also affected by other photo-inhibitory conditions; therefore, it is a dotted line. (Adopted from[10])

The photoprotective mechanisms that under high light conditions quench the excitations, which in return dissipate the excess photon energy as heat or fluorescence, are known as NPQ and lead to ~55 % irradiance loss (average in USA)[11]. From the absorbed sunlight, an estimated 8 - 10 % of the solar energy converts into biomass, which is significantly low. As seen in Figure 1.1 a, the A_{max}, which is the light-saturated photosynthetic rate is reached when there is too much light intensity leading to dissipation of excess excitation energy[10]. The quantum yield and CO_2 assimilation rates also drop when severe photoprotection takes place, as shown in Figure 1.1 b. To recapitulate, adjusting NPQ is a key for improving CO_2 assimilation which could assist in efficient biofuel production.

1.2 Non-photochemical quenching

NPQ takes place primarily in the antenna associated with the PSII complex located in the thylakoid membrane of chloroplasts[12]. qE, the major component of NPQ, is defined as the thermal dissipation of excess absorbed light energy. qE has two main requirements, one involves the activation of an enzyme for conversion of violaxanthin to zeaxanthin[13] during the VAZ cycle and the other is the protonation of light stress sensor proteins[14]. The requirements for the fast component of NPQ, qE are explained below:

1.2.1 Role of low lumenal pH

The most important aspect for qE is the lowering of the lumenal pH in the thylakoid membrane, which senses the photosynthetic state during varying light conditions. In low light conditions, the approximate lumenal pH is 7.5 and the photosynthetic antenna is in a light harvesting state. However, in high light, the lumenal pH decreases until the acidification of the internal thylakoid compartments reaches a threshold value triggering the NPQ process[15]. This low lumenal pH is required to trigger several mechanisms involved in NPQ. The change in the pH of the lumen occurs due to the proton influx into the lumen region, the imbalance between protons at the lumen site and available ADP and NADP. The lumenal pH acts as a measure of the photosynthetic stage, that is regulated or de-regulated under excess light conditions[16]. The first step in the mechanism for NPQ in plants is the activation of a membrane protein called PsbS due to acidification of the lumenal pH. This is followed by a slow enzymatic conversion of V to Z and leads to de-excitation of chlorophylls of the PSII antenna[14].

1.2.2 Role of the VAZ cycle

The VAZ cycle is a forward reaction where the di-epoxy xanthophyll V is de-epoxidized to xanthophyll Z, with an intermediate xanthophyll A. It is one of the most important reactions in the induction of NPQ taking place in high light intensities[17,18]. The enzyme that catalyzes this reaction is called VDE, which gets activated and binds to the thylakoid membrane only under conditions where the luminal pH has lowered to ~pH 5.0. After decades of research, the function of Z still remains controversial, with the current hypothesis that Z acts as an allosteric regulator that controls the sensitivity of qE and conformational changes of LHC's during pH lowering[19–21]. Even though the role of Z is not clear, its involvement in NPQ has been explained by models[22].

1.2.3 Role of PsbS

Although the crucial importance of PsbS in NPQ in higher plants has been established[23] for the past 15 years, there is still a great deal of uncertainty about the mechanism by which PsbS is involved in NPQ[24,25]. Studies have proved that PsbS is a prime requirement for excited-state quenching (qE) upon proton accumulation *in vivo*[26,27]. Several mechanisms have been proposed for PsbS. Earlier models placed PsbS as the site of actual quenching for heat dissipation from PSII, but later it was proposed that PsbS has the role of an antenna organizer that senses pH lowering and facilitates structural changes leading to quenching of LHCII[28]. The LHCII associated with PSII emerged as one of the site of NPQ and may undergo aggregation after conversion of V to Z under low pH conditions[14,29,30]. Along with LHCII, the minor antenna proteins like CP29, CP26 and CP24 have also been proposed to be the site of quenching during NPQ[19].

PsbS is one of the major components in triggering photoprotection due to its role in rearrangement and structural changes during NPQ associated with lowering of the lumenal pH[23,31]. In the absence of PsbS, low levels of NPQ have been observed, suggesting that PsbS is essential for effective pH sensing and rearrangement of antenna proteins under high irradiance[27].

1.2.4 Recent models for NPQ

In the early 1990s, the first model for NPQ was proposed[14,19]. The model proposed four states for NPQ. State 1 occurs in low light conditions, where the LHCII is in a non-aggregated state and the excitation energy is used to drive electron transport. The VAZ cycle starts with the presence of V in the VAZ binding pocket in State 1. With high light intensities, state 4 occurs. LHCII is aggregated and excess of excitation energy is present and the VAZ binding pocket contains Z. State 3 consists of NPQ levels lower than state 4 and is found in the thylakoid membrane immediately after high illumination. The VAZ binding pocket still contains V. State 2 is found when the change from high light to low light occurs. LHCII is unprotonated and Z is present in the VAZ binding pocket. However, the exact role of PsbS in NPQ is still unclear. Another model for NPQ suggests the occurrence of two quenching states: Q1 and Q2. This model is based on time-resolved fluorescence measurements of the two states[31]. Q1 occurs during high light conditions and detachment of the LHCII from PSII and its aggregation takes place. Here, PsbS is in the protonated form and heat dissipation of excess light energy takes place. No Z is required during Q1. Here, the fast phase of NPQ occurs within 1-5 mins. Q2, on the other hand, takes place in minor LHCII complexes like CP29, CP26 and CP24, which are still attached to PSII. Conversion of V to Z in Q2 is hypothesized. Here, the slow phase of NPQ takes ~10-15 mins. NPQ in the Q2 state majorly depends on the VAZ cycle.

Two models for the function of PsbS in NPQ have been proposed, both assigning PsbS as the pH sensor for sensing lumen acidification during high light irradiance. One model proposes that PsbS triggers conformational changes in LHCII leading to aggregation and NPQ, while the other model suggests PsbS to be the quenching site along with its binding to the pigment Z[16]. NPQ mechanism to regulate photosynthesis is quite biodiverse in nature. In plants, PsbS is known to be the only protein for pH sensing while in green algae, another class of proteins called LHCSR are found. In the moss *Physcomitrella patens,* the presence of both PsbS and LHCSR proteins are found to play equal roles in photoprotection[32]. Why plants adopted for PsbS-dependent NPQ, why LHCSR was lost in vascular plants and where did PsbS come from, are some intriguing questions to ask[33]. Is moss the intermediate during the evolution to land and holds answers to how the PsbS gene came into its role as a pH sensor?

From an evolutionary standpoint, photoprotection has evolved to achieve survival under high light-stress conditions over maximum carbon fixation efficiency[8]. An improvement of the efficiency of photosynthesis by reduction of the size of the antenna system and spread of the excitation throughout the canopy has been demonstrated[11]. Other ways, like deletion or inactivation of genes coding for antenna proteins or accessory pigments, have resulted in a balanced dispersion of energy to the two antenna systems[11,34,35]. Overexpression of membrane protein PsbS in Tobacco plants, together with xanthophyll-cycle enzymes, led to an increase in qE along with accelerating NPQ relaxation, which significantly increased the quantum yield of CO_2 assimilation[36]. In conclusion, understanding the mechanism of PsbS is vital for improving biomass production.

1.3 Discovery and mechanism of PsbS

The membrane protein PsbS was first discovered as a component of PSII preparation in 1986[37] and co-precipitated with other subunits[38]. Sequencing of PsbS showed[39] that it is a unique protein containing four transmembrane helices.

After more than 20 years of research, it is clear that PsbS has a central role in sensing the thylakoid luminal pH and activation of a series of complex structural rearrangements[40] that lead to chlorophyll de-excitation in the antenna, which is the basis of NPQ[23,41]. A model of the hypothesized function of PsbS in photoprotection is depicted in Figure 1.2. PsbS belongs to the LHC protein family[42]. It has a molecular weight of 22 kDa and has four transmembrane helices in its structure, unlike all other members of the LHC family.

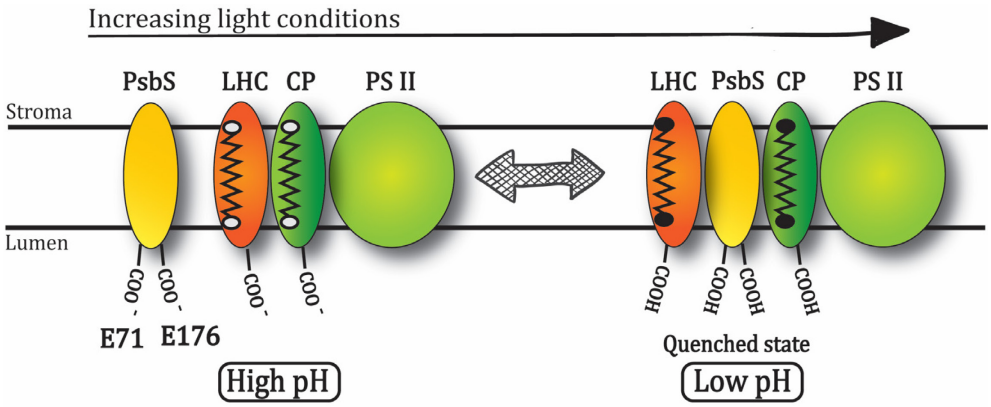

Figure 1.2 Top: The hypothesized role of PsbS during NPQ adopted from Niyogi *et al.*, 2005[13]. V to Z (white to black dots) conversion takes place with protonation of glutamate residues.

A homology structure of PsbS from *Physcomitrella patens* and the crystal structure of PsbS from *Spinacia oleracea* is shown in Figure 1.3 followed by a protein sequence alignment between PsbS from *P. patens, S. oleracea* and *A. thaliana* species. PsbS does not bind specific Chl pigments and acts as a pH sensor to trigger structural changes in PSII-LHCII super-complexes leading to qE and NPQ[24,43]. Recent studies, focusing on PsbS interaction, showed that Patens-PsbS associates with one of the monomeric unit of LHCII trimer[44]. For PsbS of higher plants, enhanced interactions with Lhcb1 antenna complexes were observed under high-light conditions[45] and increased binding of PsbS to minor antenna complexes was observed with the combination of low pH and zeaxanthin[46].

Mutational studies on proton-accepting residues in the lumen region of PsbS, especially on two glutamate residues located at the lumenal loops, have shown to severely influence qE, indicating that they are critical for the function of PsbS[47]. In Patens-PsbS, these two glutamate sites are at Glu-71 and Glu-176 that protrude at the lumenal side of the membrane (Figure 1.3c, red box). Protonation of these two active glutamates is proposed to induce a dimer to monomer transition, which is suggested to be the first step in PsbS activation[28]. The recent crystallography structure, however, shows that PsbS forms a stable dimer under low-pH conditions[48].

Apart from the structure of the protein PsbS, its evolution and existence in vascular plants are also very intriguing. In *Chlamydomonas reinhardtii*, which is an alga, previously it was believed that the PsbS gene is present but it is not active and NPQ is LHCSR-dependent[49], however, recently PsbS was shown to be transiently expressed and to play a transient role during NPQ in algae[50]. Recent studies showed that in *P. patens*, both PsbS and LHCSR genes are present and active during NPQ[51]. This role is however taken over by PsbS in higher green plants like *S. oleracea* and *A. thaliana*[52]. A reason for this switch is proposed to be the less robust LHCSR-dependent NPQ that was discarded during evolution[32]. Another explanation lies in the function of LHCSR as both a sensor of excess light and quenching site in lower organisms and mosses, that was later replaced by PsbS as sensor and LHCII as a site of quenching in higher plants[33].

The sequence alignment between *P. patens*, *S. oleracea* and *A. thaliana* shows that several regions are conserved for all the three species (Figure 1.3c).

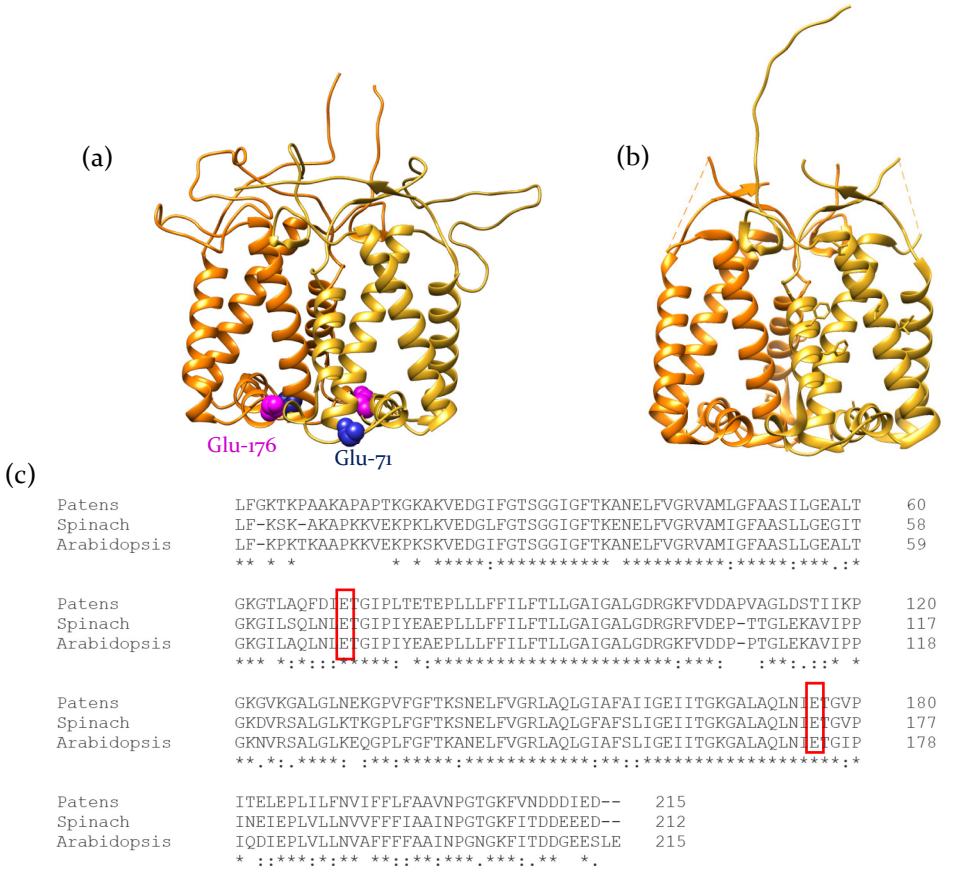

Figure 1.3 A homology model of (a) Patens-PsbS[53] in comparison with (b) Spinach-PsbS, PDB 4RI2 [48]. Two glutamate residues are shown as pink and blue spheres that are hypothesized to be the site of protonation. (c) Protein sequence alignment of *P. patens*, *S. oleracea* and *A. thaliana* using Clustal Omega from EMBL-EBI. In red marked are the two active glutamates.

1.4 Challenges in PsbS structural characterization

In vivo and *in vitro* studies have been carried out on PsbS to understand its underlying mechanism in the regulation of NPQ and its interaction with antenna proteins[43,46,47,54]. It is challenging to determine the molecular function of PsbS, due to its lack of specific-bound pigments, its low production in plants, and the difficulty of PsbS purification. Some studies performed *in vitro* synthesis of PsbS[24,28,43,54] producing detergent-refolded PsbS in moderate quantities, and PsbS has also been refolded in liposomes together with LHCII to study its quenching mechanism *in vitro*[54,55].

However, the yield of PsbS attained is not enough for carrying out spectroscopic studies and there are many challenges to solve.

The first challenge is to produce recombinant PsbS in high quantity for biochemical and NMR studies. This can be achieved by either cell-free protein expression or overexpression using *E. coli*. Both techniques have great potential in membrane protein production. While cell-free expression allows for easy labelling of isotopic amino acids with minimal scrambling, it is still challenging to produce large amounts of soluble membrane proteins[56]. This makes overexpression using *E. coli* more favorable. Even though this procedure can produce sufficient amounts of proteins, it often leads to the production of inclusion bodies. Inclusion bodies are aggregated protein structures within the bacteria when membrane proteins foreign to *E. coli* system are overexpressed[57]. These inclusion bodies contain the membrane protein in an unfolded form and are very hard to isolate and purify.

The next challenge is to refold the unfolded PsbS into its proper conformation. The refolding of membrane proteins is quite critical to their function. Factors like CMC, aggregation number of detergents, temperature and concentration of PsbS have to be considered for a successful refolding[58–60].

The determination of oligomeric states of PsbS is important as it has been proposed that PsbS activation is associated with dimer to monomer transition upon protonation under high-light conditions[28]. Determining the exact size of PsbS and oligomeric states can be very challenging since the detergent micelles surrounding it will contribute to the total molecular weight of the protein-detergent micelles. Therefore the use of complementary techniques for correct size determination is required[61–63].

The final challenge and major aim of this thesis is to resolve the molecular pH sensing mechanism of PsbS by observing structural changes and dynamics of PsbS. NMR spectroscopy is emerging as a powerful tool[64] to observe the dynamics of a protein in solution, unlike X-ray crystallography that requires crystallization. Resolving the "fingerprint" of a protein can be performed by using 2D ^{1}H-^{15}N HSQC, where each backbone amide bond corresponds to a peak[65]. However, solution-state NMR studies of PsbS are challenging due to the total size of PsbS in detergent micelles being too large, while solid-state NMR requires high quantities of properly folded, membrane reconstituted PsbS, which is challenging to prepare. In this thesis, other spectroscopic techniques like IR and CD spectroscopy have been explored as well to overcome the limitations of NMR spectroscopy.

1.5 Research objectives and dissertation outline

PsbS has been a mysterious protein in photosynthetic research. Its role in NPQ has been hypothesized in various models but the exact mechanism of function is still unclear. How PsbS interacts with other membrane components (like antenna proteins, PSII, zeaxanthin) to induce qE is still unknown as is its molecular pH-response mechanism. Mutation of two key glutamate residues in the lumenal loops of PsbS has shown to reduce NPQ significantly[47]. The exact molecular mechanism of these two glutamate residues in PsbS leading to structural changes have not been determined yet. Several challenges like the proper folding of PsbS, right environmental conditions for NMR or CD spectroscopy, while maintaining the stability of PsbS in different pH and temperature conditions have been overcome in this thesis. Finally, the role of the two glutamate residues in the pH sensing-mechanism of PsbS has been elucidated.

The main research objectives are outlined below:

1. *Can sufficient quantities of recombinant PsbS be produced and purified for spectroscopic studies?*

With the goal to perform structural and biochemical studies on recombinant PsbS, the first step is to produce enough purified PsbS in a proper fold. Two approaches for the production of PsbS were explored: cell-free expression and overexpression by *E. coli*. In Chapter 2, production of PsbS using cell-free expression system is described. After temperature and detergent optimization steps, cell-free production of soluble PsbS was achieved. PsbS was successfully refolded after its production. In Chapter 3, the production of PsbS using overexpression in *E. coli* is documented. Plasmid and temperature optimization led to maximal yields of PsbS of ~120 mg/L. A novel purification protocol was set up, which reduced losses by ~60 %.

2. *What is the optimal environment for PsbS folding and stability?*

In Chapter 3, PsbS was refolded using different detergents and was characterized by CD spectroscopy. Detergents FC-12 and OG proved optimal for the folding and stability of Patens-PsbS.

3. *What is the influence of pH on the oligomeric states of PsbS?*

In Chapter 4, PsbS refolded under high and low pH conditions were analyzed to determine pH-induced changes in oligomerization state using SEC, SDS-gel analysis, DLS and DOSY NMR spectroscopy. The dimer-to-monomer transitions were explored,

which might be the first step in the activation of PsbS. ^{15}N-^{1}H HSQC NMR was performed on PsbS to detect pH-dependent changes in structure or dynamics.

4. *What is the molecular pH response mechanism of PsbS? What is the role of the two active Glu residues in bringing about pH-dependent conformational changes?*

The fold and oligomeric state of selective Glu mutants of PsbS were compared with the WT PsbS by NMR, FTIR and CD spectroscopy, presented in Chapter 5. The roles of Glu-71 and Glu-176 were explored and a model suggesting the structural response of PsbS to low pH was proposed.

1

1.6 References

1. FAO's Director-General on How to Feed the world in 2050. *population and development review* **35,** 837–839 (2009).
2. Beller, H. R. *et al.* Discovery of enzymes for toluene synthesis from anoxic microbial communities. *Nature Chemical Biology* **14,** 451–457; 10.1038/s41589-018-0017-4 (2018).
3. Melis, A. Photosynthesis-to-fuels: From sunlight to hydrogen, isoprene, and botryococcene production. *Energy and Environmental Science* **5,** 5531–5539; 10.1039/c1ee02514g (2012).
4. Ghirardi, M. L., Togasaki, R. K. & Seibert, M. Oxygen sensitivity of algal H2-production. *Applied Biochemistry and Biotechnology* **67,** 182; 10.1007/BF02787851 (1997).
5. Robin Purchase, Huib De Vriend, Huub de Groot. *Artificial photosynthesis : for converstion of sunlight to fuel. Published as part of the series "Groene Grondstoffen" ("Green Raw Materials") ,*
6. Govindjee & Krogmann, D. Discoveries in oxygenic photosynthesis (1727-2003): A perspective. *Photosynthesis Research* **80,** 15–58; 10.1023/B:PRES.0000030443.63979.e6 (2004).
7. L.N.M.Duysens, J.Amesz, B.M.Kamp. Two photochemical systems in photosynthesis. *Nature* **190,** 510–511 (1961).
8. Blankenship, R. E. *Molecular Mechanisms of Photosynthesis.* 2nd ed. (Wiley Blackwell, 2014).
9. Melis, A., Neidhardt, J. & Benemann, J. R. Dunaliella salina (Chlorophyta) with small chlorophyll antenna sizes exhibit higher photosynthetic productivities and photon use efficiencies than normally pigmented cells. *Journal of Applied Phycology* **10,** 515–525; 10.1023/A:1008076231267 (1998).
10. Murchie, E. H. & Niyogi, K. K. Manipulation of photoprotection to improve plant photosynthesis. *Plant Physiology* **155,** 86–92; 10.1104/pp.110.168831 (2011).
11. Melis, A. Solar energy conversion efficiencies in photosynthesis: Minimizing the chlorophyll antennae to maximize efficiency. *Plant Science* **177,** 272–280; 10.1016/j.plantsci.2009.06.005 (2009).
12. Kiss, A. Z., Ruban, A. V. & Horton, P. The PsbS protein controls the organization of the photosystem II antenna in higher plant thylakoid membranes. *Journal of Biological Chemistry* **283,** 3972–3978; 10.1074/jbc.M707410200 (2008).
13. Niyogi, K. K., Li, X. P., Rosenberg, V. & Jung, H. S. Is PsbS the site of non-photochemical quenching in photosynthesis? *Journal of Experimental Botany* **56,** 375–382; 10.1093/jxb/eri056 (2005).
14. Horton, P. & Ruban, A. V. Regulation of Photosystem II. *Photosynthesis Research* **34,** 375–385; 10.1007/BF00029812 (1992).

15. Brooks, M. D., Jansson, S., and Niyogi, K. K. . in *Non-Photochemical Quenching and Energy Dissipation in Plants, Algae and Cyanobacteria,* edited by Barbara Demmig-Adams, Gyozo Garab, William Adams III, Govindjee (Springer, Dordrecht2014).

16. Goss, R. & Lepetit, B. Biodiversity of NPQ. *Journal of plant physiology* **172,** 13–32; 10.1016/j.jplph.2014.03.004 (2014).

17. H. Y. Yamamoto, T. O. M. Nakayama, C. O. Chichester. Studies on the light and dark interconversions of leaf Xanthophylls. *Archives of Biochemistry and Biophysics.,* 168–173 (1962).

18. Hager, A. Studies on the light-induced reversible Xanthophyll conversions in Chlorella and spinach leaves. *Planta* **172,** 148–172 (1967).

19. Horton, P., Johnson, M. P., Perez-Bueno, M. L., Kiss, A. Z. & Ruban, A. V. Photosynthetic acclimation: Does the dynamic structure and macro-organisation of photosystem II in higher plant grana membranes regulate light harvesting states? *FEBS Journal* **275,** 1069–1079; 10.1111/j.1742-4658.2008.06263.x (2008).

20. Ruban, A. V., Johnson, M. P. & Duffy, C. D. P. The photoprotective molecular switch in the photosystem II antenna. *Biochimica et Biophysica Acta - Bioenergetics* **1817,** 167–181; 10.1016/j.bbabio.2011.04.007 (2012).

21. Johnson, M. P., Zia, A. & Ruban, A. V. Elevated ΔpH restores rapidly reversible photoprotective energy dissipation in Arabidopsis chloroplasts deficient in lutein and xanthophyll cycle activity. *Planta* **235,** 193–204; 10.1007/s00425-011-1502-0 (2012).

22. Jahns, P. & Holzwarth, A. R. The role of the xanthophyll cycle and of lutein in photoprotection of photosystem II. *Biochimica et biophysica acta* **1817,** 182–193; 10.1016/j.bbabio.2011.04.012 (2012).

23. Li, X. P. *et al.* A pigment-binding protein essential for regulation of photosynthetic light harvesting. *Nature* **403,** 391–395; 10.1038/35000131 (2000).

24. Bonente, G., Howes, B. D., Caffarri, S., Smulevich, G. & Bassi, R. Interactions between the photosystem II subunit PsbS and xanthophylls studied in vivo and in vitro. *Journal of Biological Chemistry* **283,** 8434–8445; 10.1074/jbc.M708291200 (2008).

25. Barbara Demmig-Adams, Gyozo Garab, William Adams III, Govindjee. *Non-Photochemical Quenching and Energy Dissipation in Plants, Algae and cyanobacteria. Chapter 13 PsbS-Dependent Non-Photochemical Quenching* (Springer US, 2014).

26. Johnson, M. P. & Ruban, A. V. Arabidopsis plants lacking PsbS protein possess photoprotective energy dissipation. *Plant Journal* **61,** 283–289; 10.1111/j.1365-313X.2009.04051.x (2010).

27. Johnson, M. P. & Ruban, A. V. Restoration of rapidly reversible photoprotective energy dissipation in the absence of PsbS protein by enhanced by pH. *Journal of Biological Chemistry* **286,** 19973–19981; 10.1074/jbc.M111.237255 (2011).

28. Bergantino, E. *et al.* Light- and pH-dependent structural changes in the PsbS subunit of photosystem II. *Proceedings of the National Academy of Sciences of the United States of America* **100,** 15265–15270; 10.1073/pnas.2533072100 (2003).

29. Ruban, A. V., Phillip, D., Young, A. J. & Horton, P. Carotenoid-dependent oligomerization of the major chlorophyll a/b light harvesting complex of photosystem II of plants. *Biochemistry* **36,** 7855–7859; 10.1021/bi9630725 (1997).

30. Phillip, D., Ruban, A. V., Horton, P., Asato, A. & Young, A. J. Quenching of chlorophyll fluorescence in the major light-harvesting complex of photosystem II: a systematic study of the effect of carotenoid structure. *Proceedings of the National Academy of Sciences* **93,** 1492–1497; 10.1073/pnas.93.4.1492 (1996).

31. Holzwarth, A. R., Miloslavina, Y., Nilkens, M. & Jahns, P. Identification of two quenching sites active in the regulation of photosynthetic light-harvesting studied by time-resolved fluorescence. *Chemical Physics Letters* **483,** 262–267; 10.1016/j.cplett.2009.10.085 (2009).

32. Gerotto, C., Alboresi, A., Giacometti, G. M., Bassi, R. & Morosinotto, T. Role of PSBS and LHCSR in Physcomitrella patens acclimation to high light and low temperature. *Plant, Cell and Environment* **34,** 922–932; 10.1111/j.1365-3040.2011.02294.x (2011).

33. Niyogi, K. K. & Truong, T. B. Evolution of flexible non-photochemical quenching mechanisms that regulate light harvesting in oxygenic photosynthesis. *Current Opinion in Plant Biology* **16,** 307–314; 10.1016/j.pbi.2013.03.011 (2013).

34. Nakajima, Y. & Ueda, R. Improvement of photosynthesis in dense microalgal suspension by reduction of light harvesting pigments. *Journal of Applied Phycology* **9,** 503–510; 10.1023/A:1007920025419 (1997).

35. Blankenship, R. E. & Chen, M. Spectral expansion and antenna reduction can enhance photosynthesis for energy production. *Current Opinion in Chemical Biology* **17,** 457–461; 10.1016/j.cbpa.2013.03.031 (2013).

36. Kromdijk, J., Głowacka, K., Leonelli, L., Gabilly, S. T., Iwai, M., Niyogi, K., Long, S. P. Improving photosynthesis and crop productivity by accelerating recovery from photoprotection. *Science* **354,** 857–860 (2016).

37. Ghanotakis, D. F. & Yocum, C. F. Purification and properties of an oxygen-evolving reaction center complex from photosystem II membranes. *FEBS Letters* **197,** 244–248; 10.1016/0014-5793(86)80335-0 (1986).

38. Ljungberg, U., Akerlund Hans-Erik & Andersson Bertil. Isolation and characterization of the 10-kDa and 22-kDa polypeptides of higher plant photosystem 2. *European Journal of Biochemistry* **158,** 477–482; 10.1111/j.1432-1033.1986.tb09779.x (1986).

39. Kim, S. *et al.* Characterization of a spinach psbS cDNA encoding the 22 kDa protein of photosystem II. *FEBS Letters* **314,** 67–71 (1992).

40. Kereïche, S., Kiss, A. Z., Kouřil, R., Boekema, E. J. & Horton, P. The PsbS protein controls the macro-organisation of photosystem II complexes in the grana membranes of higher plant chloroplasts. *FEBS Letters* **584,** 759–764; 10.1016/j.febslet.2009.12.031 (2010).

41. Li, X. P. *et al.* Regulation of photosynthetic light harvesting involves intrathylakoid lumen pH sensing by the PsbS protein. *Journal of Biological Chemistry* **279,** 22866–22874; 10.1074/jbc.M402461200 (2004).

42. Funk, C. *et al.* The PS II-S protein of higher plants : a new type of pigment binding protein. *Biochemistry* **34,** 11133–11141 (1995).

43. Dominici, P. *et al.* Biochemical properties of the PsbS subunit of photosystem II either purified from chloroplast or recombinant. *Journal of Biological Chemistry* **277,** 22750–22758; 10.1074/jbc.M200604200 (2002).

44. Gerotto, C., Franchin, C., Arrigoni, G. & Morosinotto, T. In vivo Identification of Photosystem II Light Harvesting Complexes Interacting with Photosystem II subunit S. *Plant Physiology* **168,** 1747–1761; 10.1104/pp.15.00361 (2015).

45. Correa-Galvis Viviana & Gereon Poschmann , Michael Melzer, Kai Stühler and Peter Jahns. PsbS interactions involved in the activation of energy dissipation in Arabidopsis. *Nature Plants* **2,** 15225–15232; 10.1038/nplants.2015.225 (2016).

46. Sacharz, J., Giovagnetti, V., Ungerer, P., Mastroianni, G. & Ruban, A. V. The xanthophyll cycle affects reversible interactions between PsbS and light-harvesting complex II to control non-photochemical quenching. *Nature Plants* **3**; 10.1038/nplants.2016.225 (2017).

47. Li, X. P., Phippard, A., Pasari, J. & Niyogi, K. K. Structure-function analysis of photosystem II subunit S (PsbS) in vivo. *Functional Plant Biology* **29,** 1131–1139; 10.1071/FP02065 (2002).

48. Fan, M. *et al.* Crystal structures of the PsbS protein essential for photoprotection in plants. *Nature structural and molecular biology* **22,** 729–735; 10.1038/nsmb.3068 (2015).

49. Bonente, G. *et al.* The occurrence of the psbs gene product in chlamydomonas reinhardtii and in other photosynthetic organisms and its correlation with energy quenching. *Photochemistry and Photobiology* **84,** 1359–1370; 10.1111/j.1751-1097.2008.00456.x (2008).

50. Tibiletti, T., Auroy, P., Peltier, G. & Caffarri, S. Chlamydomonas reinhardtii PsbS Protein Is Functional and Accumulates Rapidly and Transiently under High Light. *Plant Physiology* **171,** 2717–2730; 10.1104/pp.16.00572 (2016).

51. Alboresi, A., Gerotto, C., Giacometti, G. M., Bassi, R. & Morosinotto, T. Physcomitrella patens mutants affected on heat dissipation clarify the evolution of photoprotection mechanisms upon land colonization. *Proceedings of the National Academy of Sciences* **107,** 11128–11133; 10.1073/pnas.1002873107 (2010).

52. Roach, T. & Krieger-Liszkay, A. The role of the PsbS protein in the protection of photosystems i and II against high light in Arabidopsis thaliana. *Biochimica et Biophysica Acta - Bioenergetics* **1817,** 2158–2165; 10.1016/j.bbabio.2012.09.011 (2012).

53. Krishnan, M., Moolenaar, G. F., Gupta, Karthick Babu Sai Sankar, Goosen, N. & Pandit, A. Large-scale in vitro production, refolding and dimerization of PsbS in different microenvironments. *Scientific Reports* **7,** 1–11; 10.1038/s41598-017-15068-3 (2017).

54. Wilk, L., Grunwald, M., Liao, P.-N., Walla, P. J. & Kühlbrandt, W. Direct interaction of the major light-harvesting complex II and PsbS in nonphotochemical quenching. *Proceedings of the National Academy of Sciences of the United States of America* **110,** 5452–5456; 10.1073/pnas.1205561110 (2013).

55. Liu, C. *et al.* Simultaneous refolding of denatured PsbS and reconstitution with LHCII into liposomes of thylakoid lipids. *Photosynthesis Research* **127,** 109–116; 10.1007/s11120-015-0176-z (2016).

56. Shimono, K., Shirouzu, M. & Yokoyama, S. Production of Membrane Proteins Using Cell-free Protein Synthesis. *Seibutsu Butsuri* **51,** 128–129; 10.2142/biophys.51.128 (2011).

57. Singh, S. M. & Panda, A. K. Solubilization and refolding of bacterial inclusion body proteins. *Journal of bioscience and bioengineering* **99,** 303–310; 10.1263/jbb.99.303 (2005).

58. Garavito, R. M. & Ferguson-Miller, S. Detergents as Tools in Membrane Biochemistry. *Journal of Biological Chemistry* **276,** 32403–32406; 10.1074/jbc.R100031200 (2001).

59. Oliver, R. C. *et al.* Dependence of Micelle Size and Shape on Detergent Alkyl Chain Length and Head Group. *PLoS ONE* **8**; 10.1371/journal.pone.0062488 (2013).

60. Tzitzilonis, C., Eichmann, C., Maslennikov, I., Choe, S. & Riek, R. Detergent/Nanodisc Screening for High-Resolution NMR Studies of an Integral Membrane Protein Containing a Cytoplasmic Domain. *PLoS ONE* **8,** 2–9; 10.1371/journal.pone.0054378 (2013).

61. Chaptal, V. *et al.* Quantification of Detergents Complexed with Membrane Proteins. *Scientific Reports* **7,** 41751; 10.1038/srep41751 (2017).

62. Bowman, G. R. *et al.* Oligomerization and higher-order assembly contribute to sub-cellular localization of a bacterial scaffold. *Molecular microbiology* **90,** 776–795; 10.1111/mmi.12398 (2013).

63. Das, S., Stivison, E., Folta-Stogniew, E. & Oliver, D. Reexamination of the role of the amino terminus of SecA in promoting its dimerization and functional state. *Journal of bacteriology* **190,** 7302–7307; 10.1128/JB.00593-08 (2008).

64. Kwan, A. H., Mobli, M., Gooley, P. R., King, G. F. & MacKay, J. P. Macromolecular NMR spectroscopy for the non-spectroscopist. *FEBS Journal* **278,** 687–703; 10.1111/j.1742-4658.2011.08004.x (2011).

65. Bodenhausen, G. & Ruben, D. J. Natural abundance nitrogen-15 NMR by enhanced heteronuclear spectroscopy (1980).

Incubate for 4 hours
Cell Extract
in vitro
Protein Production

2

Cell-free expression of PsbS

PsbS is a membrane protein playing an exclusive role in NPQ for photoprotection of plants under high-light conditions. The activation mechanism of PsbS and its pH-induced conformational changes are currently unknown. For structural investigation of PsbS, effective synthesis of PsbS with selective isotopes or electron-spin labels or non-natural amino acids incorporated would be a great asset. This chapter presents cell-free expression as a successful method for *in vitro* production of PsbS that would allow label incorporation. Optimization of the cell-free expression to yield soluble PsbS of ~500 ng/µl using a continuous-exchange method at 30 °C, along with a successful purification and refolding of PsbS in β-DM detergent was done. The presented protocols can be applied for *in vitro* expression of other membrane proteins of the LHC family.

This chapter is based on
Maithili Krishnan, T.J.J.F. de Leeuw and Anjali Pandit "Cell-free expression of the membrane protein PsbS" *Protein Expression and Purification, DOI:* 10.1016/j.pep.2019.02.010

2.1 Introduction

The discovery of PsbS has revealed that it has a prominent role in sensing changes in thylakoidal pH. PsbS is hypothesized to undergo structural conformational changes to bring about rearrangements in the neighbouring photosynthetic proteins, thus, leading to de-excitation of the neighbouring antenna Chls[1,2]. To study its mechanism, PsbS was overexpressed using *E. coli* and refolded into helical structures using several types of detergents[3,4]. Although this overexpression method is well established, there are challenges like inclusion bodies production, low yield while isotope and selective labelling, losses upon insertion into liposomes or nanodiscs and toxic effects to the host cells upon overexpression.

Cell-free expression systems are emerging to resolve the problems in the conventional overexpression of membrane proteins[5–8], with simple operation protocols, high success rates and flexibility in applications[9]. The concept of the cell-free system allows to easily control all kinds of reaction parameters. The addition of agents, like RNase and protease inhibitors, can stabilize expressed proteins and limit proteolytic degradation. For resolving protein structures via NMR spectroscopy, isotope labelled amino acids can be added to the cell-free reaction. In contrast to *in vivo* expression, this can be achieved very easily, as labelled amino acids can be added directly to the reaction mixture. Commercialized *E. coli* cell-free systems are composed of extracted cell components, including ribosomes, tRNAs, plasmid DNA, T7 RNA polymerase, translation factors and tRNA synthetases nucleoside triphosphates and amino acids[10]. The procedure of small-scale cell-free protein synthesis involves incubation of these components with an mRNA or DNA template in small reaction vessels and can yield up to several micrograms of proteins. Methods for batch incubation or continuous exchange have also been developed to increase productivity.

Since the cell-free expressions system is open and easily accessible, supplementing specific target compounds such as ligands, substrates or inhibitors, or even protein components serving as chaperones, subunits or coenzymes, at any point of incubation is not a limitation. Furthermore, labelling of proteins using seleno-methionine, ^{15}N- or ^{13}C-labelled amino acids or fluorescence-enhanced non-natural amino acids can be achieved[11–13] without problems of metabolic scrambling. Successful backbone assignments of membrane proteins have been performed using cell-free expression enabling selective labelling of certain amino acids and even specific positions of amino acids[14].

Optimal expression of membrane proteins is defined by both high yields of protein and a stable structure that plays an equal role in the quality of expression. Several

parameters affecting the biophysical properties of the microenvironment like lipid composition, detergent characteristic, protein-lipid interactions, protein aggregation, pH, fluidity, tension, all attributing to correct folding of a membrane protein help in deciding the best expression system[8]. *In vitro* refolding of various membrane proteins during the cell-free reaction can be achieved by adding detergents, liposomes or lipid nanodiscs to the reaction mixture[15–17]. However, the yields for membrane proteins produced using the cell-free technique is still far below the yields achieved for soluble proteins[18].

This chapter shows that PsbS from *P. patens* can be synthesized by using a commercial cell-free system and be successfully refolded. Various detergents and lipid nanodiscs were added to the reaction mixtures to achieve soluble PsbS using the fed-batch system. Purification and refolding of both pellet and soluble PsbS produced using cell-free reactions was successfully achieved in the detergent β-DM.

2.2 Materials and Methods

2.2.1 Cell-free expression protocol

The PsbS gene from *P. patens*[4] was inserted in a pExp5 vector for the cell-free reactions (described in Chapter 3). The Expressway™ Cell-Free Expression System (Invitrogen) was used to carry out the cell-free reactions. 25 µl reaction mixture was used containing the template DNA plasmid and incubated for 2-4 hours at 30 °C or 37 °C while shaking at 1200 rpm. After 30 minutes, 25 µl of feeding mixture was added into the reaction volume. To produce soluble PsbS, cell-free reactions were carried out in the presence of detergents, or in the presence of liposomes or lipid nanodiscs (preparation protocols according to Crisafi *et, al.*[19]). In the batch feeding method, 12.5 µl of feeding mixture was added every 30 minutes for up to 7 hours. The continuous exchange method was carried out in 0.1 ml 96-well microdialysis plates (Thermo Scientific - Pierce) containing a 10 kDa cut-off membrane. 50 µl of the reaction mixture and 1 ml of feeding mixture diluted in HEPES buffer was added to this system.

2.2.2 SDS-page gel analysis

SDS-page gel electrophoresis analysis (12.5 % running gel, 4 % stacking gel stained with Coomassie brilliant blue R-250 Bio-Rad) was carried out to check the yield of PsbS synthesis along with 2.5 µl of Precision Plus Protein™ Dual Color Standard from Sigma and BSA standard protein.

2.2.3 Purification of cell-free produced PsbS from pellet

Cell-free production of PsbS in the absence of detergents results in a pellet containing PsbS. This pellet, P, was subjected to urea wash protocol[4] to achieve soluble PsbS.

2.2.4 Purification of cell-free produced soluble PsbS

Soluble PsbS containing His-tag was purified after cell-free synthesis in the presence of 1 % Brij-78 or lipid nanodiscs using Ni-NTA Agarose beads (QIAGEN). The soluble fraction was diluted in equal amounts of binding buffer (50 mM NaH_2PO_4, 300 mM NaCl, 10 mM imidazole and appropriate detergent, pH 8.0) and added to the resin, followed by a 4-hour incubation at 4 °C. After the incubation step, the supernatant was removed from the resin by centrifuging for 1 minute at 200 x g, 4 °C. Washing of the resin was carried out three times using 3 volumes of wash buffer (binding buffer + 20 mM imidazole). The elution step was carried out 3 times using 1.5 volumes of elution buffer (binding buffer + 250 mM imidazole) to achieve purified PsbS.

2.2.5 CD spectroscopy

A Jasco J-815 spectropolarimeter (Jasco Labortechnic, Japan) was used to perform CD spectroscopy to check the refolding of the cell-free synthesized PsbS. The purified PsbS was buffer exchanged to 50 mM NaH_2PO_4, pH 8.0 with 0.12 % β-DM to remove the high salts and imidazole or urea concentrations. The spectra were recorded between 190 nm and 260 nm with a scanning rate of 100 nm/min, a response time of 8 seconds and an optical path length of 1 mm.

2.3 Results and discussion

2.3.1 Cell-free synthesis of PsbS as pellet

For carrying out the cell-free reaction, the PsbS plasmid was added to the cell-free *E. coli* reaction mix and incubated at 37 °C for 3 hours. Using 1330 ng of the plasmid in the cell-free reaction, a yield of 200 ng/µl PsbS was produced with this standard reaction protocol (Fig 2A.1). As PsbS is a membrane protein that would aggregate without the presence of detergents, it precipitated as a pellet, P, in the cell-free reaction (Figure 2.1a). Figure 2.1b shows the purification of PsbS by washing with UP buffer to separate impurities (SS1 and SS2) from the pellet. Upon addition of 0.05 % LDS, most of the PsbS from the pellet P was solubilized (SS3). Further addition of 0.5 % LDS to the remaining pellet solubilized the remaining PsbS (SS4). The soluble fraction SS4 was buffer exchanged to remove the urea and stored in the buffer containing 0.1 % LDS for further use. Refolding of PsbS from SS4 was carried out in the presence of 0.12 % β-DM according to a published protocol and analysis of the refolded protein is discussed further[3,4].

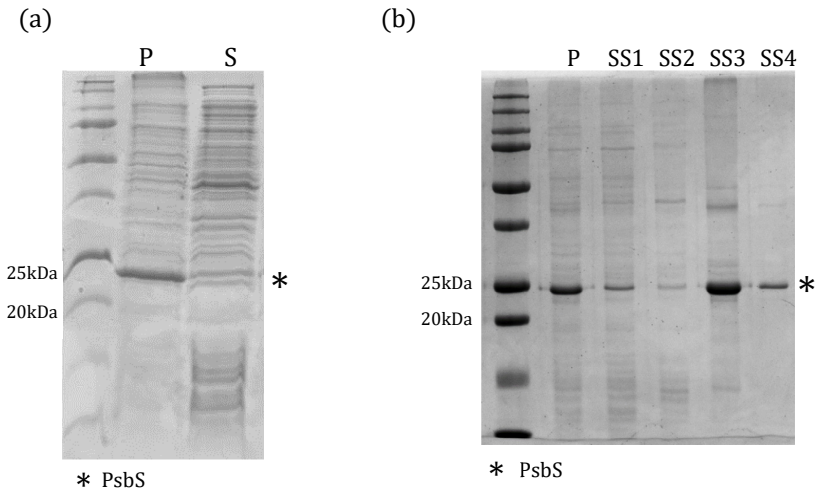

Figure 2.1 (a) Cell-free production of PsbS (*) in the absence of detergents. Cell-free reactions were separated in the pellet (P), and supernatant (S). (b) Purification of cell-free PsbS from pellet: SS1 and SS2 are soluble fractions after washing the pellet P with UP buffer, SS3 is the soluble fraction after washing with UP buffer and 0.05 % LDS and SS4 is the soluble fraction after washing with UP buffer and 0.5 % LDS.

2.3.2 Cell-free synthesis of soluble PsbS

In order to solubilize the expressed PsbS during the cell-free reaction, the effects of the addition of various detergents to the reaction mixture were analyzed. Here optimization on PsbS solubilization was carried out by cell-free reaction in the presence of detergents like β-DM, Triton X-100, Brij-35 and Brij-78 (Fig 2A.2). Furthermore, the addition of liposomes and lipid nanodiscs were tested as a method to directly fold synthesized PsbS into lipid membranes (Fig 2A.3 and Fig 2A.4). The results are summarized in Table 2.1 and show successful production of PsbS in the presence of all the tested detergents, liposomes and lipid nanodiscs. In the presence of detergents, PsbS still precipitated as a pellet, except for reactions carried out in the presence of sufficient amounts of polyoxyethylene-alkyl-ether detergents, Brij-35 and Brij-78. The flexible long chains of polyoxyethylene-alkyl-ethers and their relatively small hydrophilic head might be favouring the solubilization of PsbS[20,21]. Although some studies showed that the addition of liposomes was beneficial in improving membrane protein yields in cell-free synthesis[22], by the data presented in this chapter the presence of asolectin liposomes lowered the production of PsbS considerably.

Table 2.1 Cell-free expression of PsbS in membrane-mimicking environments. The reaction was carried out at 37 °C and PsbS yield as soluble or pellet fraction were classified into four groups: -, no detectable expression; □, spurious expression < 50 ng/µl; +, 51–200 ng/µl; ++, > 200 ng/µl. Different concentrations were tested for β-DM and Brij-35 (x CMC). SDS-page gels of the different reactions are presented in Fig. 2A.1-2A.4 in the appendix 2A.

Membrane mimicking environment	Concentration mM (%)	x CMC	Soluble	Pellet
Control	..	..	-	++
β-DM	0.51 (0.03)	4	-	+
	1.53 (0.1)	14	-	+
	3.06 (0.2)	28	-	-
Triton X-100	0.23 (0.15)	10	-	++
Brij-35	0.32 (0.04)	4	□	□
	1.6 (0.2)	20	□	□
	6.4 (0.8)	80	□	□
Brij-78	9.2 (1.0)	200	□	-
Asolectin liposomes	24 (lipid)	..	□	□
Asolectin nanodiscs	2.4 (lipid)	..	□	-

2.3.3 Incubation temperature

The cell-free reactions were further optimized by varying the incubation temperature, to 37 °C, 30 °C and 25 °C. Since Brij-78 was optimal for expression of soluble PsbS, this detergent was used in the temperature variance experiments. As shown in Fig 2A.5 and Table 2.2, reactions carried out at 30 °C and 25 °C gave higher yields of PsbS than reactions at 37 °C. This suggests that lower temperatures are better suited, possibly due to a slower rate of protein translation. Because part of the produced PsbS precipitated at 25 °C, for further experiments 30 °C was selected as the optimal temperature for cell-free PsbS production in soluble form.

Table 2.2 Temperature-dependent cell-free expression of PsbS. PsbS yields as soluble or pellet fractions were classified into four groups: -, no detectable expression; □, spurious expression < 50 ng/µl; +, 51–200 ng/µl; ++, > 200 ng/µl.

Temp	Soluble	Pellet
37 °C	□	-
30 °C	+(+)	□
25 °C	+	+

2.3.4 Batch feeding

During the cell-free transcription and translation reactions, conditions change because of the consumption of substrates and accumulation of products and by-products, which inhibit the reaction itself[10]. To upscale the PsbS production, the batch feeding method was tested. In this procedure, instead of adding 25 µl of feeding mixture after 30 minutes, 12.5 µl feeding mixture was added up to 10 times every 30 minutes after the reaction was started. The reaction was prolonged up to 8 hours and ~23 µg of PsbS was produced (Figure 2.2).

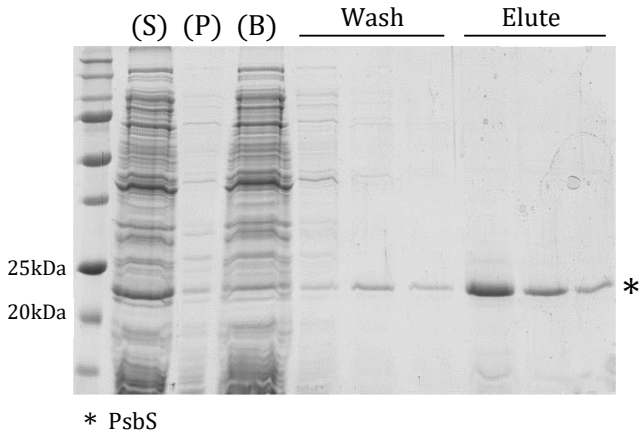

Figure 2.2 PsbS (*) was expressed at 30 °C in the presence of 1 % Brij-78 using the batch feeding method; P, pellet and S, supernatant of the reaction mixture before loading with Ni-NTA beads. B is the supernatant that was removed after incubation with Ni-NTA beads. Comparison of S and B shows that most of the soluble PsbS bind to the beads. The beads were washed with buffer containing 20 mM imidazole and PsbS was eluted with buffer containing 250 mM of imidazole.

Although the total amount of protein was increased by batch feeding, a substantial amount of feeding mixture was added to the reaction. Besides that, after 3 hours reaction time, white flakes were formed, suggesting that a part of PsbS was precipitated. The PsbS produced by cell-free batch feeding reactions in the presence of Brij-78 was purified for analysis (Figure 2.2). In addition, PsbS produced in lipid nanodiscs were also purified (Fig 2A.6).

2.3.5 Continuous exchange

In order to avoid precipitation during batch feeding and to improve the yield of cell-free production, the use of continuous-exchange reactions were explored, where dialysis is used to dilute the inhibitory products that are formed during the reaction

when fresh amino acids and co-factors are added. The continuous-exchange reaction was carried out using 1 % Brij-78 at 30 °C for 9 hours with the addition of 12.5 µl feeding mixture at three-time intervals. Using this set-up, the yield of PsbS was not significantly higher than with the batch-feeding method. However, the PsbS produced with continuous-exchange was in a soluble state and no white aggregates were observed. The results are shown in Fig 2A.7. The yield of PsbS in this reaction was estimated to be ~500 ng/µl and could be further improved by increasing the reaction time.

2.3.6 CD spectroscopy of refolded cell-free produced PsbS

To check the fold of the cell-free produced soluble PsbS, CD spectroscopy was carried out by pooling the eluted fractions of PsbS shown in Figure 2.2. The initial CD spectrum of the cell-free produced PsbS in Brij-78 suggests that the soluble PsbS is in a partly folded molten-globule state and does not show the characteristics of α-helix structure (Fig 2A.8). To overcome this issue, PsbS was first unfolded by removal of Brij-78 in the presence of 0.1 % LDS followed by refolding in the presence of 0.12 % β-DM using the standard refolding protocol[3,4]. In addition, PsbS pellets produced from the cell-free reaction carried out in the absence of detergent (Figure 2.1) were refolded using the standard protocol. The CD spectra of cell-free produced, refolded PsbS is shown in Figure 2.3. According to the CD spectral analysis, the refolded PsbS has ~50 % helical structure (Table 2.3). This number agrees with the crystal structure of *S. oleracea* PsbS that shows that PsbS is ~48 % α-helical, with the remaining part random coil and a small contribution of β-sheet[23] and is consistent with CD analyses of detergent-refolded PsbS produced from *E. coli* (Chapter 3)[4]. Comparing the CD spectrum of cell-free produced PsbS in β-DM to the CD spectrum of *E. coli* produced PsbS in β-DM, different amplitudes for the characteristic bands at 210 nm and 222 nm are observed. It was demonstrated that the PsbS CD signature varies for different detergent types, while the estimated helical content is similar[4]. The variations in the CD spectra were attributed to differences in the stromal loop and tail structures of which the folds may depend on the detergent micro-environment. The CD spectra of *E. coli* and cell-free produced PsbS that are compared in Figure 2.3, are both taken from samples where PsbS is solubilized in β-DM. The observed differences could originate from the presence of lipids from the *E. coli* host system in the *E. coli* produced PsbS. Supporting this view are NMR spectra showing the presence of protein-associated lipids that are purified along with the protein (data not shown). A possible explanation can be that lipids mediate the refolding of PsbS and influence the conformations of the non-helical contents. The influence of lipids on the refolding of membrane proteins is an interesting and important aspect, which is not easily controlled in recombinant expression systems using host cells, but which could be

further explored in cell-free synthesis, where selective lipids can be added to the synthesis reaction or during the subsequent refolding steps.

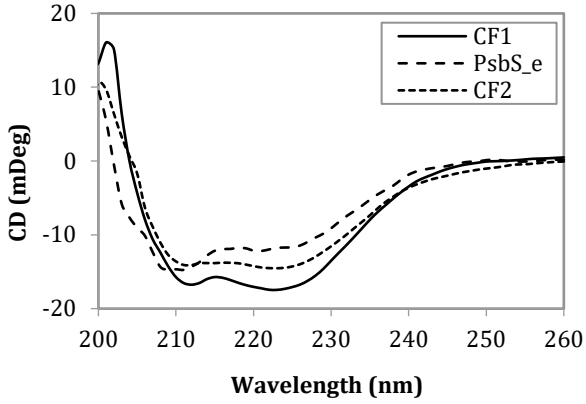

Figure 2.3 CD spectra of cell-free produced PsbS in comparison with *E. coli* produced PsbS refolded in 0.12 % β-DM. CF1 is PsbS cell-free produced with Brij-78, purified, unfolded and *in vitro* refolded in β-DM. CF2 was cell-free produced without detergent as a pellet, purified and refolded in β-DM, PsbS_e was produced from *E. coli*, purified as inclusion bodies and refolded in β-DM (Chapter 3).

Table 2.3 Estimation of secondary structures using BeStSel (Beta Structure Selection[24])

Secondary structures (%)	**PsbS_e**	**CF1**	**CF2**
Helix	51.4	54.9	50.4
Antiparallel	30.5	7.7	0.9
Parallel	0	10.9	27.1
Turn	2.3	14.8	3.8
Others	15.8	11.8	17.9

2.4 Conclusion

In this chapter using cell-free synthesis, PsbS can be produced either as an aggregated pellet or in a soluble state in the presence of membrane-mimicking additives, in contrast to the *E. coli* overexpression, where PsbS is always overexpressed as inclusion bodies. The cell-free produced PsbS protein could successfully be refolded into detergent micelles, showing ~50 % helical content. The protocols were optimized to yield ~500 ng/µl PsbS production in a single reaction, which could be upscaled for structural studies to produce milligram amounts of PsbS.

2.5 References

1. Li, X. P. *et al.* A pigment-binding protein essential for regulation of photosynthetic light harvesting. *Nature* **403,** 391–395; 10.1038/35000131 (2000).
2. Li, X. P. *et al.* Regulation of photosynthetic light harvesting involves intrathylakoid lumen pH sensing by the PsbS protein. *Journal of Biological Chemistry* **279,** 22866–22874; 10.1074/jbc.M402461200 (2004).
3. Wilk, L., Grunwald, M., Liao, P.-N., Walla, P. J. & Kühlbrandt, W. Direct interaction of the major light-harvesting complex II and PsbS in nonphotochemical quenching. *Proceedings of the National Academy of Sciences of the United States of America* **110,** 5452–5456; 10.1073/pnas.1205561110 (2013).
4. Krishnan, M., Moolenaar, G. F., Gupta, Karthick Babu Sai Sankar, Goosen, N. & Pandit, A. Large-scale in vitro production, refolding and dimerization of PsbS in different microenvironments. *Scientific Reports* **7,** 1–11; 10.1038/s41598-017-15068-3 (2017).
5. Junge, F. *et al.* Advances in cell-free protein synthesis for the functional and structural analysis of membrane proteins. *New biotechnology* **28,** 262–271; 10.1016/j.nbt.2010.07.002 (2011).
6. Fenz, S. F., Sachse, R., Schmidt, T. & Kubick, S. Cell-free synthesis of membrane proteins: tailored cell models out of microsomes. *Biochimica et biophysica acta* **1838,** 1382–1388; 10.1016/j.bbamem.2013.12.009 (2014).
7. Hein, C., Henrich, E., Orbán, E., Dötsch, V. & Bernhard, F. Hydrophobic supplements in cell-free systems: Designing artificial environments for membrane proteins. *Eng. Life Sci.* **14,** 365–379; 10.1002/elsc.201300050 (2014).
8. Sachse, R., Dondapati, S. K., Fenz, S. F., Schmidt, T. & Kubick, S. Membrane protein synthesis in cell-free systems: from bio-mimetic systems to bio-membranes. *FEBS Letters* **588,** 2774–2781; 10.1016/j.febslet.2014.06.007 (2014).
9. Smith, M. T., Wilding, K. M., Hunt, J. M., Bennett, A. M. & Bundy, B. C. The emerging age of cell-free synthetic biology. *FEBS Letters* **588,** 2755–2761; 10.1016/j.febslet.2014.05.062 (2014).
10. Shimizu, Y. *et al.* Cell-free translation reconstituted with purified components. *Nature Biotechnology* **19,** 751–755; 10.1038/90802 (2001).
11. Reckel, S. *et al.* Transmembrane segment enhanced labeling as a tool for the backbone assignment of alpha-helical membrane proteins. *Proceedings of the National Academy of Sciences of the United States of America* **105,** 8262–8267; 10.1073/pnas.0710843105 (2008).
12. Ozawa, K., Dixon, N. E. & Otting, G. Cell-free synthesis of 15N-labeled proteins for NMR studies. *IUBMB Life* **57,** 615–622; 10.1080/15216540500217859 (2005).
13. Koglin, A. *et al.* Combination of cell-free expression and NMR spectroscopy as a new approach for structural investigation of membrane proteins. *Magnetic Resonance in Chemistry* **44,** 17–23; 10.1002/mrc.1833 (2006).
14. Trbovic, N. *et al.* Efficient strategy for the rapid backbone assignment of membrane proteins. *Journal of the American Chemical Society* **127,** 13504–13505; 10.1021/ja0540270 (2005).

15. Ishihara, G. *et al.* Expression of G protein coupled receptors in a cell-free translational system using detergents and thioredoxin-fusion vectors. *Protein Expression and Purification* **41,** 27–37; 10.1016/j.pep.2005.01.013 (2005).

16. Schwarz, D., Dötsch, V. & Bernhard, F. Production of membrane proteins using cell-free expression systems. *Proteomics* **8,** 3933–3946; 10.1002/pmic.200800171 (2008).

17. Katzen, F., Peterson, T. C. & Kudlicki, W. Membrane protein expression: no cells required. *Trends in Biotechnology* **27,** 455–460; 10.1016/j.tibtech.2009.05.005 (2009).

18. Liguori, L., Marques, B., Villegas-Méndez, A., Rothe, R. & Lenormand, J. L. Production of membrane proteins using cell-free expression systems. *Expert Review of Proteomics* **4,** 79–90; 10.1586/14789450.4.1.79 (2007).

19. Crisafi, E. & Pandit, A. Disentangling protein and lipid interactions that control a molecular switch in photosynthetic light harvesting. *Biochimica et Biophysica Acta - Biomembranes* **1859,** 40–47; 10.1016/j.bbamem.2016.10.010 (2017).

20. De Grip, W. J. Thermal stability of rhodopsin and opsin in some novel detergents. *Methods in Enzymology 81* (Elsevier1982), pp. 256–265 (1982).

21. Külheim, C., Agren, J. & Jansson, S. Rapid regulation of light harvesting and plant fitness in the field. *Science (New York, N.Y.)* **297,** 91–93; 10.1126/science.1072359 (2002).

22. Klammt, C. *et al.* Evaluation of detergents for the soluble expression of alpha -helical and beta-barrel-type integral membrane proteins by a preparative scale individual cell-free expression system **272,** 6024–6038; 10.1111/j.1742-4658.2005.05002.x (2005).

23. Fan, M. *et al.* Crystal structures of the PsbS protein essential for photoprotection in plants. *Nature structural and molecular biology* **22,** 729–735; 10.1038/nsmb.3068 (2015).

24. Micsonai, A. *et al.* Accurate secondary structure prediction and fold recognition for circular dichroism spectroscopy. *Proceedings of the National Academy of Sciences of the United States of America* **112**; 10.1073/pnas.1500851112 (2015).

2.6 Appendix 2A

Fig 2A.1
SDS-PAGE analysis demonstrating the successful production of cell-free expressed PsbS (*, 22kDa). The pellet of 2.5 µl reaction mixture was compared with a concentration range of BSA protein on a 12.5 % SDS- polyacrylamide gel. The PsbS yield was ~200 ng/µl. Total protein yield is 10 µg from 50 µl.

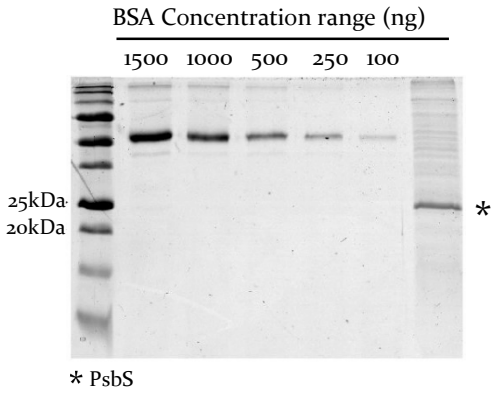

Fig 2A.2
Cell-free expression of PsbS in the presence of different concentrations of β-DM or Brij-35 at 37 °C for 4 hours (PsbS, control without detergent; Negative, control without PsbS plasmid). The reaction mixture was separated in (a) pellet and (b) soluble fractions by centrifugation for 10 minutes at 14,000 x g and loaded on gel.

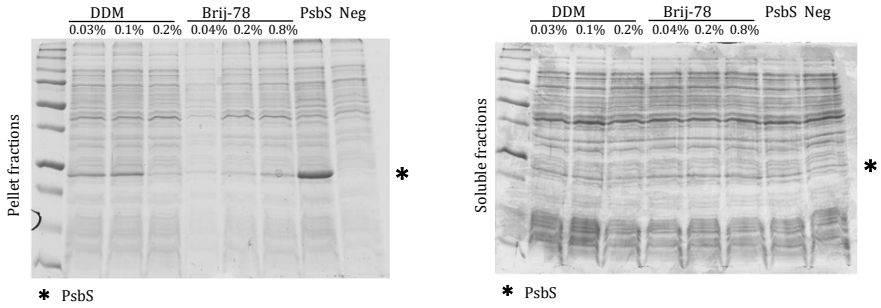

Fig 2A.3
Cell-free expression of PsbS in the presence of lipid nanodiscs that were prepared from asolectin lipids and MSP1E3D1 scaffold proteins (MSP; 2.4 nmol and 120 nmol asolectin per cell-free reaction) or in the presence of Brij-78 (B78, 1 %). The reaction was carried out at 37 °C for 4 hours. Total fraction (T) was separated in (P) pellet and (S) soluble fractions by centrifugation (PsbS: control without detergent; MSP: Nanodiscs with PsbS; B78: control with detergent).

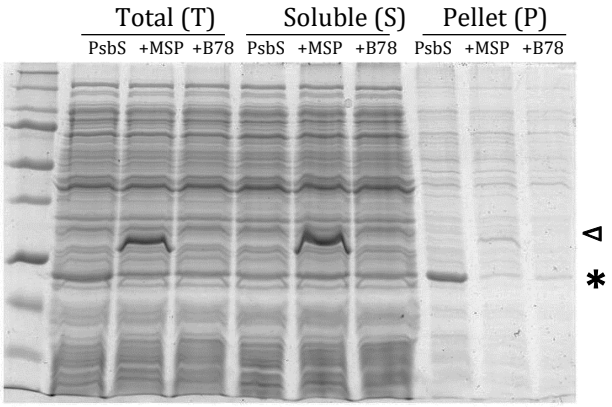

* PsbS ◁ MSP nanodiscs

Fig 2A.4
Cell-free expression of PsbS in the presence of asolectin liposomes (1200 nmol asolectin per cell-free reaction). The reaction was carried out at 37 °C for 4 hours. Total fraction (T) was separated in (P) pellet and (S) soluble fractions by centrifugation. PsbS: control reaction without liposomes, PsbS + Buffer: control reaction with the addition of HEPES buffer that was used for the liposomes, PsbS + Liposomes: reaction in the presence of liposomes.

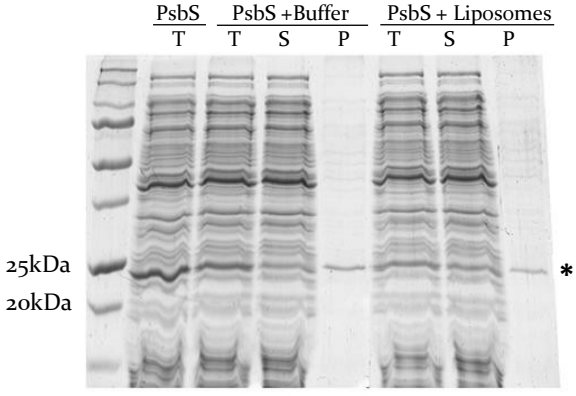

* PsbS

Fig 2A.5
Cell-free expression of PsbS (*) in the presence of 1 % Brij-78 comparing the yield efficiencies at 30 °C (a) and at 25 °C (b). T, total reaction; P, pellet; S, supernatant containing the soluble protein content, Neg, control without PsbS plasmid.

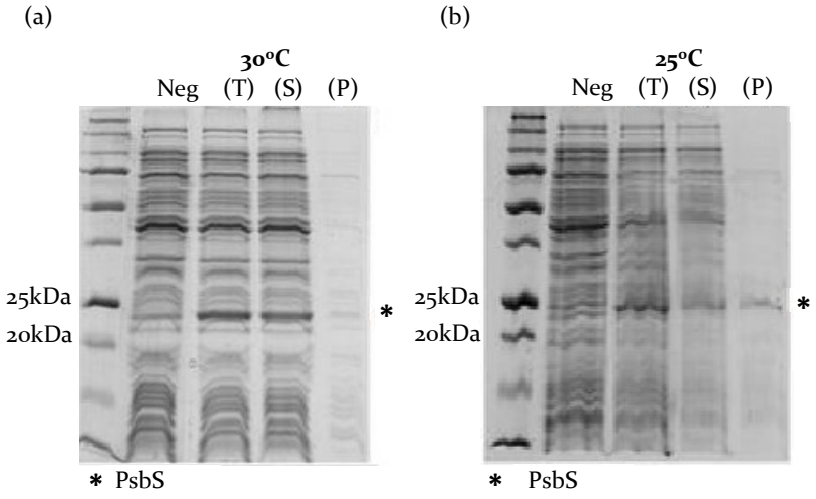

Fig 2A.6
Purification of soluble PsbS (*) expressed at 30 °C in the presence of lipid nanodiscs (arrow: MSP1E3D1 scaffold protein). S, supernatant of the reaction mix containing soluble PsbS before loading with Ni-NTA beads. For purification of PsbS after loading with Ni-NTA beads, the beads were washed with buffer containing 20 mM imidazole and PsbS was eluted with buffer containing 250 mM of imidazole.

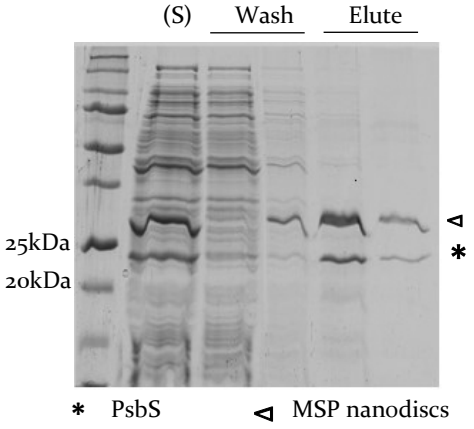

Fig 2A.7
Continuous-exchange reaction. PsbS (*) was expressed at 30 °C in the presence of 1 % Brij-78 and the reaction was incubated for 9 hours. Neg, control without PsbS plasmid; T, total reaction mix; P, pellet; S, supernatant containing the soluble protein content. Total yield was estimated as ~500 ng/µl. The continuous-exchange reaction was carried out in a 2 mL test tube holding a 10 kDa cut-off dialysis device containing a 1:15 ratio of reaction mixture: feeding mixture (50 µl internal volume of the reaction mixture, 750 µl external volume). Total protein yield is 25 µg from 50 µl.

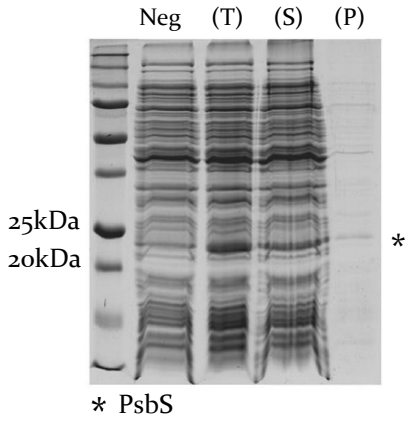

Fig 2A.8
The CD spectrum of purified PsbS that was produced via cell-free expression in the presence of 1 % Brij-78.

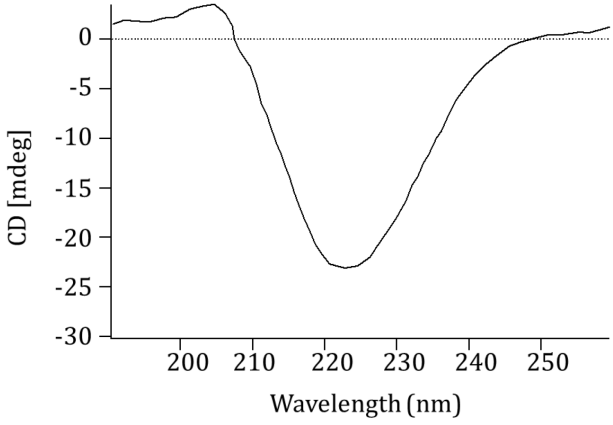

3

Production, purification and refolding of PsbS

This chapter outlines the optimization of overproduction of PsbS in *E. coli* cells, enabling a protocol for PsbS production in milligram quantities. The overproduction of PsbS was improved by optimizing the choice of the expression vector and strain. To decrease the loss of PsbS during the purification protocol, a new method of purification has been developed. This method results in minimal loss of membrane protein PsbS and complete solubilization of the inclusion body pellet containing PsbS using urea and LDS detergents. Furthermore, refolding of PsbS using various detergents was performed to find the optimal condition for its structural characterization. PsbS from *P. patens*, *A. thaliana* and *S. oleracea* were refolded and characterized. The optimal detergents for refolding Patens-PsbS are OG and FC-12, showing ~50 % helical structure, in agreement with the Spinach-PsbS PDB 4RI2. FC-12 is zwitterionic, which favours PsbS to remain soluble. In addition, FC-12 also forms detergent micelles of small size which make it a good candidate for solution-state NMR experiments.

This chapter is based on a part of
Maithili Krishnan, Geri Moolenaar, Karthick Sai Sankar Gupta, Nora Goosen, and Anjali Pandit "Large-scale *in vitro* production, refolding and dimerization of PsbS in different microenvironments." *Scientific Reports*, **2017**, DOI:10.1038/s41598-017-15068-3

3.1 Introduction

Membrane proteins account for 20 - 30 % of all proteins in prokaryotes and eukaryotes[1]. One of the important roles of membrane proteins is their key role in diseases and almost 70 % of all drug targets are membrane proteins[2,3]. There are very few membrane protein structures solved to date since working with membrane proteins is challenging[4,5]. In particular, the yield of membrane proteins is often low after isolation for *in vitro* functional and structural studies[3]. For overexpression of membrane proteins generally *E. coli* bacteria are used. Since membrane proteins contain large hydrophobic surfaces, they are produced either in the cytoplasmic membrane or as inclusion bodies in the cytoplasm. For reasons unknown, the formation of inclusion bodies can be very toxic to the bacterial system and leads to reduced yield of membrane proteins. The overexpression of membrane proteins affects the membrane integrity and cell viability leading to reduced growth and faulty cell division[4]. Refolding of functional membrane proteins is challenging and often refolding procedures are unsuccessful[6]. Additionally, very little knowledge about stability, quality, folding and degradation of membrane proteins and how this might affect the overexpression yields are available. Therefore, attempts to optimize overexpression of membrane proteins are most often based on "trial and error"[4].

Using the *E. coli* system for overexpression for production of membrane protein such as PsbS is beneficial because of its fast growth kinetics, high cell densities and easy DNA tranformations[7]. Factors affecting the success of overexpression are the nature of the host, the promoter employed, the growth conditions, the origin and type of the protein overexpressed[8]. When expressions levels are high and the recombinant protein is not soluble, inclusion bodies are formed. Due to the lack of right membrane composition of the bacteria or absence of detergents or lipids during overexpression, most membrane proteins aggregate into inclusion bodies. They are densely packed denatured proteins found in both cytoplasmic and periplasmic spaces of *E. coli* in the form of cellular units[9]. When the genes that are being overexpressed are further away in evolutionary distances from their host species, inclusion bodies are commonly formed but they are favorable for effective purification. Inclusion bodies have advantages of easy isolation, high concentration and minimal degradation of the protein along with resistance to proteolytic attack and homogeneity of the protein inside the inclusion bodies. However having these advantages, the challenge in the recovery of protein from inclusion bodies lies in proper solubilization of the aggregated protein and in proper refolding of protein into its active form[9].

In Chapter 2, the cell-free synthesis of the membrane protein PsbS was demonstrated. Although the yields are satisfactory, the protocol needs up-scaling and further

optimization. The cell-free expression also yields insoluble PsbS or soluble PsbS that is not properly folded. Therefore, in this chapter, overproduction of PsbS in *E. coli* and subsequent refolding of PsbS in detergent micelles have been optimized.

To best solve the structures of membrane proteins techniques like X-ray crystallography, IR or NMR spectroscopy have to be used. These techniques require high yields and isotope labeling of the membrane proteins, especially for NMR spectroscopy. The incorporation of ^{15}N and ^{13}C isotopes into the protein for NMR studies is possible by growing the *E. coli* cells in minimal media with ^{15}N ammonium salts or ^{13}C glucose[10,11]. Membrane proteins like LHCII have been successfully overexpressed and purified from the *E. coli* system[8,12,13]. Although successful attempts to produce recombinant PsbS using *E. coli* exist[14–17], the yields are significantly too low to perform NMR or IR spectroscopy.

For refolding PsbS using detergents, there are two important parameters, CMC and aggregation number of the detergent, that have to be considered[18]. Detergents lose their micellar round shape when the concentration is lower than the CMC limit. The aggregation number is the number of monomers needed to form a micelle. Using estimated aggregation numbers and the molecular weight of the detergent molecule, the micellar molecular weight can be estimated[19]. CMC and aggregation number depend on environmental conditions like pH, temperature, ionic strength and more. The physical-chemical properties of detergents that affect the structure of membrane proteins have to be evaluated[20]. By comparing the size and shape of the micelles they form, optimal detergents can be selected. Some zwitterionic detergents like FC-12 micelles have been successfully used in NMR studies[21]. FC-12 forms small sized micelles that are beneficial for solution-state NMR experiments. Proteins in OG or β-DM detergents have been crystallized upon detergent removal to carry out X-ray diffraction[22]. PsbS was refolded using OG and was confirmed for its proper refolding by CD spectroscopy[14]. The X-ray crystal structure of Spinach-PsbS was determined from crystals formed after detergent removal from PsbS in detergent NG[23]. In this chapter, six detergents have been selected for refolding PsbS, shown in Figure 3.1. The refolded PsbS structures were analyzed by CD spectroscopy.

Since there is no functionality assay for isolated PsbS, a careful CD analysis of the refolded PsbS was performed. In Table 3.1, six detergents and their different characteristics that help to mimic the membrane micro-environmental conditions are listed[24].

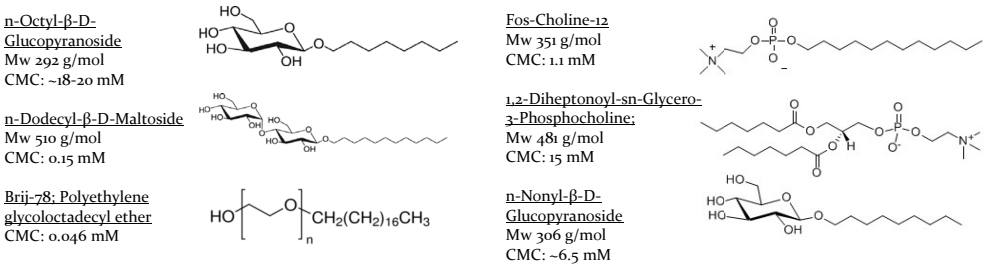

Figure 3.1 Chemical structures, CMC, aggregation numbers and charges of various detergents that were selected for refolding PsbS are shown.

Table 3.1 Different detergents with their aggregation number, CMC, MW and charges

Detergents	Aggregation no	CMC	MW	Charges
OG	27-100	18-20 mM	292 g/mol	N
β-DM	98	0.15 mM	510 g/mol	N
Brij-78	133	0.046 mM	-	N
FC-12	54	1.1 mM	351 g/mol	Z
DHPC	70-80	15 mM	481 g/mol	Z
NG	130	6.5 mM	306 g/mol	N

In this chapter an optimized procedure to produce and purify recombinant PsbS in milligram quantities has been established. The overproduction of PsbS is improved by optimizing the choice of the expression vector, strain optimization and by modification of the purification protocol. Cloning of the PsbS gene from three species *P. patens*, *A. thaliana*, and *S. oleracea* was done in order to set up a PsbS library. For carrying out biochemical experiments, screening for the best detergent condition for the refolding of PsbS was performed. After a successful optimization of recombinant PsbS, isotope-labelled ^{15}N *P. patens* PsbS at neutral and low pH were prepared to perform NMR spectroscopy, as documented in Chapter 4.

3.2 Materials and Methods

3.2.1 Cloning of recombinant PsbS

The *P. patens* PsbS mature coding gene was obtained from the Morosinotto Lab. (University of Padova) and the gene for PsbS from *A. thaliana* was obtained from the Croce Lab. (VU Amsterdam). The PsbS gene for *S. oleracea* was ordered from Baseclear®. To clone the PsbS gene into the pEXP5-NT expression vector (Invitrogen) two primers for each species and two for the vector were synthesized. The gene and the pEXP5-NT vector were amplified by standard polymerase chain reactions (PCR)

using the CloneAmp HiFi polymerase. The gene was inserted into the vector via the Gibson Assembly method (In-Fusion HD Cloning Kit, Clontech Laboratories, Inc). Colony PCR and commercial sequencing were used to check successful cloning. Plasmid map of pExp5-PsbS gene is shown in Fig 3A.6. Primers used for each species are shown in the Table 3.2.

Table 3.2 Primers used for cloning PsbS into pExp-NT vector

Primer	Sequence
Vector pExp5 forward	5'- AGGGTGATCCGGCTGCTAAC – 3'
Vector pExp5 reverse	5'- AAGGGACTGAAAATACAGGTTTTCGCC – 3'
Patents-PsbS forward	5'-AGCGGCGAAAACCTGTATTTTCAGTC CCTTGGCAAAACTAAACCCGCCGC – 3'
Patents-PsbS reverse	5'-TTCGGGCTTTGTTAGCAGCCGGATCACCC TTCAGTCCTCGATGTCGTCGTCGTTGAC – 3'
Arabidopsis-PsbS forward	5' - CCTGTATTTTCAGTCCCTTCTCTTCA AACCCAAAACCAAAGCTG - 3'
Arabidopsis-PsbS reverse	5' - CAGCCGGATCACCCTCTCGAGGCTT TCTTCACCATCATCGG - 3'
Spinach-PsbS forward	5' - AGCGGCGAAAACCTGTATTTTCAG TCCCTTCTCTTTAAGTCCAAAGCCAA - 3'
Spinach-PsbS reverse	5' - TTCGGGCTTTGTTAGCAGCCGGAT CACCCTCTAATCTTCTTCTTCATCAT - 3'

3.2.2 Optimization of overexpression

Overexpression of PsbS was carried out by inducing *E. coli* strain BL21(DE3) pLysS grown on LB media containing 75 µg/mL ampicillin and 25 µg/mL chloramphenicol by addition of 0.05 mM of IPTG at a cell density of 0.3 - 0.4. After 12 - 14 hours at 18 °C, the cells were harvested.

Plasmid optimization was done by using a pExp5 vector over a pETite vector. The optimal temperature for overexpression of PsbS was found to be 18 °C. BL21 and BL21-pLyS strains were compared for the highest yield of PsbS. Different concentrations of IPTG, 1 mM, 0.5 mM and 0.05 mM, were tested to induce the overexpression (Fig 3A.1) which showed no significant differences. 0.05 mM ITPG was used for further experiments.

3.2.3 Isotope labeling of NMR samples

For NMR HSQC experiments, bacteria were grown in M9 minimal media containing $^{15}NH_4Cl$. In appendix Fig 3A.2, the comparison between LB media and M9 overexpression is shown. The cell pellets were stored at –80 °C until further use.

3.2.4 Protein purification protocols

The purification of inclusion bodies was performed using a detergent buffer and Triton buffer [12]. Several washes of Triton buffer resulted in a white pellet, which was abundant in unfolded PsbS. Two different methods were compared for purification of PsbS from the pellet: nickel affinity column and urea wash. For His-Tag purification, a nickel-affinity column protocol was followed to isolate denatured protein (Qiagen). At the end of this step, purified unfolded PsbS was obtained. The latter method used a novel protocol that was designed to optimize the yield of purified PsbS. UP buffer was used here to prevent the loss of protein during nickel affinity column purification. The inclusion body pellet was dissolved in urea buffer and incubated at 25 °C, 900 rpm shaking for 30 minutes. The sample was centrifuged at 20,000 x g at room temperature for 10 minutes. This step produced a pellet containing PsbS and a soluble fraction containing impurities.

The urea wash and centrifugation steps were repeated twice. Washing was done with UP buffer and 0.05 % LDS, which further removed impurities. Next, the remaining PsbS pellet was dissolved in urea buffer by adding 0.5 % of LDS which helped dissolve PsbS. Immediate buffer exchange (PD-10 Desalting gravity column, GE Healthcare) to 50 mM Hepes, 0.1 % LDS, pH 5.0 was performed to remove the high concentration of urea and to adjust the pH. The recombinant PsbS in 50 mM Hepes, 0.1 % LDS, pH 5.0 was stored at 4 °C until further use.

3.2.5 Refolding of recombinant PsbS

Refolding of the LDS-solubilized PsbS was performed adopting the protocol from[14], using various detergents purchased from Anatrace for refolding: OG, β-DM, Brij-78, FC-12, DHPC and NG. The refolding buffer contained 0.1 M HEPES (adjusted to pH 5.0 or pH 7.5 with NaOH), 4 % (w/v) LDS, and 25 % (w/v) sucrose. Unfolded PsbS (~1 mg/mL) was mixed with an equal volume of refolding buffer and heated to 100 °C for 1 min. The desired detergent was added to the mixture and 200 mM KCl was used to precipitate LDS. CMC ($N_{det,CMC}$), aggregation number ($N_{det,\ Agg}$)[21] of each detergent type and volume of the sample were taken into account while calculating the amount of detergent ($N_{det,tot}$) to add (Equation 3.1).

$$N_{det,tot} = N_{det,CMC} + N_{det,Agg}[PsbS] \quad (3.1)$$

As a final step, buffer exchange to 100 mM sodium phosphate for pH 7.5 or to 100 mM sodium acetate for pH 5.0 was carried out (PD-10 Desalting gravity column, GE Healthcare), to remove the excess sucrose. For NMR experiments, samples were concentrated using Amicon Ultra-4 centrifugal filters containing 10 kDa filter membranes.

3.2.6 Gel electrophoresis

SDS-page gel electrophoresis analysis (12.5 % running gel, 4 % stacking gel stained with Coomassie brilliant blue R-250 Bio-Rad) was carried out for checking the yield of PsbS at every step of overexpression, purification and refolding. 2.5 µL of Precision Plus Protein™ Dual Color Standard from Sigma was used in all the SDS-page gels.

3.2.7 CD spectroscopy

The secondary folds of the refolded PsbS were analyzed by Jasco J-815 spectropolarimeter (Jasco Labortechnic, Japan) using a step size of 1 sec/nm, the bandwidth of 1 nm and a scanning speed of 100 nm/min. CD spectra were analyzed using BeStSel (Beta Structure Selection[25]) for estimating the content of α-helical, β-sheet and coil or other conformations for each CD spectrum.

3.3 Results and Discussion

3.3.1 Cloning and overexpression of PsbS

After successful cloning of PsbS gene into an efficient vector pExp5, overexpression of the PsbS was optimized. In Figure 3.2a, IPTG (+) shows the overexpression of PsbS using the vector pETite. About 9 mg of PsbS was expressed from 200 mL of culture solution (*i.e.* ~45 mg PsbS/L). With the new vector system pExp5, PsbS overexpression was increased considerably (Figure 3.2b, IPTG (+)). The PsbS expression yield was estimated by comparing the intensities of the PsbS bands to the intensity of a known concentration of BSA protein. About 25 mg PsbS from 200 mL of cell culture (*i.e.* ~125 mg PsbS/L) was obtained, giving almost a three-fold increase in production compared to expression using the pETite vector.

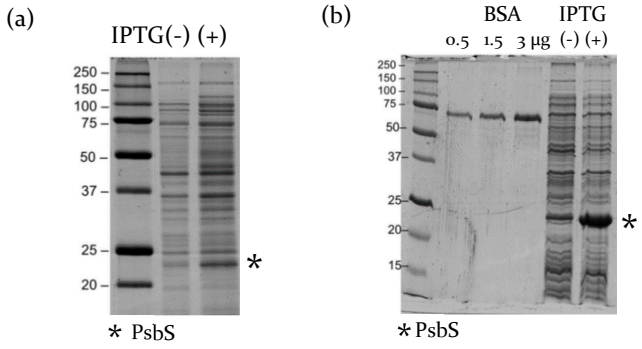

Figure 3.2 Overproduction of PsbS. (a) PsbS overexpression using the pETite vector (yield: ~9 mg from 200 mL cells); (b) PsbS overexpression using the pExp5 vector (yield: ~25 mg from 200 mL cells).

3.3.2 Optimization of PsbS purification

To further improve the production of PsbS, the loss of protein PsbS during its purification steps must be reduced. The basic purification of inclusion bodies containing PsbS from the cell pellets is shown in appendix Fig 3A.3, using a detergent buffer and Triton buffer wash. The final inclusion bodies pellet (P4) contained about 19 mg of PsbS, which was used as a starting material for PsbS purification. Figure 3.3 (a and b) demonstrate that with standard nickel-affinity column purification using the N-terminal His-tag, significant loss of protein occurs. In Figure 3.3a, the inclusion bodies pellet was first dissolved in 8 M urea in phosphate buffer pH 8.0 (UP-buffer) containing 0.5 % LDS and centrifuged to give pellet (p1) and supernatant (s1). Fraction s1 was loaded on the nickel-affinity column. During the column purification process, ~14 mg of PsbS was discarded in flow through from the 19 mg starting material. The overall efficiency of the column method was estimated to be ~19 %, with about 80 % of the protein lost in the flow through or in other eluted fractions.

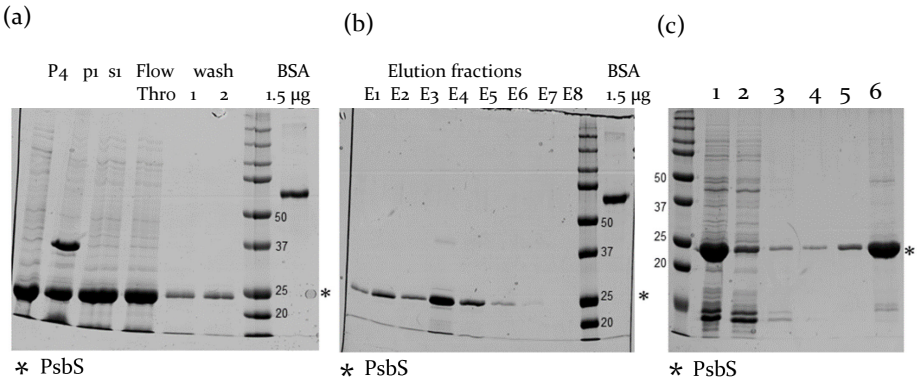

Figure 3.3 Purification of PsbS from inclusion bodies using nickel-affinity column or the urea-wash protocol. (a) Inclusion bodies pellet P4 (lane 1) containing 19 mg of PsbS was solubilized in urea buffer containing 0.5 % LDS. Pellet (lane 2, p1) and supernatant (lane 3, s1) were obtained after centrifuging at 10000 x g for 10 minutes. The supernatant was loaded on the nickel affinity column. The loss fractions of PsbS are shown as the flow through (lane 4) and wash (lane 5,6), and together give a loss of ~14 mg PsbS; (b) Nickel-affinity column purified elution fractions of PsbS (1 µl loaded on the gel). Elution fraction E3 (0.7 µg/µl), fraction E4 (1 µg/µl) and fraction E5 (0.7 µg/µl) were further used to refold PsbS (lane 3, 4, 5). In total, the collected fractions (1.5 ml) contained ~3.6 mg of PsbS out of 19 mg starting material. (c) UP-wash protocol; Lane 1: About 3.2 mg of PsbS from the inclusion bodies pellet was dissolved in buffer containing 8 M urea. Several washes of UP buffer were carried out (Lane 2, 3, 4). Lane 5 is the washing step of the pellet with UP buffer with 0.05 % LDS. The last wash step was carried out using UP buffer with 0.5 % of LDS to dissolve all the PsbS from inclusion bodies (Lane 6). The concentration of PsbS in the 0.5 % LDS buffer was ~2 µg/µL (2.5 µL sample loaded on the gel). In total ~2 mg of PsbS was present after urea-wash purification from 3.2 mg starting material.

To reduce the loss of protein during the purification steps, a new purification protocol that circumvents the use of nickel-affinity column purification was implemented. This new method to purify PsbS was based on the poor solubility of PsbS in UP-buffer either without LDS or in the presence of 0.05 % LDS. After two times washing the pellet with UP-buffer without LDS, the washing was continued several times with UP-buffer containing 0.05 % LDS to remove contaminating proteins. Finally, the purified PsbS pellet was dissolved in UP-buffer containing 0.5 % LDS (Figure 3.3c). The starting material for purification contained about 3.2 mg of protein (lane 1). Several washes with UP buffer showed the removal of background proteins (lane 2, 3, 4, 5). The final amount of purified PsbS was about 2 mg (lane 6), by which the efficiency of this method was 60 %, compared to 19 % using the nickel-affinity column.

Summarizing, the combination of using pExp5 expression vectors and the UP-buffer wash method for purification gave an almost three-fold increase in overproduction and another three-fold increase of purification yield, by which these modifications resulted in about 9-fold increase of PsbS production. A possible reason for the loss of PsbS during nickel-affinity column purification could be that proteins are unfolded in the presence of urea leading to poor binding to the column. Moreover, the presence of 2 % LDS in the nickel column can interfere with the affinity for PsbS, making the nickel-column protocol quite tedious for large-scale purification. The UP-wash method, on the other hand, can be easily applied for obtaining large quantities of PsbS, circumvents the use of column purification and does not require engineering of a His-tag. To test the applicability of the new purification method for other LHC proteins, the UP-wash protocol was applied to purify the Lhcb1 protein of *A. thaliana,* a protein homolog to PsbS and one of the polypeptides forming trimeric LHCII (appendix Fig 3A.4). The UP-wash method applied to Lhcb1 gave yields that were comparable to PsbS for purification of the protein from inclusion bodies, confirming that the method is extendable to other proteins of the LHC family.

3.3.3 Refolding of Patens-PsbS

The second step for successful sample preparation was to choose an optimal detergent for refolding of PsbS. Refolding of recombinant PsbS in detergent micelles has been shown successfully using OG or β-DM, and the crystal structure of Spinach-PsbS was obtained from PsbS purified in NG buffer[23]. In addition to these glucoside-based detergents, refolding was tested in the phosphocholine detergents FC-12 and DHPC, which have been used successfully as membrane mimics for solution NMR, owing to their short chains and small micelle sizes. Further, refolding in Brij-78 was tested, which is an oxyethylene-polymer based detergent that has suitable properties for *in vitro* expression and refolding using cell-free expression systems (Chapter 2).

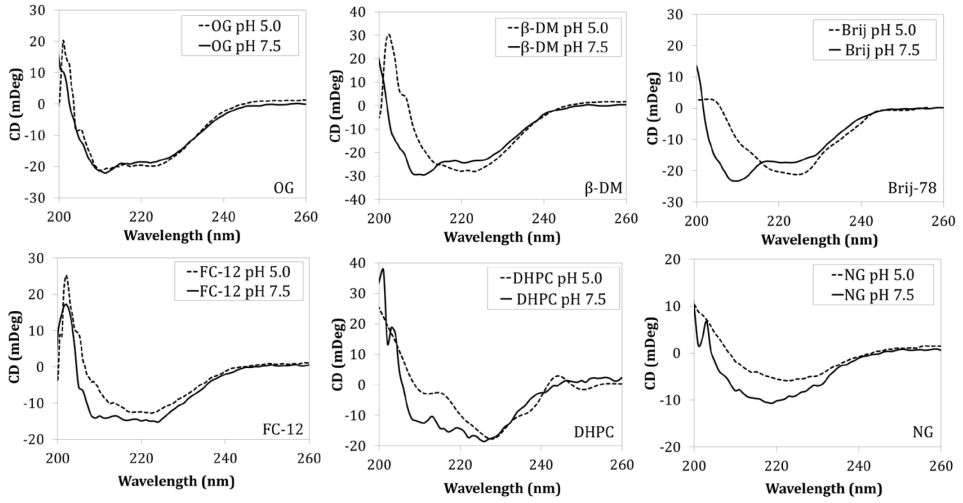

Figure 3.4 Circular dichroism spectra of Patens-PsbS refolded in various detergent buffers at pH 7.5 (solid line) and at pH 5.0 (dashed line). CD spectra of PsbS refolded in buffer containing (a) 2 % OG (b) 0.1 % β-DM (c) 1 % Brij-78 (d) 1 % FC-12 (e) 1 % DHPC and (f) 1 % NG.

Figure 3.4 shows CD spectra of refolded PsbS from *P. patens* using various detergents under neutral (solid line) and low pH conditions (dashed line). PsbS was successfully refolded in OG, β-DM, Brij-78 and FC-12, as seen from the CD spectral shapes that are representative of helical structures in Figure 3.4 a–d (solid line, pH 7.5). However, refolding in DHPC (e) or NG (f) would significantly reduce the amount of helicity. Table 3.3 presents a CD spectral component analysis giving an estimated percentage of the helix, antiparallel, parallel or turn structures present in the refolded PsbS for the six detergents at pH 7.5. Using the homologous crystal structure of PsbS from *S. oleracea*, for the *P. patens* PsbS amino-acid sequence 47 % α-helical structure is predicted closely matching with the CD analyses except for NG and DHPC. For NG, this is surprising since this detergent was successfully used for crystallization of native PsbS. It is interesting to notice that for PsbS refolded in OG, β-DM, Brij-78 and FC-12, which all gave samples with a similar percentage of helicity, the percentage of sheet structure differs for the various detergent types. In the appendix, Fig 3A.5 shows a homology structure of *P. patens* PsbS. The structure contains two small anti-parallel sheet stretches at the stromal site. In addition, the stromal site contains a large loop segment that is not resolved in the crystal structure and contains the N- and C-terminal stretches that are only partly resolved. At the luminal site, the trans-membrane protein helices are connected via short connected loops that contain the proposed Glu active residues and a short helix segment.

One observation is that the non-helical protein sites can adopt different folds depending on the detergent micelles in which the protein is solubilized. The CD spectrum of the recombinant PsbS in β-DM looks very similar to the published CD spectrum of native plant PsbS in β-DM, with characteristic peaks at 208 nm and 222 nm, of which the 208 nm peak is very pronounced. The 208 nm peak is less pronounced in the CD spectrum of PsbS refolded in OG, and this spectrum of PsbS in OG buffer looks very similar to the CD spectrum reported by Wilk *et al.*,[14] who refolded plant PsbS in OG micelles. The CD spectral differences for PsbS solubilized in various detergents likely reflect structural differences that are induced by the detergent micellar shapes. β-DM micelles form oblate structures, whereas OG and FC-12 micelles form prolate structures and Brij-78 is a polymeric surfactant that forms random-coil arrangements.

Table 3.3 CD Secondary-structure analysis of PsbS in various detergent buffers.

Secondary structures (%)	**OG pH 7.5**	**β-DM pH 7.5**	**Brij-78 pH 7.5**	**FC-12 pH 7.5**	**DHPC pH 7.5**	**NG pH 7.5**
Helix	51.8	51.4	42.3	49.6	17.2	25.2
Antiparallel	11.5	30.5	17.5	1.1	10.1	10.6
Parallel	0	0	0	0	0	9.8
Turn	8.6	2.3	8.4	8.1	21	14.5
Others	28.1	15.8	31.8	41.2	51.6	39.8

Figure 3.4 also contains the CD spectra of refolded PsbS, in pH 5.0 conditions (dashed line). The pH 5.0 spectra for PsbS refolded in detergents β-DM, Brij-78 and DHPC has structural variations as compared to the pH 7.5 conditions. From sample preparation experience, the stability of PsbS in pH 5.0 conditions is challenging to achieve and perhaps β-DM, Brij-78 and DHPC fail to maintain the solubility of PsbS under pH 5.0 conditions. PsbS refolded in OG and FC-12, pH 5.0 conditions adopt a ~50 % α-helical structure. There are minor changes in the non-helical spectral regions that are small fluctuations compared to the structural variation. In conclusion, the optimal detergents for refolding Patens-PsbS were OG and Fc-12 due to their proper folding and stability of PsbS. OG and FC-12 have small micellar size, which is favorable for size-determination analyses and NMR experiments. Additionally, FC-12 detergent is zwitterionic that provided more stability to PsbS.

3.3.4 Refolding of Arabidopsis-PsbS and Spinach-PsbS

Structural characterization using CD spectroscopy was done for PsbS from *Arabidopsis thaliana* and *Spinacia oleracea* by refolding using various detergents in pH 7.5 and pH 5.0 (shown in Figure 3.5).

(a) Arabidopsis-PsbS

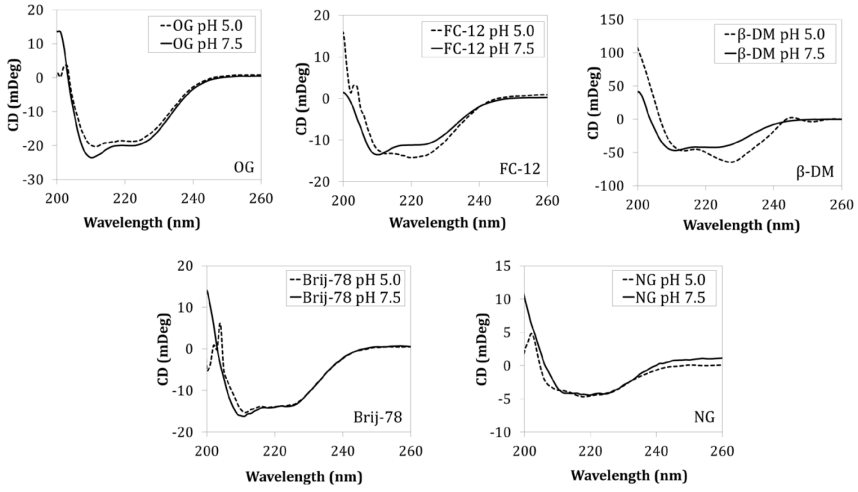

(b) Spinach-PsbS

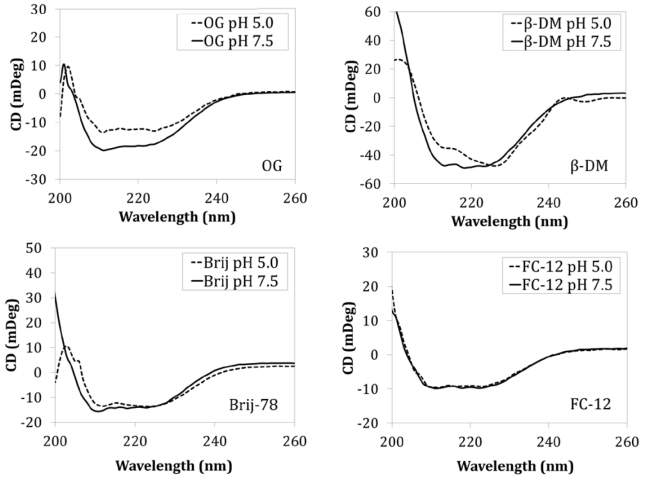

Figure 3.5 CD spectra of PsbS from *A. thaliana* (Arabidopsis-PsbS) (a) and *S. oleracea* (Spinach-PsbS) (b) refolded in various detergent buffers at pH 7.5 (solid line) and at pH 5.0 (dashed line)

From Figure 3.5, Arabidopsis-PsbS and Spinach-PsbS forms ~40 – 50 % helical structures in all detergents for both pH conditions. Arabidopsis-PsbS and Spinach-PsbS could be refolded at low and high pH in all detergent conditions that were tested. Slight structural variations in the fold of PsbS with pH lowering for all detergent conditions are observed, arising mainly from variations in the non-helical part of PsbS. As compared to Patens-PsbS, refolding of Arabidopsis-PsbS and Spinach-PsbS were better successful at both low and neutral pH in all detergents screened.

3.4 Conclusion

This chapter shows the successful development of a protocol for large-scale overproduction and refolding of PsbS, opening routes for structural characterization of this important light-stress sensor protein. The conformational structures of PsbS in detergent micelles are influenced by the choice of detergent, underlining the importance of the protein microenvironment.

Refolding of PsbS from three different species was shown to be successful. Selection of the optimal detergent condition was determined based on proper refolding showing ~40 – 50 % helical structures, as observed in the crystal structure of Spinach-PsbS[23]. The overall conclusion is that the fold of non-helical parts of PsbS varies with the choice of detergent. From all the detergents that were screened, OG, Fc-12, β-DM and Brij-78 show proper refolding of PsbS at pH 7.5, corresponding to ~50 % helical structures. For the proper refolding of Patens-PsbS OG and FC-12 were the best detergents, since they showed good refolding in both pH conditions. These detergent types are recommended for solubilization of isolated PsbS and the protocols mentioned in this chapter can be used in further studies focused on PsbS pH-dependent conformational changes.

3.5 References

1. Erik Wallin, Gunnar van Heijne. Genome wide analysis of intergral membrane proteins from eubacterial, archean and eukaryotic organisms. *Protein Science* **7,** 1029–1038 (1998).
2. Lundstrom, K. Structural genomics and drug discovery. *Journal of cellular and molecular medicine* **11,** 224–238; 10.1111/j.1582-4934.2007.00028.x (2007).
3. Schlegel, S. *et al.* Revolutionizing membrane protein overexpression in bacteria. *Microbial Biotechnology* **3,** 403–411; 10.1111/j.1751-7915.2009.00148.x (2010).
4. Wagner, S., Bader, M. L., Drew, D. & Gier, J.-W. de. Rationalizing membrane protein overexpression. *Trends in Biotechnology* **24,** 364–371; 10.1016/j.tibtech.2006.06.008 (2006).
5. Grisshammer, R. Understanding recombinant expression of membrane proteins. *Current opinion in biotechnology* **17,** 337–340; 10.1016/j.copbio.2006.06.001 (2006).
6. Wagner, S. *et al.* Consequences of membrane protein overexpression in Escherichia coli. *GBM Annual Spring meeting Mosbach 2007* **2007**; 10.1240/sav_gbm_2007_m_001709 (2007).
7. Rosano, G. L. & Ceccarelli, E. a. Recombinant protein expression in Escherichia coli: Advances and challenges. *Frontiers in Microbiology* **5,** 1–17; 10.3389/fmicb.2014.00172 (2014).
8. Rogl, H., Kosemund, K., Kühlbrandt, W. & Collinson, I. Refolding of Escherichia coli produced membrane protein inclusion bodies immobilised by nickel chelating chromatography. *FEBS Letters* **432,** 21–26; 10.1016/S0014-5793(98)00825-4 (1998).
9. Singh, S. M. & Panda, A. K. Solubilization and refolding of bacterial inclusion body proteins. *Journal of bioscience and bioengineering* **99,** 303–310; 10.1263/jbb.99.303 (2005).
10. Verardi, R., Traaseth, N. J., Masterson, L. R., Vostrikov, V. V. & Veglia, G. Isotope labeling in Biomolecular NMR. *Advances in Experimental Medicine and Biology* **992**; 10.1007/978-94-007-4954-2 (2012).
11. Paliy, O. & Gunasekera, T. S. Growth of E. coli BL21 in minimal media with different gluconeogenic carbon sources and salt contents. *Applied Microbiology and Biotechnology* **73,** 1169–1172; 10.1007/s00253-006-0554-8 (2007).
12. Paulsen, H., Rümler, U. & Rüdiger, W. Reconstitution of pigment-containing complexes from light-harvesting chlorophyll a/b-binding protein overexpressed in Escherichia coli. *Planta* **181,** 204–211; 10.1007/BF02411539 (1990).
13. Horton, P. & Ruban, A. V. Regulation of Photosystem II. *Photosynthesis Research* **34,** 375–385; 10.1007/BF00029812 (1992).
14. Wilk, L., Grunwald, M., Liao, P.-N., Walla, P. J. & Kühlbrandt, W. Direct interaction of the major light-harvesting complex II and PsbS in nonphotochemical quenching. *Proceedings of the National Academy of Sciences of the United States of America* **110,** 5452–5456; 10.1073/pnas.1205561110 (2013).

15. Aspinall-O'Dea, M. *et al.* In vitro reconstitution of the activated zeaxanthin state associated with energy dissipation in plants. *Proceedings of the National Academy of Sciences* **99,** 16331–16335; 10.1073/pnas.252500999 (2002).

16. Dominici, P. *et al.* Biochemical properties of the PsbS subunit of photosystem II either purified from chloroplast or recombinant. *Journal of Biological Chemistry* **277,** 22750–22758; 10.1074/jbc.M200604200 (2002).

17. Bonente, G., Howes, B. D., Caffarri, S., Smulevich, G. & Bassi, R. Interactions between the photosystem II subunit PsbS and xanthophylls studied in vivo and in vitro. *Journal of Biological Chemistry* **283,** 8434–8445; 10.1074/jbc.M708291200 (2008).

18. Arora, a. & Tamm, L. K. Biophysical approaches to membrane protein structure determination. *Curr. Opin. Struct. Biol.* **11,** 540–547; 10.1016/S0959-440X(00)00246-3 (2001).

19. Chaptal, V. *et al.* Quantification of Detergents Complexed with Membrane Proteins. *Scientific Reports* **7,** 41751; 10.1038/srep41751 (2017).

20. Garavito, R. M. & Ferguson-Miller, S. Detergents as Tools in Membrane Biochemistry. *Journal of Biological Chemistry* **276,** 32403–32406; 10.1074/jbc.R100031200 (2001).

21. Oliver, R. C. *et al.* Dependence of Micelle Size and Shape on Detergent Alkyl Chain Length and Head Group. *PLoS ONE* **8**; 10.1371/journal.pone.0062488 (2013).

22. Raman, P., Cherezov, V. & Caffrey, M. The Membrane Protein Data Bank. *Cellular and molecular life sciences : CMLS* **63,** 36–51; 10.1007/s00018-005-5350-6 (2006).

23. Fan, M. *et al.* Crystal structures of the PsbS protein essential for photoprotection in plants. *Nature structural and molecular biology* **22,** 729–735; 10.1038/nsmb.3068 (2015).

24. Krishnan, M., Moolenaar, G. F., Gupta, Karthick Babu Sai Sankar, Goosen, N. & Pandit, A. Large-scale in vitro production, refolding and dimerization of PsbS in different microenvironments. *Scientific Reports* **7,** 1–11; 10.1038/s41598-017-15068-3 (2017).

25. Micsonai, A. *et al.* Accurate secondary structure prediction and fold recognition for circular dichroism spectroscopy. *Proceedings of the National Academy of Sciences of the United States of America* **112**; 10.1073/pnas.1500851112 (2015).

3.6 Appendix 3A

Fig 3A.1 (a) Plasmid pExp5-PsbS optimized for overexpression at 18 °C, overnight with 1 mM IPTG induction in BL21-pLysS and BL21 strains. (b) IPTG optimization for PsbS overexpression using pExp5-PsbS in BL21-pLysS strain at 18 °C, overnight. 0.05 mM was used in all experiments.

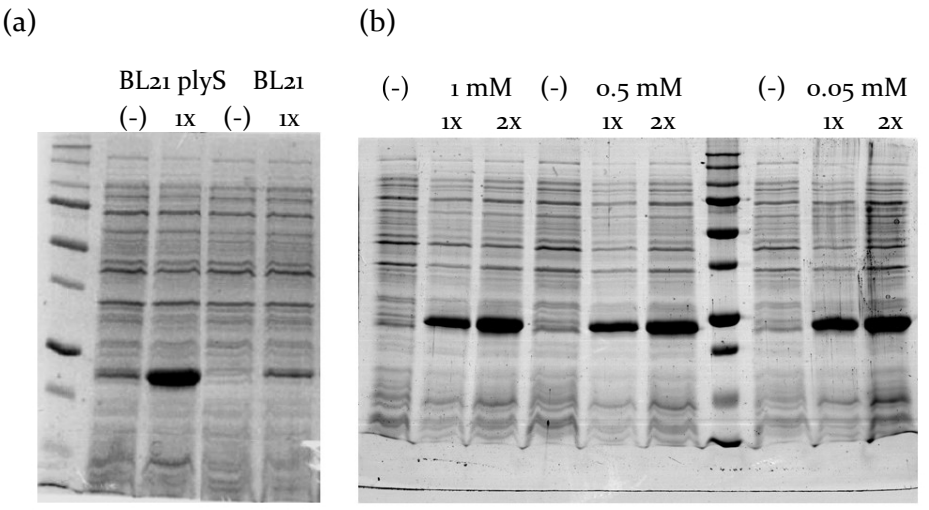

Fig 3A.2 Comparison of PsbS overexpression from enriched LB and minimal M9 media grown at 18 °C, overnight in a volume of 200 mL. BSA is loaded as a marker for comparison of yield. Equal amounts of protein were loaded on gel.

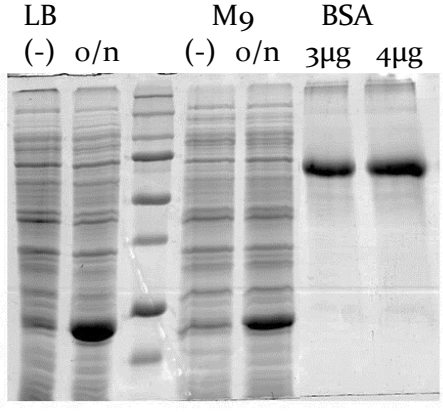

Fig 3A.3 Inclusion body purification from 200 mL cell pellet.
(+) IPTG sample shows the overexpression of PsbS from 200 mL culture. Different steps of inclusion body purification were carried out (supernatant S1 to pellet P4). BSA protein (5 µg) is shown for comparison of yield. In the final step, pellet P4 contains PsbS of ~19 mg, which is used for the next step, urea wash purification.

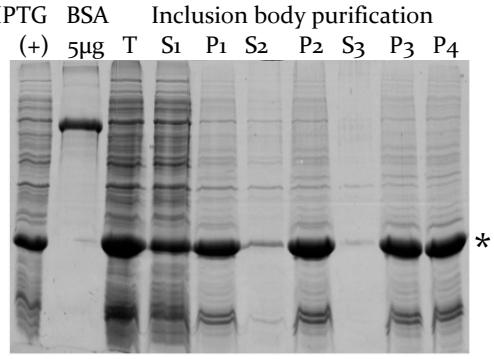

* PsbS

Fig 3A.4 Purification of Lhcb1 (*A. thaliana*) from inclusion body pellet using the urea wash protocol. Lane 1: Lhcb1 from the inclusion bodies pellet was dissolved in buffer containing 8 M urea. Several washes of urea buffer were carried out (Lane 2,3,4). Lane 5 is a washing step of the pellet with 8 M urea buffer with 0.05 % LDS. The last wash step was carried out using urea buffer with 0.5 % of LDS to dissolve all the PsbS from inclusion bodies (Lane 6). Lane 7 contains 3 µg of BSA for yield comparison.

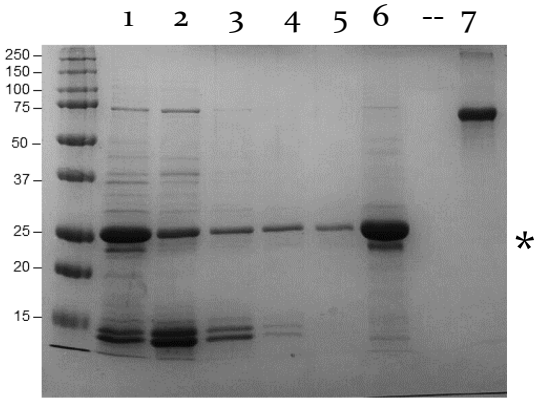

* PsbS

Fig 3A.5 Homology model of dimeric PsbS from *P. patens*

A homology model of *P. patens* PsbS constructed by SWISS-MODEL based on the crystal structure of PsbS from *S. oleracea* (PDB-ID 4RI2). The homology structure includes the stromal loops that are not resolved in the crystal structure and was energy-minimized using Chimera software. (a) front view of *P. patens* PsbS (b) side view of *P. patens* PsbS.

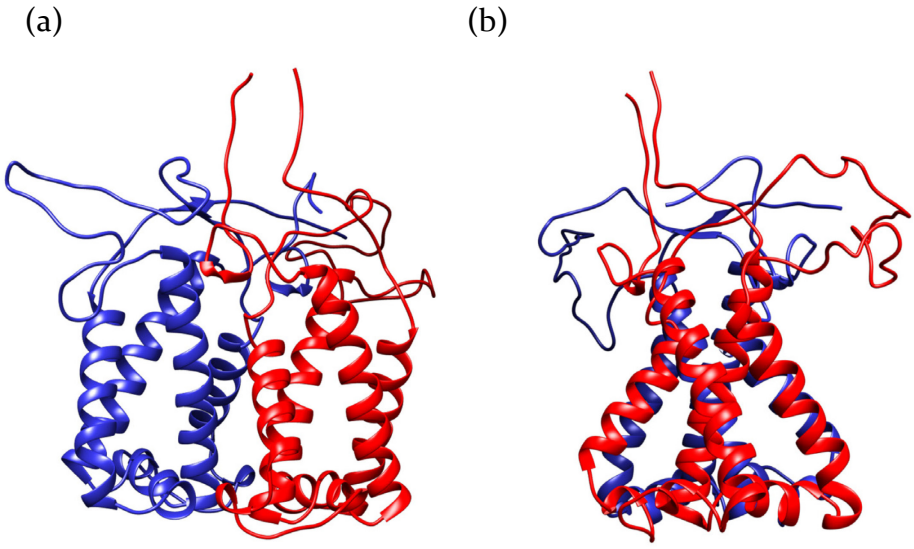

Fig 3A.6 Plasmid map of pExp5-6X His-NT PsbS

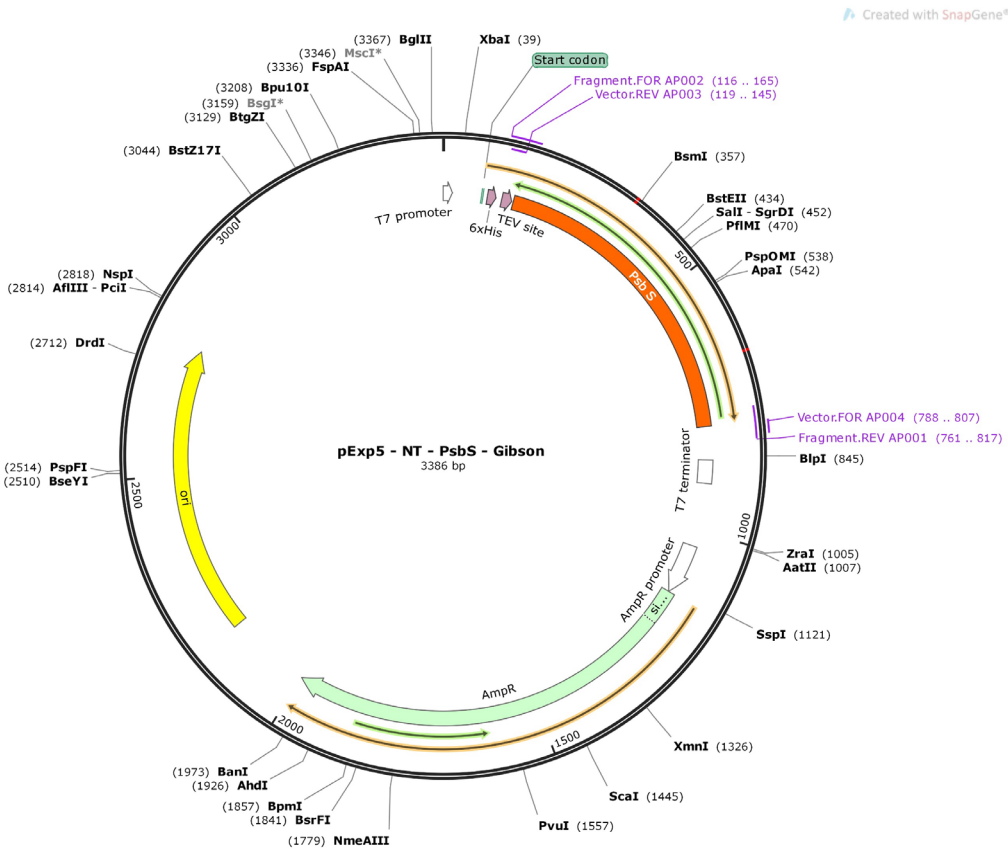

Stroma
H2
H1
Lumen
E2
E1

4

Oligomeric states of PsbS

In this chapter, the effect of pH lowering on the oligomeric states of PsbS are explored. Using a combination of techniques like SDS-gel analysis, dynamic light scattering, size exclusion chromatography, diffusion-ordered spectroscopy and heteronuclear single quantum coherence NMR spectroscopy, it was concluded that recombinant PsbS form dimers similarly to native PsbS, at neutral and low pH.

Part of this chapter is based on

Maithili Krishnan, Geri Moolenaar, Karthick Sai Sankar Gupta, Nora Goosen, and Anjali Pandit "Large-scale *in vitro* production, refolding and dimerization of PsbS in different microenvironments." *Scientific Reports*, **2017**, DOI:10.1038/s41598-017-15068-3

4.1 Introduction

PsbS was first discovered in 1984 as CP22, which co-precipitated along with PSII[1]. Recent studies on the mechanism of PsbS suggest that it triggers the rearrangement of LHCII in thylakoid membrane thus impacting NPQ[2–6]. PsbS is also proposed to be a dimer in the dark conditions or alkaline conditions and monomeric in acidic conditions during light induction[2,7]. Challenging to this model, the X-ray crystal structure of PsbS revealed a dimer structure at low pH[8]. This structural occurrence of PsbS dimers is also consistent with the presence of two PsbS units per PSII determined with stoichiometric analysis of spinach thylakoids[9]. The effect on the dimer-monomer ratio of PsbS due to pH lowering has been proposed to play a role in its function as a photoprotector[10]. It is still unclear what is the underlying mechanism and how PsbS uses its dimer-monomer transistion to trigger NPQ.

This chapter reports the association of recombinant PsbS into native-like dimers, and analyses the oligomeric states and conformational structure of PsbS by a combination of SDS-gel analysis, DLS, SEC, DOSY and HSQC NMR spectroscopy. DOSY NMR is a technique that allows analysis of compound mixtures by separating the compounds based on their self-diffusion coefficient[18]. This is good to identify the diffusion rate for particle size calculation of PsbS under different pH conditions. DOSY NMR is a complementary but much more accurate technique to DLS. In DOSY, NMR signals of different species are separated according to their diffusion coefficient. A series of spin echo spectra are measured with different pulsed field gradient strengths, and the signal decays are analyzed to extract the translational diffusion coefficients for each species. The measured intensity curves against the gradient strength were fit with a double-exponential function (see Equation 4.1) to determine the translational diffusion coefficients D_t. 2D ^{15}N-HSQC NMR spectroscopy gives a signal for each ^{1}H-^{15}N amide group and can be performed to resolve a “fingerprint” of a protein[16,17].

Parallel to NMR spectroscopy, PsbS was analyzed using gel electrophoresis and SEC for determination of molecular size. Experiments were carried out at neutral and low pH, mimicking the inactive and active state of PsbS, to understand how PsbS folding and assembly is controlled by the pH environment.

4.2 Materials and Methods

4.2.1 Gel electrophoresis

SDS-page gel electrophoresis analysis (12.5 % running gel, 4 % stacking gel stained with Coomassie brilliant blue R-250 Bio-Rad) was carried out for checking the yield of

PsbS at every step of overexpression, purification and refolding. 2.5 µL of Precision Plus Protein™ Dual Colour Standard from Sigma was used in every SDS-page gel.

4.2.2 Dynamic light scattering

DLS was carried out at room temperature using a Malvern Zetasizer Nano S90 with VWR cuvettes PMMA semi-micro.

4.2.3 Size exclusion chromatography

SEC was carried with a Superdex 200 5/150 GL analytical column (GE Healthcare). The column was equilibrated with 100 mM sodium phosphate with 0.05 % FC12 or 1 % OG for pH 7.5 and with 100 mM sodium acetate with 0.05 % FC12 or 1 % OG for pH 5.0. All samples were filtered using 0.22 µm filters before loading on the column. The detection wavelength was set at 260 nm. The sizes of the eluted fractions were estimated with the use of molecular weight markers as shown in the appendix Fig 4A.4.

4.2.4 NMR spectroscopy

All NMR spectra were recorded with a Bruker Avance III 600-MHz instrument equipped with a cryoprobe. A standard 1D sequence with ^{15}N decoupling during acquisition was used to obtain 1D ^{1}H NMR data. For the 2D experiments, standard HSQC was performed with 2D H-1/X correlation via double inept transfer with decoupling during acquisition. The pulse program used for obtaining 1D ^{1}H DOSY spectra was stebpgp1s19, which contains a 2D sequence for diffusion measurements using stimulated echo using bipolar-gradient based diffusion-ordered spectroscopy. For all the experiments, the water signal was suppressed by using a 3-9-19 pulse sequence with gradients. The diffusion time interval (d20 or Δ) was set to 300 ms while the gradient pulse lengths (p30 or δ) was set to 12 ms for all the measurements. The pulse gradient field strength was incremented linearly from 2 % to 95 % in 16 steps. The 90° pulse for proton was found to be 11.8 µs at –7.00 dB and 64 scans were used with a relaxation delay of 8 s. The DOSY intensity curves (I) plotted versus the gradient strength (g) were fitted with a double-exponential fit according to Equation 4.1 to obtain the translational diffusion constant D_t using an Igor-Pro user-defined fit function (Igor Pro version 6.01):

$$I\left(D_{1,t}, D_{2,t}, g\right) = I_1 e^{-D_{1,t}\gamma^2 g^2 \delta^2 [\Delta - \frac{1}{3}\delta]} + I_2 e^{-D_{2,t}\gamma^2 g^2 \delta^2 [\Delta - \frac{1}{3}\delta]} \qquad (4.1)$$

The resulting fits yielded two diffusion constants D_1 and D_2 in the order of ~10^{-9} m^2/s and ~10^{-11} m^2/s, respectively. D_1 was ascribed to the effects of chemical exchange, while D_2 was taken as the translational diffusion constant D_t. Particle hydrodynamic sizes were calculated from D_t using the Stokes-Einstein equation shown in Equation 4.2:

$$D = \frac{K_B T}{6 \Pi \eta r} \qquad (4.2)$$

Where, D is the diffusion constant D_t (D_2 from Eq 4.1), K_B is Boltzmann's constant, T is absolute temperature, η is the viscosity constant and r is the radius of the spherical particle. Equation 4.2 is also used for calculation of the DLS-determined hydrodynamic sizes.

4.3 Results and discussion

4.3.1 Oligomeric states of detergent-refolded PsbS at low and neutral pH

Native PsbS exists as dimers at neutral pH and forms monomers at low pH[7,10]. The proteins may cluster into larger aggregates under NPQ conditions[2]. Fan *et al*. however determined the structure of a dimeric PsbS at low pH, and PsbS dimer states at neutral and low-pH conditions were observed by SDS-page analysis[8]. Although SDS-page analysis can provide good estimates of molecular weights, protein oligomeric states may alter after sample preparation in SDS buffer and subsequent heating. Using chemical crosslinking, protein oligomeric states are stabilized, however cross-linking efficiencies can be pH-dependent. In this chapter, three additional methods to determine the sizes of refolded PsbS directly in detergent solutions were used. DLS was applied as a rapid method to determine hydrodynamic size distributions of PsbS in detergent solution. SEC was carried out to determine the oligomeric states of PsbS. DOSY NMR was applied as an alternative to DLS to determine protein translational diffusion constants, from which the protein-micelle hydrodynamic sizes were estimated. DOSY NMR has the advantage over DLS that the proteins are probed directly via the amide protons, whereas DLS detects both empty and protein-containing micelles.

To investigate the oligomeric states and stability of PsbS, SDS-page gel analysis was carried out, where PsbS samples were analyzed between zero and 90 days after PsbS refolding in FC-12 detergent. It was observed that the dimer states were resistant to SDS solubilization when the subsequent boiling step was omitted (appendix Fig 4A.1). Therefore, the standard boiling step for the SDS-page analysis was omitted. In Figure 4.1, SDS-page gels for PsbS in FC-12 at pH 7.5 and at pH 5.0 are shown respectively, collected at different days after detergent refolding (defined as Day 0).

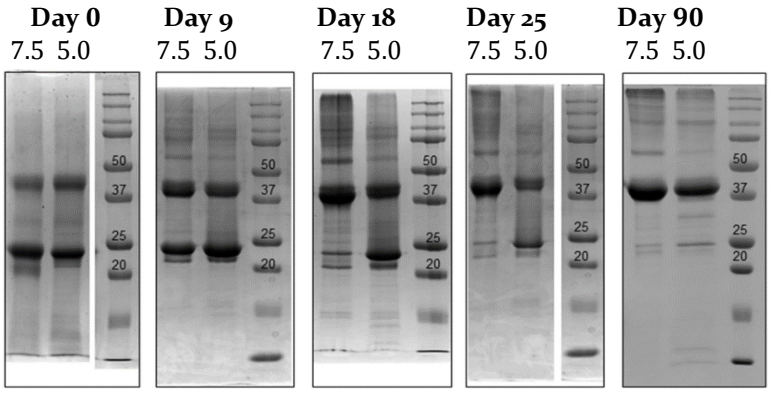

Figure 4.1 SDS-page gel analysis of samples collected at different days after PsbS refolding. SDS-page gel graphs of PsbS of PsbS collected at various days after its refolding in FC-12 detergent. Samples were not boiled before loading on the gel.

At day 0, PsbS forms mixtures of monomers and dimers both at neutral and low pH. On a time-scale of weeks, the dimer content of the samples slowly increased (Day 9 and 18). Interestingly, this process appeared to be retarded at low pH. At Day 25, the pH 7.5 sample predominantly shows as a dimer band, whereas the pH 5.0 sample contains monomer and dimer bands of similar intensities. After three months (Day 90), PsbS dimers were the most dominant observed state under both pH conditions. In addition to monomer and dimer forms, the gel graphs show that PsbS samples contained fractions of larger oligomers. From the time-dependent analysis, it can be observed that dimeric PsbS is the most stable state at both pH conditions. It is however surprising that it takes several weeks to reach this state. It is possible that PsbS dimers slowly associated into larger aggregates that were not in equilibrium anymore with the monomers. If the aggregates were not resistant to SDS solubilization, the incorporated proteins would appear as dimers on SDS-page gels. It is also possible that FC-12, which is a zwitterionic detergent that is known to prevent protein-protein interactions, retards the association of detergent-solubilized monomers into dimers. The slow observed process of dimerization is informative as it differentiates between neutral and low-pH conditions. The retarded dimerization process at low pH suggests that the PsbS dimers are destabilized, or that there is a larger energetic barrier for their association. In time, solutions also started to form visible sediments and accumulate soluble aggregates. Therefore, the following experiments were performed within a week after PsbS detergent refolding.

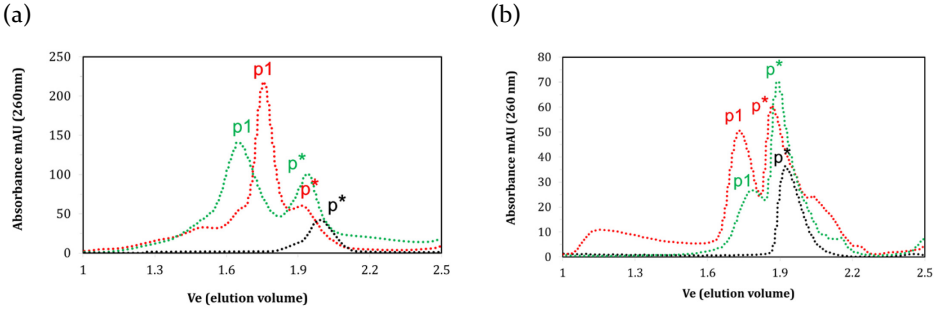

Figure 4.2 Size exclusion chromatography of PsbS in FC-12 and in OG. SEC chromatograms of (a) PsbS in FC-12 at pH 7.5 (red) and at pH 5.0 (green); (b) PsbS in OG at pH 7.5 (red) and at pH 5.0 (green). Black lines correspond to control experiments with detergent only, FC-12 (a) or OG (b). The p* peaks appear at similar elution times as the detergent micelles and are considered to be empty detergent micelles, while the p1 peaks are the PsbS fractions.

To analyze the oligomeric states of refolded PsbS in detergent buffer conditions without SDS, PsbS samples were analyzed by SEC. Figure 4.2 shows the SEC graphs for PsbS in FC-12 (a) and OG (b) at pH 7.5 (red) and pH 5.0 (green). In addition, control experiments were performed injecting 10 % of FC-12 or 10 % of OG detergent buffered at pH 7.5 (black lines). The detection wavelength was set at 260 nm to be at the maximum absorption of Phe since Patens-PsbS has 21 Phe residues but contains no Tyr or Trp. Under all conditions, two prominent peaks assigned p* and p1 were observed, together with weak peaks representative of larger aggregates. In the control experiments, OG and FC-12 eluted from the column at similar times as the p* peak of PsbS. It was assumed that the p* peak contains empty detergent micelles. In agreement, SEC experiment of PsbS in OG (pH 7.5) with the detection set at 214 nm does not show the p* peak (appendix Fig 4A.3). FC-12 and sodium-acetate buffer solutions had significant intrinsic absorption at 214 nm and therefore SEC with 214 nm detection was not applicable. The SEC estimated detergent micelle sizes were ~40 kDa for FC-12 and ~50 kDa for OG (Table 4A.1 and Table 4A.2). Considering a micelle size of ~40 kDa for FC-12, and p1 corresponding to ~90 kDa at pH 7.5, the p1 peak in Figure 4.2a would match with the size of PsbS dimers (protein size ~44 kDa). For PsbS in OG, p1 (~100 kDa) also would match with the size of PsbS dimers considering OG micelle sizes of ~50 kDa. At low pH, solutions of PsbS in OG contained visible sediments. In the SEC run of PsbS in OG, the shoulder of soluble aggregates at the void volume between 1 - 1.3 Ve (Figure 4.2b, red) disappears at low pH (Figure 4.2b, green) which is a strong indication that soluble aggregates at pH 7.5 formed sediments at pH 5.0. Because of the low intrinsic (Phe) absorption of Patens-PsbS, and incompatibility with 214 nm detection for PsbS in FC-12 and for PsbS in OG at low pH, it cannot be excluded that in the latter solutions PsbS monomers were present that were obscured by the p*

detergent peaks. The findings show that PsbS in FC-12 migrates faster from the column at pH 5.0 than at pH 7.5, is opposite to the findings of Fan *et al.*, who found that Spinach-PsbS purified in NG would migrate slower at low pH[8]. It is, therefore, suspected that low-pH solutions of FC-12 contained mixtures of dimers and larger oligomers, or that PsbS protonation changes had a different effect on the elution profile due to the zwitterionic character of FC-12.

To further analyze the PsbS particle sizes, a DLS size analysis was performed. Figure 4.3 shows the DLS size distributions for PsbS in FC-12 at neutral and acidic pH. At low pH (blue curve), a small shift of the distribution towards smaller diameter sizes is observed. Since the DLS Volume% intensities increase with the third power of the diameter sizes, a DLS size distribution of a mixture of monomers and dimers will be biased towards the dimer form.

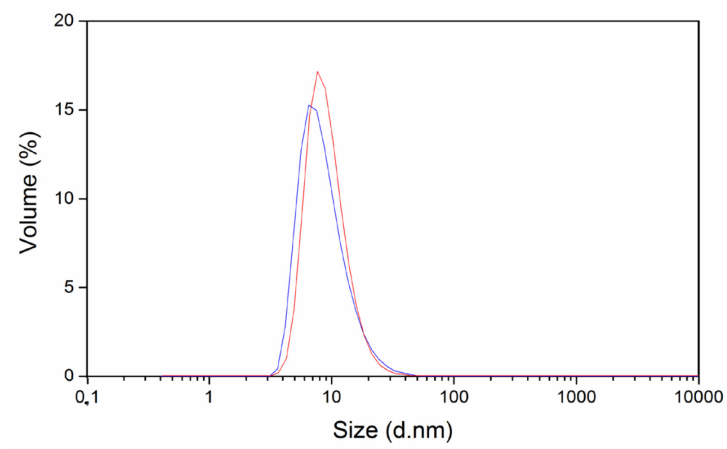

Figure 4.3 Dynamic light scattering of PsbS in FC-12. PsbS particle size determined by DLS on PsbS refolded in 0.1 % FC-12 at pH 7.5 (red) and at pH 5.0 (blue).

It was assumed that the average DLS diameter sizes reflect the size of the dimers and that the shift at low pH indicates an increase of the monomer population, in agreement with the SDS-page analysis. The DLS distributions are tailed on the right side, indicating the presence of larger aggregates. For PsbS in OG, the DLS experiments did not produce reliable results due to high polydispersity of the samples (data not shown), indicating that the solutions contained mixtures of monomers or dimers and a significant population of higher aggregates. The DLS results of PsbS in FC-12 do not show a shift into larger oligomers at low pH, indicating that the SEC peak shift at low pH is due to changes in protein conformation or protonation states.

Solutions of PsbS in FC12 and OG buffer were further analyzed by DOSY NMR spectroscopy. Figure 4.4 a and b show the H_N DOSY curves for PsbS in FC-12, at pH 7.5 (a) and at pH 5.0 (b) together with the double-exponential fits. The steep exponential component contains the actual PsbS diffusion coefficient, while the gradual decay component arises from proton exchange at water-exposed H_N sites. Remarkably, the relative amplitude of the steep decay component was larger at pH 7.5 than at pH 5.0. Adding an additional fit component, considering a mixture of PsbS monomers and dimers with different diffusion properties, did not give an additional diffusion coefficient, neither did it improve the fit.

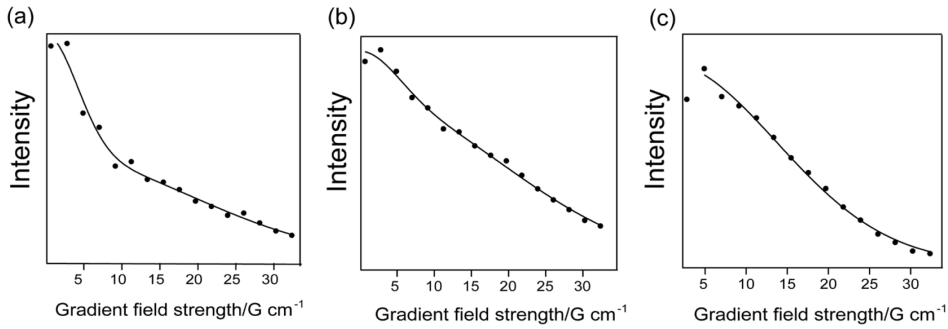

Figure 4.4 DOSY NMR of PsbS in FC-12. Integrated 1H H_N intensities (black circles) versus the gradient field strength of PsbS in FC-12 at (a) pH 7.5 and (b, c), at pH 5.0. The sample in (c) is referred to as the monomer sample. Fitted translational diffusion constants were (a) D_t = 4.0 * 10^{-11} m^2 s^{-1}; (b) D_t = 3.9 * 10^{-11} m^2 s^{-1} and (c) D_t = 7.9 * 10^{-11} m^2 s^{-1}.

In one sample of PsbS in FC-12 at pH 5.0, a steep intensity decay was observed (Figure 4.4c), corresponding with a much larger diffusion coefficient. Based on these observations, it was tentatively proposed that in this particular sample, PsbS monomers were dominant. This sample was freshly prepared and may have contained larger amounts of detergent than the other samples. The protein-detergent solutions had to be concentrated for the NMR experiments, by which the final amounts of detergent present in the samples were difficult to control. The estimated values for D_t are summarized in Table 4.1, where the sample in Figure 4.4c is indicated as 'monomer'.

Table 4.1 Translational diffusion coefficients of PsbS-detergent micelles. Estimated D_t values (standard deviation between brackets) based on the DOSY ^{1}H NMR H_N intensities (H_N), on the FC-12 trimethyl-amino peak (FC-12) or on the OG (4-7) CH_2 band (OG).

	D_t (m^2s^{-1})		
	H_N	**FC-12**	**OG**
PsbS in FC-12 pH 7.5	$4.0 * 10^{-11}$ ($3.7 * 10^{-12}$)	$5.0 * 10^{-11}$ ($5.2 * 10^{-12}$)	--
PsbS in FC-12 pH 5.0	$3.9 * 10^{-11}$ ($3.8 * 10^{-12}$)	$5.7 * 10^{-11}$ ($5.6 * 10^{-12}$)	--
PsbS in FC-12 pH 5.0 (monomer)	$7.8 * 10^{-11}$ ($6.6 * 10^{-12}$)	$9.8 * 10^{-11}$ ($1.0 * 10^{-11}$)	--
PsbS in OG pH 7.5	$3.2 * 10^{-11}$ ($1.1 * 10^{-12}$)	--	$3.9 * 10^{-11}$ ($4.2 * 10^{-12}$)

Data of PsbS in OG at pH 5.0 were omitted because the sample sedimented during the DOSY experiment. The diffusion coefficients estimated from the DOSY curves in Figure 4.4 a and b show the hydrodynamic diameter sizes of 12.1 (±1.2) nm at pH 7.5 and 12.4 (±1.3) nm at pH 5.0, and for PsbS in OG (pH 7.5) the diffusion coefficient corresponds with 15.2 (±1.5) nm (calculations using Eq 4.2). For the supposed monomeric sample in Figure 4.4 c, the diffusion coefficient corresponds to 6.2 (±1.0) nm using Eq 4.2. In addition to the H_N intensities, the trimethyl-amino peak of FC-12 and the (4-7) CH_2 peak of OG were used to estimate the translational diffusion coefficients. The diffusion coefficients measured via the detergent peaks correspond with smaller hydrodynamic sizes because the detergent signals are the average of free detergent, empty detergent micelles and protein-detergent micelles. The diameter sizes determined from the FC-12 trimethyl-amino peak intensities are 9.4 (±1.3) nm (pH 7.5) and 8.7 (±1.2) nm (pH 5.0) respectively, which are very close to the DLS determined average sizes. Indeed, the DLS determined sizes are also the average of protein and empty detergent micelles that are not resolved as separate peaks in the histograms. The DOSY results do not show significant changes at low pH, except for the one particular sample (Figure 4.4c). This suggests that under both conditions, PsbS predominantly existed as dimers. Decreased stability of the dimers at low pH could make them more sensitive to fluctuations in detergent concentrations.

4.3.2 PsbS conformational structures at low and neutral pH

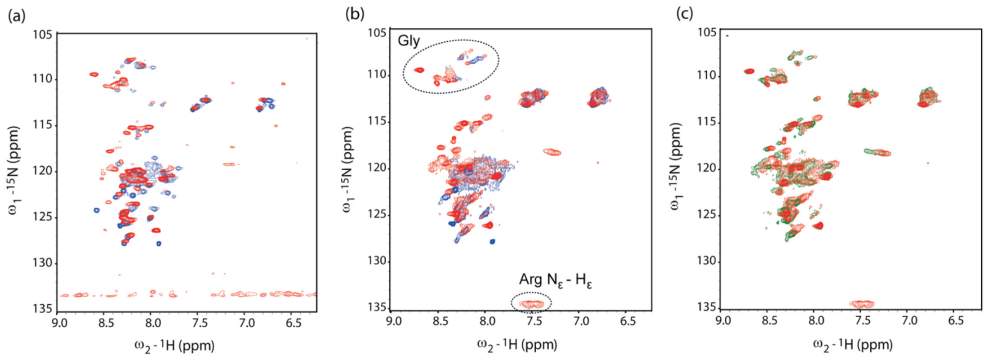

Figure 4.5 HSQC NMR spectra of PsbS in FC-12 and in OG. (a) PsbS in OG at pH 7.5 (blue) and at pH 5.0 (red); (b) PsbS in FC-12 at pH 7.5 (blue) and at pH 5.0 (red); (c) PsbS in FC-12 at pH 5.0 (red) and the supposed monomerized sample of PsbS in FC-12 at pH 5.0 (green).

To gain further insight into the structure and dynamics of PsbS, ^{1}H-^{15}N HSQC NMR spectra were recorded for the DOSY samples. The Figure 4.5a presents the HSQC spectrum of PsbS in OG at low (red) and neutral (blue) pH, and in Figure 4.5 b spectra of PsbS in FC-12 at low (red) and neutral (blue) pH are presented. In Figure 4.5 c, the DOSY samples that were analyzed in Figure 4.4 b (red, dimer) and Figure 4.4 c (green, monomer) are compared. The spectra show only a moderate set of resonances with low dispersion, reminiscent of a random-coil structure, which contrasts with the CD spectral analyses that predict ~50 % helicity. The contrast is explained if we consider that due to the large protein-micelle sizes, only the mobile protein regions might be resolved in solution NMR, which are the flexible loops, turn and terminal regions that reside in the aqueous phase. Two experimental observations agreed with this notion. First, an H-D exchange experiment reversibly deleted most of the resonance peaks (data not shown), indicating that these are from water-accessible sites. Second, the DOSY curves contain a steep decay component with a considerable amplitude that can be interpreted by fast amide proton exchange with the surrounding bulk water, which does not occur for amides involved in α-helical H-bonds. The HSQC resonance peaks are better resolved for PsbS in OG than for PsbS in FC-12, suggesting that PsbS adopts a more dynamic structure in OG micelles than in FC-12. A comparison of spectra at pH 7.5 and pH 5.0 (Figure 4.5 a and b) show several changes in the peak patterns and more resolved peaks at pH 5.0 (red spectra), including several Gly peaks and a folded peak of the Arg guanidinium side-chain nitrogens for PsbS in FC-12.

The improved resolution at pH 5.0 suggests that PsbS adopts a more ordered structure at low pH, in line with the DOSY results, where fast proton-exchange effects were more prominent at pH 7.5 than at pH 5.0. These observations match with the conclusion of Fan *et al.*, that PsbS dimers form a more loose structure at neutral pH. The supposed monomer spectrum at low pH (Figure 4.5 c, green) has several shifted peaks and lacks the Arg signal. *P. patens* PsbS contains three Arg residues, of which one is involved in an inter-monomer hydrogen bond, stabilizing the PsbS dimer[8]. The disappearance of the Arg signal could correlate with the breaking of the inter-dimer hydrogen bond, and the shifted peaks could be from sites at the monomer interfaces.

4.4 Conclusion

In conclusion, refolded *Physcomitrella patens* PsbS was observed to stabilize as dimers over time in detergent solutions that are carefully kept above the CMC limit, indicating that strong interactions between the PsbS monomers occur. The crystallographic structure of native PsbS shows a chlorophyll bound at the dimer interface, which may stabilize the dimers *in vivo*[8]. The necessity of lipid or pigments for membrane protein oligomerization is a common motif and for instance, LHCII, which is homolog to PsbS, requires 1,2-dipalmitoyl-sn-glycero-3-phospho-rac-(1-glycerol) for its trimerization[19]. In these experiments, however, PsbS dimers are observed in an *in vitro* assay, which excludes the necessity for native lipids or pigments to stabilize the inter-monomer interfaces. PsbS dimers are formed at neutral and low pH conditions, which is consistent with the observed low-pH crystal structure of a PsbS dimer. Lowering of the pH, corresponding with the active state of PsbS *in vivo*, however, appears to destabilize the dimer states or their association into higher soluble aggregates, and shifts apparent monomer-dimer equilibria towards monomers. This finding not only explains the controversies about the oligomeric states of *in vivo* PsbS at low pH reported in different studies[8,10,7] but also suggests a molecular-response model where the pH environment may control active and inactive populations of PsbS in a gradual manner. In membranes *in vivo*, other parameters like zeaxanthin could further control monomer-dimer or higher-state equilibria and shift those towards the active form. The combined results show that upon lowering the pH, local changes occur in PsbS conformational structure and dynamics that are not accompanied by large changes in the secondary structure. PsbS adopts a looser structure at neutral pH than at low pH while at the same time its dimeric form is stable. PsbS proteins in detergent solutions adapt slightly different conformational structures depending on the micellar microenvironments. *In vivo*, this plasticity might be used by PsbS to associate with different interacting partners.

Solution NMR spectroscopy forms an elegant method to simultaneously analyze protein PsbS conformational structures and oligomerization states. Due to the large protein-micelle sizes, a thorough structural analysis will require solid-state NMR approaches that have the advantage that there is no size limit. The conformational structures of PsbS in detergent micelles are influenced by the choice of detergent, underlining the importance of the protein microenvironment. The results reveal that PsbS has intrinsic properties to form dimers both at low and neutral pH but does undergo pH-dependent conformational changes that destabilize the dimer states and shift monomer-dimer equilibria. In thylakoidal membranes, additional components may further control the equilibria to create a fine-tuned photoprotective response mechanism for PsbS activation upon thylakoid-lumen acidification at excess light conditions.

4.5 References

1. Funkapb, C., Schriider, W. P., Greena, B. R., Rengerb, G. & Anderssona, B. The intrinsic 22 kDa protein is a chlorophyll-binding photosystem II subunit of **342,** 261–266 (1994).

2. Dominici, P. *et al.* Biochemical properties of the PsbS subunit of photosystem II either purified from chloroplast or recombinant. *Journal of Biological Chemistry* **277,** 22750–22758 (2002).

3. Brooks, M. D., Jansson, S., and Niyogi, K. K. . in *Non-Photochemical Quenching and Energy Dissipation in Plants, Algae and Cyanobacteria,* edited by Barbara Demmig-Adams, Gyozo Garab, William Adams III, Govindjee (Springer, Dordrecht2014).

4. Niyogi, K. K., Li, X. P., Rosenberg, V. & Jung, H. S. Is PsbS the site of non-photochemical quenching in photosynthesis? *Journal of Experimental Botany* **56,** 375–382 (2005).

5. Li, X. P. *et al.* Regulation of photosynthetic light harvesting involves intrathylakoid lumen pH sensing by the PsbS protein. *Journal of Biological Chemistry* **279,** 22866–22874 (2004).

6. Sacharz, J., Giovagnetti, V., Ungerer, P., Mastroianni, G. & Ruban, A. V. The xanthophyll cycle affects reversible interactions between PsbS and light-harvesting complex II to control non-photochemical quenching. *Nature Plants* **3** (2017).

7. Correa-Galvis Viviana & Gereon Poschmann , Michael Melzer, Kai Stühler and Peter Jahns. PsbS interactions involved in the activation of energy dissipation in Arabidopsis. *Nature Plants* **2,** 15225–15232 (2016).

8. Fan, M. *et al.* Crystal structures of the PsbS protein essential for photoprotection in plants. *Nature structural and molecular biology* **22,** 729–735 (2015).

9. Funk, C. *et al.* The PS II-S protein of higher plants : a new type of pigment binding protein. *Biochemistry* **34,** 11133–11141 (1995).

10. Bergantino, E. *et al.* Light- and pH-dependent structural changes in the PsbS subunit of photosystem II. *Proceedings of the National Academy of Sciences of the United States of America* **100,** 15265–15270 (2003).

11. Kwan, A. H., Mobli, M., Gooley, P. R., King, G. F. & MacKay, J. P. Macromolecular NMR spectroscopy for the non-spectroscopist. *FEBS Journal* **278,** 687–703 (2011).

12. Wilk, L., Grunwald, M., Liao, P.-N., Walla, P. J. & Kühlbrandt, W. Direct interaction of the major light-harvesting complex II and PsbS in nonphotochemical quenching. *Proceedings of the National Academy of Sciences of the United States of America* **110,** 5452–5456 (2013).

13. Kelly, S. M., Jess, T. J. & Price, N. C. How to study proteins by circular dichroism. *Biochimica et Biophysica Acta - Bioenergetics* **1751,** 119–139 (2005).

14. Tzitzilonis, C., Eichmann, C., Maslennikov, I., Choe, S. & Riek, R. Detergent/Nanodisc Screening for High-Resolution NMR Studies of an Integral Membrane Protein Containing a Cytoplasmic Domain. *PLoS ONE* **8,** 2–9 (2013).

15. Li, X. P., Phippard, A., Pasari, J. & Niyogi, K. K. Structure-function analysis of photosystem II subunit S (PsbS) in vivo. *Functional Plant Biology* **29,** 1131–1139 (2002).

16. Bodenhausen, G. & Ruben, D. J. Natural abundance nitrogen-15 NMR by enhanced heteronuclear spectroscopy (1980).

17. Fox, D. A. & Columbus, L. Solution NMR resonance assignment strategies for β-barrel membrane proteins. *Protein Science* **22,** 1133–1140 (2013).

18. Glanzer, S. & Zangger, K. Directly decoupled diffusion-ordered NMR spectroscopy for the analysis of compound mixtures. *Chemistry (Weinheim an der Bergstrasse, Germany)* **20,** 11171–11175 (2014).

19. Hobe, S., Prytulla, S., Kuhlbrandt, W. & Paulsen, H. Trimerization and crystallization of reconstituted light-harvesting chlorophyll a / b complex **13,** 3423–3429 (1994).

4.6 Appendix 4A

Fig 4A.1 Boiled (B) and unboiled (UnB) samples of PsbS in FC-12 neutral pH at 90 days.

Using the standard SDS-page gel protocol including sample boiling, both monomer and dimer bands of PsbS are observed. If the boiling step before loading is omitted, only dimer bands are observed. Addition of EDC crosslinker would give the same result as omitting the boiling step (data not shown).

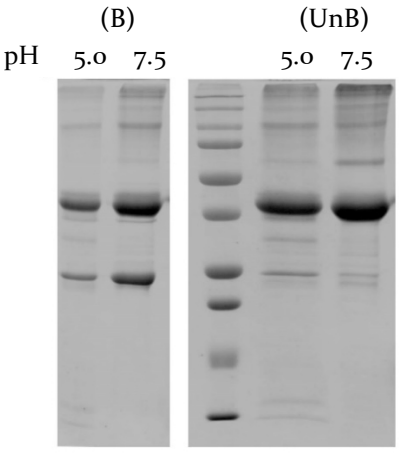

Fig 4A.2 Original SDS-page gel figure of Figure 4.1 that were presented in edited form (cutting two lanes)

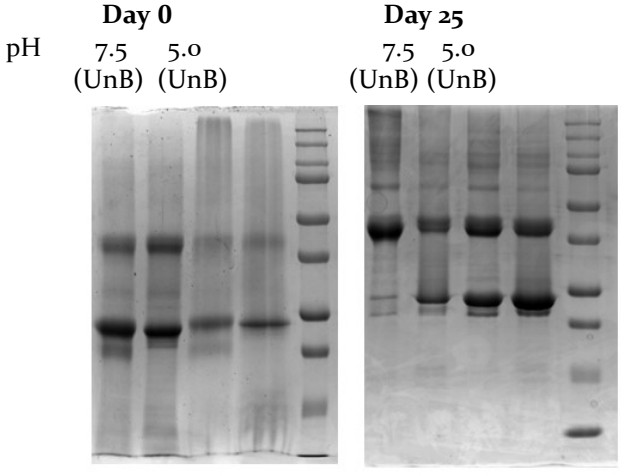

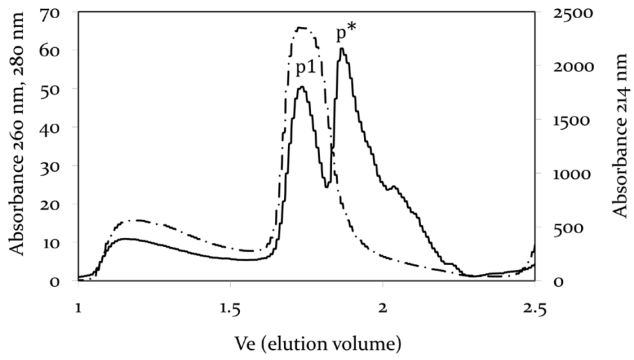

Fig 4A.3 Comparison of SEC chromatograms of PsbS in OG at pH 7.5 with the detection wavelength set at 260 nm (solid), and at 214 nm (dash) detection.

Table 4A.1 Molecular weight estimates for SEC eluted fractions of PsbS in FC12

	Markers	Ve	MW (kDa)		
1	α - amylase	1.52	200		
2	Alcohol dehydrogenase	1.65	150		
3	Bovine serum albumin	1.78	66		
4	Carbonic anhydrase	2.11	29	Exp	Y
	PsbS pH 7.5 peak *	1.92	50	0.00135	50.6531
	PsbS pH 7.5 peak 1	1.75	90	0.00243	90.9036
	FC-12 detergent	1.98	41	0.001101	41.2066
	PsbS pH 5.0 peak *	1.95	45	0.00122	45.6864
	PsbS pH 5.0 peak 1	1.65	128	0.003427	128.226

Table 4A.2 Molecular weight estimations for SEC eluted fractions of PsbS in OG

	Markers	Ve	MW (kDa)		
1	α - amylase	1.52	200		
2	Alcohol dehydrogenase	1.64	150		
3	Bovine serum albumin	1.78	66		
4	Carbonic anhydrase	2.11	29	Exp	Y
	PsbS pH 7.5 peak *	1.87	60	0.00186	60.6579
	PsbS pH 7.5 peak 1	1.72	100	0.003081	100.439
	OG detergent	1.92	51	0.001573	51.2722
	PsbS pH 5.0 peak *	1.89	56	0.00174	56.7134
	PsbS pH 5.0 peak 1	1.78	82	0.002518	82.0911

Fig 4A.4
Molecular weight estimates for SEC eluted fractions of PsbS in FC-12 (a) and for eluted fractions of PsbS in OG (b). Markers 1, 2, 3 and 4 correspond to α-amylase (200 kDa), alcohol dehydrogenase (150 kDa), BSA (66 kDa) and carbonic anhydrase (29 kDa) (green diamond).

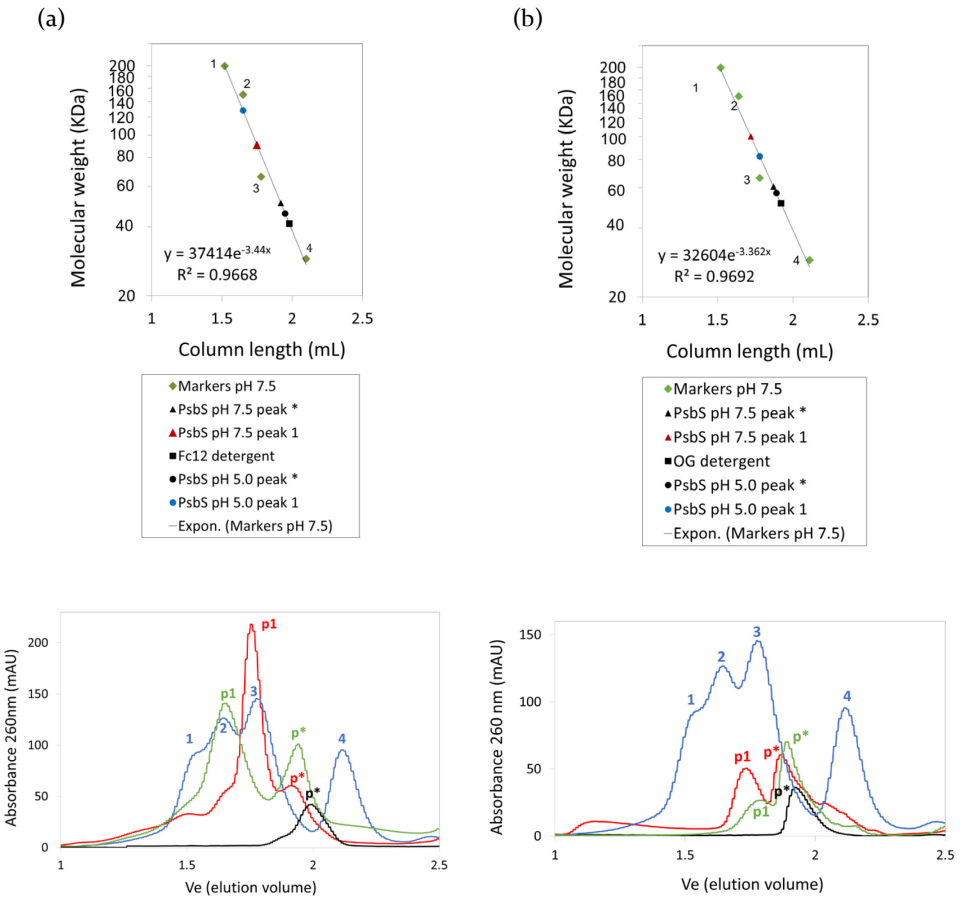

Fig 4A.5 Western blot of unfolded and refolded PsbS using Anti-PsbS (Agrisera antibodies AS09533)

(a) SDS gel containing refolded PsbS.
(b) Refolded PsbS was run on western blot using Anti-PsbS antibodies to detect the presence of PsbS protein. The presence of dimer, monomer and higher aggregates are observed.

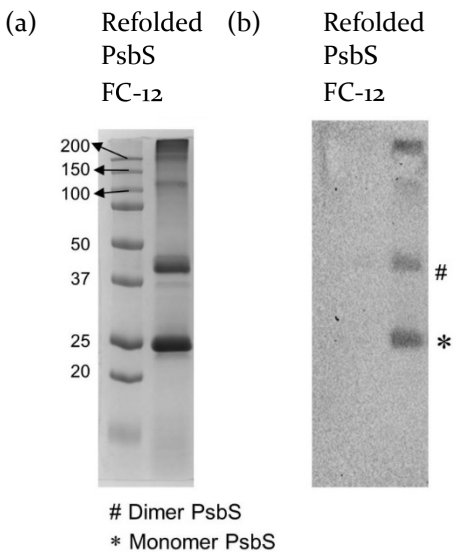

pH 7.5
pH 5.0
E1
E2
E1
E2

5

The role of Glu-71 and Glu-176 residues in PsbS function

PsbS is a key component in NPQ that is proposed to have two active glutamates which undergo protonation upon lumen acidification. Single mutations of these glutamate residues in *in vivo* studies have reduced NPQ by 60 - 70 % and a double mutation causes complete abolishment of NPQ. To understand the exact role of the active glutamates (Glu-71 and Glu-176) in the pH response of PsbS, single mutants of E71Q and E176Q and the double mutant E71Q, E176Q were analyzed by NMR and IR spectroscopy. It was observed that Glu-71 is important for stabilizing the PsbS dimer. The key finding of this chapter is the repositioning of the amphipathic short lumenal helix H2, containing Glu-176, from aqueous to membrane phase upon protonation. Thus, leading to a structural response of PsbS as a fu nction of pH, which in turn may regulate photosynthesis. In addition, protonation of all the titratable Glu and Asp residues in PsbS upon pH lowering are observed.

This chapter is based on

Maithili Krishnan, Patrick Konold, John T.M. Kennis, Anjali Pandit "The two active glutamates of the plant stress sensor PsbS contribute non-equivalently to its pH-activated molecular response mechanism." *In preparation, [Preprint BioRxiv*, DOI: 10.1101/457614]

5.1 Introduction

The PsbS-dependent mechanism of NPQ has not been clearly understood[1,2]. Across the plant species, the PsbS gene is highly conserved and specific residues have been hypothesized to play a role in its regulatory mechanism[3]. Several conserved acidic residues on the lumen-exposed side of PsbS were discovered, suggesting their role in pH sensing ability of PsbS to detect acidification of the thylakoid lumen under light stress[4]. The binding of DCCD to PsbS has led to the hypothesis that two proton accepting amino acid residues in PsbS undergo changes with protonation at low pH triggering its activity[5]. Using site-directed mutations, two glutamate residues were identified to be critical for PsbS function[6–8]. The single mutation of either of the two glutamates reduced qE to 60 – 70 %, while there was a complete absence of qE in the double mutant[7]. These two glutamate residues were demonstrated to be critical for the function of PsbS.

In PsbS from *Physcomitrella patens,* Glu-71 and Glu-176 are the two glutamate residues that assist in pH sensing and are critical for qE (in Spinach-PsbS those residues are Glu-69 and Glu-173). For ease of explanation, the two glutamates are termed E1 and E2 throughout this chapter. The pH-dependent monomer-to-dimer transitions of PsbS are very intriguing as it may play a role in the activation of PsbS since it was reported that PsbS is present in thylakoid membranes as a homodimer in alkaline conditions while at low pH, it is monomeric[1]. However, this was challenged by the dimer structure of PsbS obtained at low pH using X-ray crystallography[9]. Thus, it would be interesting to also explore how the pH-sensing glutamates affect the monomer-dimer transition[10].

From the crystal structure of Spinach-PsbS, the two glutamate residues E1 and E2 are located symmetrically at the luminal amphiphilic loops/helices that connect the two transmembrane helices. Despite the high sequence similarity between the two connecting stretches, they adapt very different conformations[9]. Several intermolecular interactions help to stabilize the dimer structure of PsbS. The X-ray structure of PsbS reveals hydrophobic interactions between the transmembrane helices, 13 hydrogen bonds, one salt bridge and one Arg-Arg pair at the stromal side, and most importantly four hydrogen bonds at luminal side formed by one of the two glutamate residues[9]. These four hydrogen bonds at the luminal side are formed between the carboxyl and carbonyl of E2 and the backbone amide nitrogen of Ile-74 and Tyr-75 from the adjacent monomer[9]. It was indicated from the structure of Spinach-PsbS that structural conformations adopted by luminal loops of monomer PsbS are important for the intermolecular hydrogen bonds.

In Figure 5.1, the structure of PsbS highlighting E1 (green) in the luminal loop region and E2 (red) in the luminal amphiphilic helix (a) and a schematic model (b) of the hydrogen bond formation between E2 and amino acids in the loop of the adjacent monomer are shown.

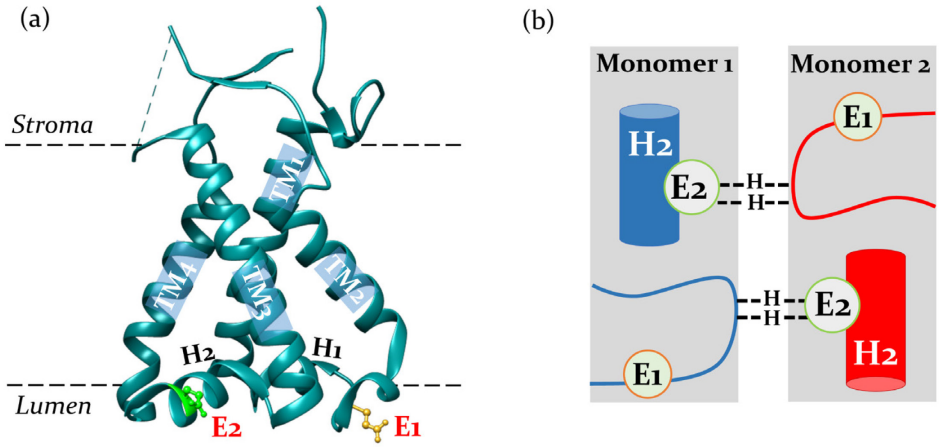

Figure 5.1 (a) Structure of monomer PsbS showing the E1 and E2 residues (Glu-69, Glu-173 for Spinach-PsbS; Glu-71, Glu-176 for Patens-PsbS) that are proposed to be involved in pH-induced conformational changes (b) Schematics of inter-monomer hydrogen bonding between E2 and the loop in the adjacent monomer containing E1 [9].

pH-dependent structural changes in WT PsbS were observed using ^{15}N - ^{1}H HSQC NMR spectroscopy in Chapter 4[11]. However, due to uniform isotope-labelling of PsbS, and due to the large PsbS-detergent micelle size hampering further structural investigation by solution NMR, assignment of the NMR chemical shifts from the Glu-71 and Glu-176 residues were not possible. Here site-directed mutations made at the site of the two active Glu residues have been used to understand the role of E1 and E2 in the pH-dependent PsbS response. This chapter introduces FTIR spectroscopy as a favorable tool to study the pH-dependent structural changes in PsbS using unlabeled samples. FTIR is also favourable over CD spectroscopy, as membrane proteins tend to scatter strongly in the range 190-200 nm in the UV region, which is avoided in FTIR spectroscopy[12].

This chapter outlines the role of E1 and E2 residues in PsbS function, for which two single mutants and one double mutant were created and studied by different spectroscopic techniques. Through NMR and IR spectroscopy it is concluded that the two active Glu residues are non-equivalent in their response to pH. Finally, the pH response mechanism of PsbS is explained in this chapter and was found to depend on protonation of E2.

5.2 Materials and Methods

5.2.1 Creation of mutants, protein expression, refolding and purification

Three plasmids of mutant *P. patens* PsbS were purchased from Baseclear B.V.®. Two single mutants with Glu-71 and Glu-176 replaced by Gln were created and named as M1 and M2 respectively. One double mutant with both Glu at sites 71 and 176 replaced by Gln was created and named as M3. These plasmids were transformed, and the mutant proteins were overexpressed, purified and refolded in FC-12 detergent buffer as per protocols (Chapter 3)[11].

5.2.2 Gel electrophoresis

SDS-PAGE gel electrophoresis analysis (12.5 % running gel, 4 % stacking gel stained with Coomassie brilliant blue R-250 Bio-Rad) was carried out for checking the yields of PsbS at every step of overexpression, purification and refolding. 2.5 µL of Precision Plus Protein™ Dual Color Standard from Sigma was used in all the SDS-page gel.

5.2.3 CD spectroscopy

The secondary folds of the refolded PsbS were analyzed by Jasco J-815 spectropolarimeter (Jasco Labortechnic, Japan) and using a step size of 1 sec/nm, the bandwidth of 1 nm and scanning speed of 100 nm/min. CD spectra were analyzed using BeStSel (Beta Structure Selection[13]) for estimating the content of α-helical, β-sheet and coil or other conformations for each protein sample.

5.2.4 Isotope labelling

For NMR spectroscopy, U-^{13}C ^{15}N labelled PsbS WT and M3 were overexpressed in minimal media using ^{13}C-glucose and ^{15}N-ammonium chloride. Further, they were purified and refolded as per protocols described in Chapter 3. The samples were buffer exchanged to sodium phosphate buffer, pH 7.5 or sodium acetate pH 5.0 in 1 % FC-12 detergent and concentrated using 0.22 µm filters for NMR experiments. Both 1D ^{13}C solid state and solution state NMR along with ^{15}N - ^{1}H HSQC experiments were performed.

5.2.5 NMR spectroscopy

Solution-state NMR spectra were recorded on a Bruker Avance III 600-MHz instrument equipped with a cryoprobe. A standard 1D sequence with ^{15}N decoupling during acquisition was used to obtain 1D ^{1}H NMR data. For the 2D experiments, standard HSQC was performed with 2D H-1/X correlation via double inept transfer with decoupling during acquisition. Parameters for 1D ^{1}H DOSY NMR spectra are described in Chapter 4. For all the experiments, the water signals were suppressed by using a 3-9-19 pulse sequence with gradients.

Solid-state NMR measurements were performed with a Bruker Avance I 750-MHz wide-bore solid-state NMR spectrometer operating at a 17.6 Tesla magnetic strength. In this field, ^{13}C and ^{1}H resonate at 188.66 and 750.23 MHz respectively. A standard 4 mm triple resonance MAS probe was used. The samples were packed in 4 mm zirconium rotors and were spun at the magic angle (54.74°). The spinning frequency was varied between 5 and 13 kHz depending upon the experiment. The temperature was varied from 232 K to 293 K.

Approximately 70 µl of sample volume containing ~8 mg of PsbS was loaded in the 4 mm rotor. The sample was cooled down to the required temperature during slow spinning. With the sample frozen, the spinning frequency was gradually increased to the desired value and kept constant throughout the experiment.

Direct polarization 1D MAS ^{13}C spectra were obtained with 'hpdec' sequence. An acquisition time of 36.2 ms was used. For all the experiments, 1024 scans were acquired with a constant recycle delay of 5 s. A line exponential broadening function of 50 Hz was applied while processing the spectra. ^{13}C spectra were externally referenced to tetramethylsilane.

5.2.6 FTIR spectroscopy

Infrared difference spectra were recorded using an FTIR spectrometer (IFS 66s Bruker) equipped with a nitrogen-cooled photovoltaic Mercury Cadmium Telluride detector (20 MHz, KV100, Kolmar Technologies). The samples were contained between CaF_2 windows separated with a 20 µm Teflon spacer for D_2O buffer and the concentration was tuned for OD ~0.8 absorptions at 1650 cm^{-1}. The measurements were carried out at room temperature and the spectral resolution of the instrument was 3 cm^{-1}.

5.3 Results and Discussion

5.3.1 Refolding and oligomerization

An initial structural analysis was done using CD spectroscopy to verify proper refolding of the PsbS samples. In the appendix, Fig 5A.1 shows that the refolding of PsbS WT and the three mutants M1, M2 and M3 have ~50 % helical structure but have structural variation in their non-helical contents. In particular, there is a more pronounced negative band at 210 nm for the M1 mutant under pH 7.5 conditions. Under pH 5.0 conditions, the samples show a decrease in the peak intensity at 210 nm suggesting they undergo structural changes that are associated with acidification.

PsbS WT and mutants M1, M2 and M3 refolded in 0.1 % FC-12 were analyzed by SDS-PAGE gel electrophoresis at pH 5.0 and pH 7.5 as shown in Figure 5.2. The samples

were loaded on gels both before and after boiling in order to observe any solubilization of dimer structures into monomers due to the boiling step.

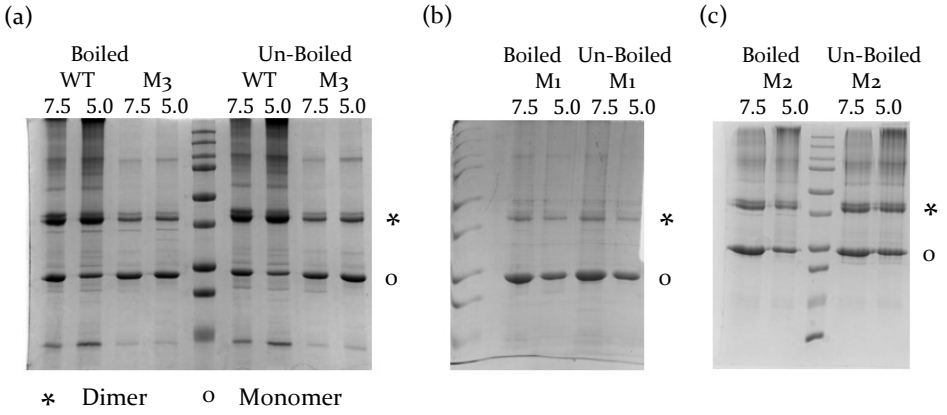

Figure 5.2 SDS gel analysis of WT, M1, M2 and M3 after refolding in 0.1 % FC-12 detergent after boiled and un-boiled conditions under pH 7.5 and pH 5.0 conditions

Figure 5.2 shows that the mutants M2 and M3 form both monomers and dimers, like the WT sample. However, the dimer contents of PsbS in M2 and M3 samples were lower than the dimer content of the WT, which suggests that the dimers were destabilized by the mutations. However, according to the DOSY analysis (Figure 5.5), the size of M3 at pH 5.0 is larger, which suggests that M3 dimers are actually stabilized at low pH. The single mutation of E1 has a more prominent effect on the dimerization of PsbS. According to the SDS page analysis, the M1 samples formed only monomers, suggesting that the mutation E71Q affects the stability of the dimer quite drastically and inhibits dimerization (Figure 5.2b).

5.3.2 Protonation and dynamics of WT and M3

The WT PsbS and double mutant M3 were further analyzed by solid-state and solution-state NMR spectroscopy as presented below. DOSY NMR was used to further characterize the folds and sizes of the PsbS-detergent micelles.

Figure 5.3 shows the 1D ^{13}C solution state NMR spectra of U-^{13}C labelled PsbS WT and M3 at pH 7.5 and pH 5.0 conditions. In the WT spectrum at pH 7.5 conditions, the deprotonated carboxylic acid carbons of the titratable Glu and Asp residues were observed as two peaks centered at 181.9 ppm (accumulated Glu) and 178.4 ppm (accumulated Asp).

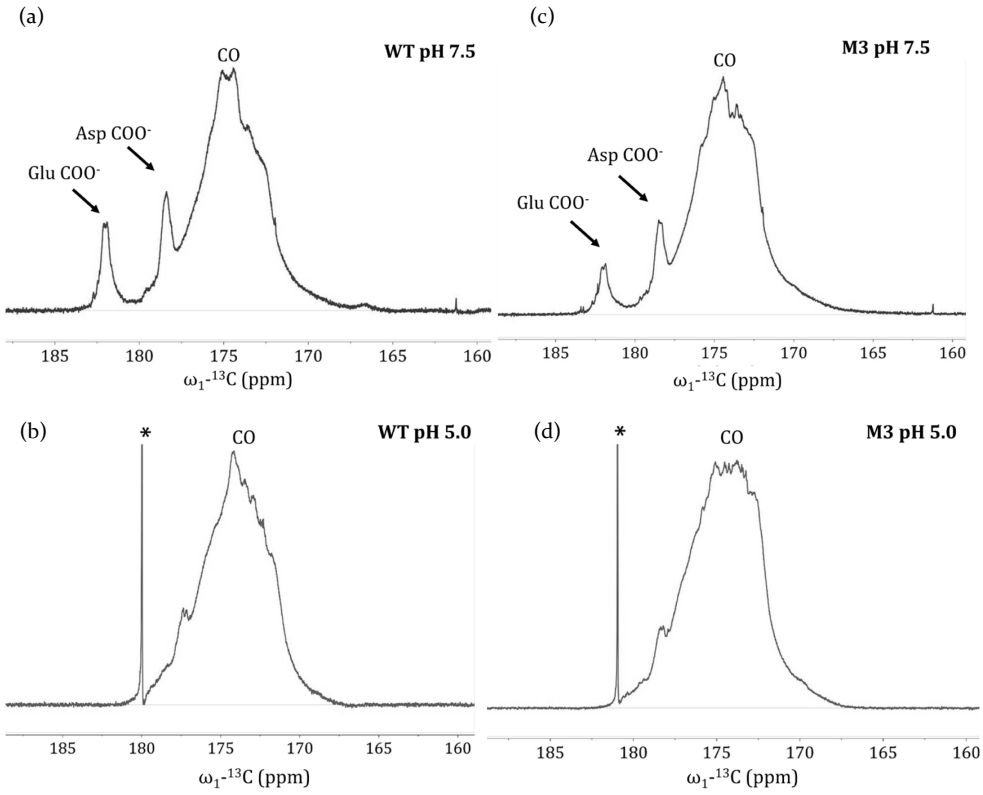

Figure 5.3 1D ^{13}C spectra of WT and M3 at 293 K, neutral and low pH measured using solution NMR showing the carbonyl region and carboxylic acids side chains from Glu and Asp residues.

At pH 5.0 conditions, all the titratable Glu and Asp residues were protonated, which is reflected by the upfield shifting of the carboxyl peaks that are merged with the carbonyl region. Similarly, for mutant M3 all the titratable Glu and Asp residues were protonated at low pH.

Since with solution-state NMR only the mobile parts of PsbS were observed due to its large size in detergent micelles, additional solid state 1D ^{13}C MAS NMR experiments using direct polarization were carried out to observe the effect of change to low pH on the full structure of PsbS. Standard ssNMR experiments apply cross polarization for signal enhancement. However, in cross polarization, magnetization is transferred via dipolar couplings and cross polarization efficiencies are reduced for dynamic molecules with short rotational correlation times because the dipolar couplings are averaged to zero during the pulse experiment. Direct polarization NMR is efficient over the whole dynamics range and therefore direct polarization experiments were suitable for the samples of PsbS in detergent micelles that are too dynamic for

detection by cross polarization-MAS NMR and too large for full detection by solution-state NMR.

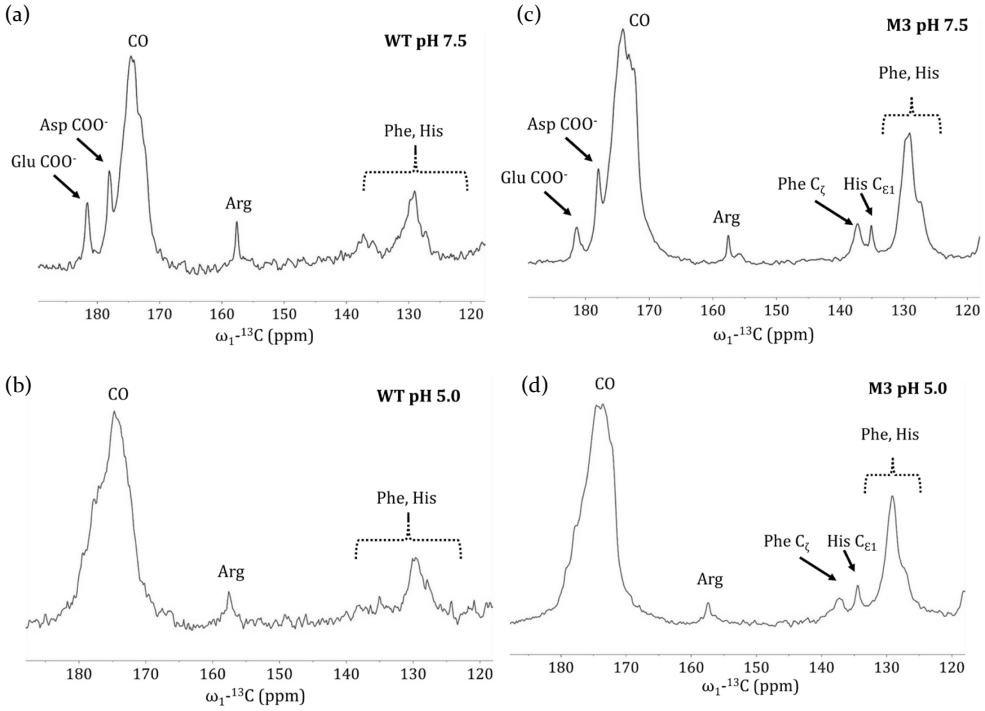

Figure 5.4 1D ^{13}C spectra of WT and M3 at 293K, neutral and low pH measured using solid-state NMR showing the carbonyl region, carboxylic acids side chains and aromatic side chains.

Figure 5.4 shows the 1D 13C Direct Polarization NMR spectra of WT and M3 in pH 7.5 and 5.0 conditions. The backbone carbonyl peak (180 - 170 ppm), carboxylic acid carbons of Glu and Asp (181.5 and 178.1 ppm) and aromatic side chain atoms from Phe ring (Cδ1, Cδ2, Cε1, Cε2, Cɣ) and His residues (~128 to 137 ppm) along with a peak from the Arg residues (~158 ppm) can be identified in the spectra as indicated.

Differences in the carbonyl peak of PsbS comparing the WT and M3 sample at pH 7.5 or at pH 5.0 show that the E1 and E2 mutation in mutant M3 has an effect on the secondary structure of the protein. Changing the pH from pH 7.5 to 5.0, both WT and M3 show changes in the carbonyl region indicating that the proteins undergo conformational changes in their secondary structure upon acidification.

At pH 7.5, two clear peaks were observed of deprotonated Glu and Asp carboxyl acid side chains (Figure 5.4a). At pH 5.0, these peaks were shifted upfield and overlap with the large 13C' peak centered at 175 ppm of the protein carbonyls, indicating that all the 23 protonatable residues of PsbS (Asp and Glu) are protonated at pH 5.0 (Figure 5.4b). The shape of the carbonyl 13C' band of the M3 mutant differs from the WT, both at pH 7.5 and at pH 5.0 (Figure 5.4 c,d, respectively), which indicates that there are differences between the secondary structure of the WT and the M3 mutant, with more coil structure for the M3 mutant. This protonation effect was also observed in the solution state NMR spectra (Figure 5.3) where only the dynamic parts of the protein could be measured. However, the solid-state NMR spectra confirm that protonation of all the titratable Glu and Asp residues occurs at pH 5.0 for both the WT and M3. The peak of the accumulated Glu at 181.5 ppm in the M3 spectrum at pH 7.5 shows less intensity relative to the carbonyl peak as compared to the WT spectrum, in agreement with the fact that two Glu residues were mutated.

From Figure 5.4, insights into the dynamics of aromatic amino acids (140 - 120 ppm) can be obtained. PsbS contains 3 Arg and 18 Phe residues. Additionally, the recombinant PsbS contains 6 His residues at the N-terminus. The aromatic side chain atoms from Phe (Cδ1, Cδ2, Cε1, Cε2, Cγ Cζ) or His (Cε1, Cγ) residues were observed between 120 - 140 ppm. Remarkably, the Phe ring signals have more intensity in the M3 spectrum than for the WT. The direct polarization signals should not be sensitive to dynamics, but if the Phe rings flip slowly between two conformations, the NMR peaks would broaden and intensities would be reduced[14,15]. The differences in Phe intensity between the WT and M3 were, therefore, attributed to differences in the dynamics of the Phe rings. The Phe NMR signal intensities do not change with pH, which means that the Phe dynamics was not influenced by the pH lowering.

The Arg Cζ peak that for both WT and M3 mutant appears at 160.3 ppm has lower intensity and was broadened at low pH, which suggests increased heterogeneity in the environment or structural conformation of the Arg residues. This is an interesting observation as one of the Arg residues is involved in stabilizing PsbS dimer via a hydrogen bond[9].

Furthermore, DOSY NMR experiments were carried out on the M3 samples at pH 7.5 and pH 5.0 and compared with the WT pH 7.5 sample (shown in Figure 5.5). The plot of the NMR intensity versus the magnetic gradient field strength is used to estimate the value of the lateral diffusion coefficient, D_t . The value of D_t is directly related to the diameter of particles according to the Stokes-Einstein equation as described in Chapter 4. Comparing the D_t values for all three samples in Figure 5.5 showed that

WT and M3 at pH 7.5 have smaller sizes than M3 pH 5.0 sample. The M3 sample at pH 5.0 has a D_t value similar to WT at pH 5.0 (Table 5.1). The M3 sample at pH 7.5 has the largest D_t value, *i.e.* smaller particle size, suggesting more monomers.

According to data in Table 5.1, the WT PsbS shows very little size variation with pH difference whereas M3 sample shows a significant reduction in diameter size at high pH conditions. The plots in Figure 5.5 collected at pH 7.5 had to be analysed with two diffusion components. The largest diffusion component contains the actual diffusion coefficient reflecting the Stokes diameter sizes of the protein particles and is also given in Table 5.1, while the steep decay component arises from proton exchange at water exposed sites of the PsbS, reflecting the diffusion of protons. The presence of a steep decay component in the DOSY curves at pH 7.5 of M3, similar to DOSY curve of WT, suggests that M3 adopts a loose structure at pH 7.5 with several water-exposed sites. This steep component is not observed in the DOSY curve of M3 at low pH, suggesting that the M3 adopts a less loose structure at low pH, which was also observed for the WT in Chapter 4.

Table 5.1 Estimated D_t values (standard deviation between brackets) based on DOSY $^{-1}$H NMR H_N intensities for PsbS WT at pH 7.5 and M3 at pH 7.5 and at pH 5.0 in Fc-12 conditions

	D_t (m^2s^{-1}) at H_N
PsbS WT pH 7.5	$4.2 * 10^{-11}$ ($3.2 * 10^{-12}$)
PsbS WT pH 5.0 *(Chapter 4)*	$3.9\ 10^{-11}$ ($3.8\ 10^{-12}$)
PsbS M3 pH 7.5	$5.1 * 10^{-11}$ ($4.6 * 10^{-12}$)
PsbS M3 pH 5.0	$3.9 * 10^{-11}$ ($4.0 * 10^{-12}$)

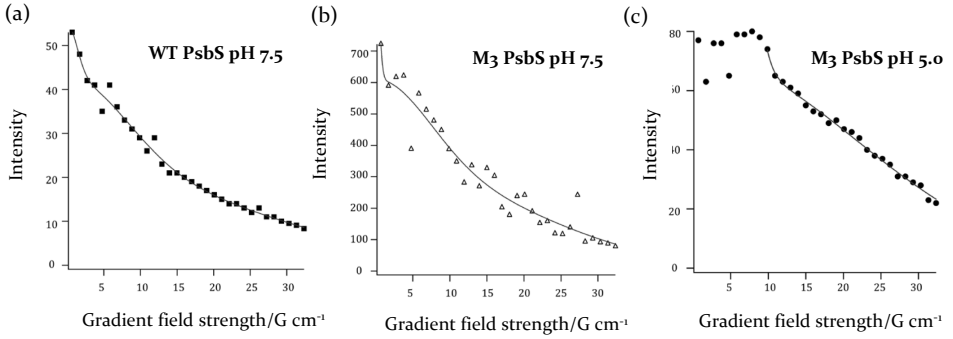

Figure 5.5 Comparison of DOSY NMR experiments on WT at pH 7.5 (a) and M3 samples at pH 7.5 (b) and pH 5.0 conditions (c).

To further observe the structural changes in the amide region due to the change to low pH, 2D ^{15}N - ^{1}H HSQC solution NMR spectra were collected of U - ^{15}N labelled WT and M3 samples. Figure 5.6 shows that, at low pH conditions, more signals were visible in WT and M3 spectra, suggesting that PsbS adopts a more defined structure with less dynamics or disorder for both the WT and the mutant. HSQC is a solution state NMR experiment and can only observe the dynamic parts of the PsbS. In the case of PsbS, since it is surrounded by Fc-12 detergent micelles, the overall size is large for solution NMR to detect the protein amides of the transmembrane parts.

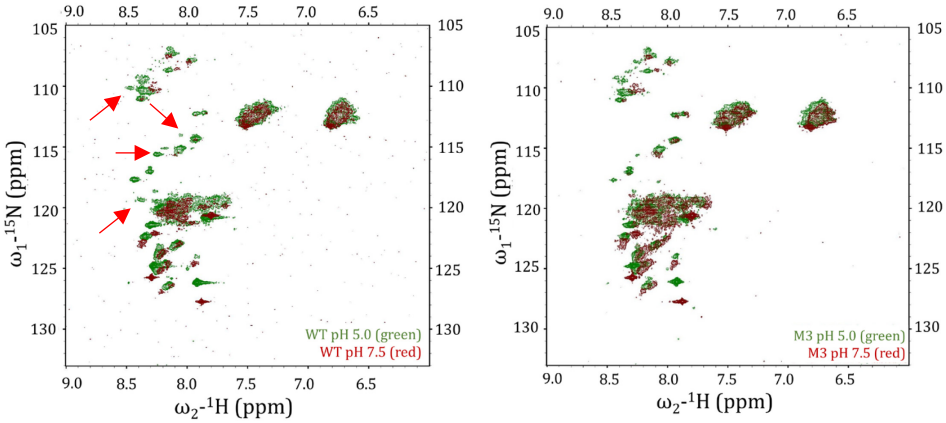

Figure 5.6 2D ^{15}N - ^{1}H HQSC NMR spectra of WT and M3 at pH 7.5 (red) and pH 5.0 (green). The red arrows indicate peaks that are observed for the WT at low pH but are missing in the M3 spectrum.

Hence, the HSQC spectra are expected to be dominated by signals coming from the flexible stromal loops. Some of the peaks that appear only at low pH in the WT spectrum and absent in the M3 spectrum (red arrows). The overall comparison suggests that the flexible parts of PsbS undergo similar structural changes due to change to low pH.

From the NMR analysis, it was concluded that for both WT PsbS and the M3 mutant, all the titratable Glu and Asp residues protonated when the pH was lowered to pH 5.0 and both the WT and M3 mutant undergo changes in the secondary structure and protein dynamics at low pH.

In the next part, IR spectroscopy experiments were carried out to determine the individual role of the two active Glu residues in the PsbS structural response to pH. Figure 5.7 shows the 1D FTIR spectra of WT PsbS and of the M1, M2 and M3 mutants at low and at neutral pH (black and red), together with the pH difference spectra (in green).

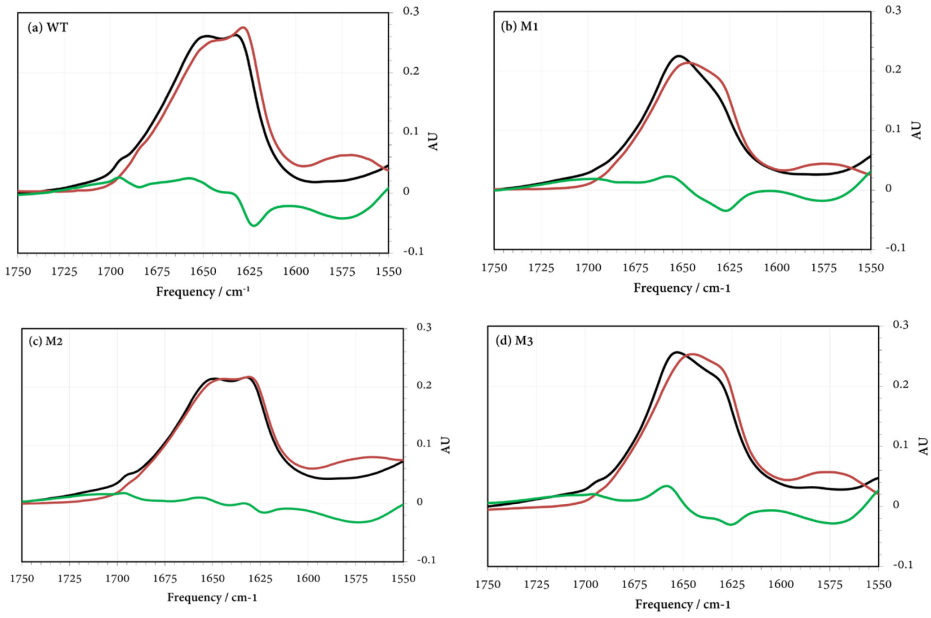

Figure 5.7 1D FTIR spectra showing the Amide I region, at pH 7.5 (red line), pH 5.0 (black line) and IR difference spectra (pH 5.0 minus pH 7.5, green line) for WT PsbS (a), M1 (b), M2 (c) and M3 (d).

The FTIR spectrum of the WT PsbS at pH 7.5 (Figure 5.7a, red line) shows a band at ~1570 cm^{-1} that corresponds to vibrations of carboxylic acids from deprotonated Glu and Asp residues. Upon protonation, this band disappeared and a shoulder appeared in the region 1700 - 1690 cm^{-1}. This can be observed in the spectrum of PsbS at pH 5.0 condition (black line). The same protonation effect can be observed in the spectra of the three mutants (Figure 5.7 b, c, d). This indicates that at low pH, all Glu and Asp were protonated, in agreement with the NMR data results. The Amide I band vibrations of the CO stretch are observed in the region 1600 to 1700 cm^{-1} and are representative of the protein backbone conformation[16]. In the amide I IR spectrum contributions of α helices, β sheet and turns can be distinguished based on their different CO stretch frequencies[17]. Turns and α helices have amide I frequency maxima at ~1680 cm^{-1} and ~1650 cm^{-1} respectively, while β sheet contents have lower amide I frequencies. The Amide I spectrum of WT PsbS has a dominant peak at ~1650 cm^{-1} that is representative of helix structure, in addition to a sharp shoulder peak centered at 1630 cm^{-1}. In the Amide I spectra of the M1 and M3 mutants, this shoulder was broadened and the overall shape of the Amide I was different, which indicated that both M1 and M3 have a secondary structure that differs from that of the WT protein, which corresponds to conclusions from Figure 5.4. In the M2 mutant, the distinct

shoulder peak at 1630 cm^{-1} was preserved and remarkably no significant structural change was observed in the amide I region with a change in pH.

The difference spectra of pH 5.0 and pH 7.5 (green line) show changes that occur in the secondary structure of PsbS upon lowering of the pH. Between the range of 1690 and 1650 cm^{-1} positive structural gain while at ~1630 cm^{-1} the disappearance of structural character due to the pH change to pH 5.0 can be observed for WT M1 and M3 but not for M2. The positive bands appearing were due changes in the turns and loops, while at ~1630 cm^{-1} the negative band appearing can be attributed to arise from the disappearance of low vibrational frequency α-helixes[12,18].

5.3.3 Discussion - the role of active Glu residues

Monomer/dimer content of wild-type and mutant PsbS

To interpret the observed pH-dependent changes observed in WT PsbS and the M1, M2 and M3 mutants, the crystal structure of Spinach-PsbS was used as a starting reference, which represents PsbS at low pH[9]. In the crystal structure, E1 (Glu-69 in the X-ray structure) is located in a luminal loop that connects two transmembrane helices TM1 and TM2, whereas E2 (Glu-173 in the X-ray structure) is located in the amphipathic short helix H2 at the water-membrane interface facing the lumen, and connects TM3 and TM4 (Figure 5.1). In the PsbS structure, the backbone carbonyl and side chain carboxyl of E2 each can form a hydrogen bond with two backbone amides of Ile-74 and Tyr-75 in the luminal loop of the adjacent monomer. The residues Ile-74 and Tyr-75 are part of a short 3-10 helix fragment. In Patens-PsbS, the latter two amino acids are Leu-74 and Thr-75. At the luminal side, the dimer is stabilized by four hydrogen bonds, connecting E2 in the amphipatic helix H2 (Glu-173 or Glu-176 in Spinach-PsbS, resp. Patens-PsbS) of monomer 1 to the luminal loop, which contains E1 (Glu-69 or Glu-71 in Spinach-PsbS, resp. Patens-PsbS) of monomer 2 and *vice versa*.

The M1 mutant is strongly impaired in dimerization (Figure 5.2b), even though E1 is not close to the dimer interface and in fact, is at the exterior side of the PsbS dimer as shown in Figure 5.1. Yet, as mentioned, this residue is part of the luminal loop that is connected to E2 of the adjacent monomer via two hydrogen bonds. The highly reduced dimer content of M1 at acidic and neutral pH conditions suggests that the site of E1 has an allosteric effect on the dimerization of PsbS. Possibly, substitution of this residue by Gln may re-orient the luminal loop, disrupting the inter-monomer hydrogen bonds to E2.

The M2 mutant is still capable of dimer formation, even though this mutant lacks E2 that is involved in forming two inter-monomer hydrogen bonds to two amide NH groups of the adjacent monomer (Figure 5.1). This can be explained since in the M2

mutant, E2 is substituted by Gln, which contains a side chain carbonyl that is equally capable of receiving a hydrogen, whilst the H bond involving the E2 backbone carbonyl can equally be formed by the Gln backbone carbonyl.

Assignment of wild-type PsbS conformational changes to re-positioning of amphipatic helix H2

The origin of the Amide I difference signals observed in FTIR spectroscopy will be discussed now, which indicate conformational changes in the secondary structure. In FTIR, a distinct negative/positive Amide I signal at 1625 (-) or 1660 (+) cm^{-1}, and a positive-going shoulder at 1638 cm^{-1} in WT PsbS was observed (Figure 5.7). This signal is also reflected and refined in 2DIR spectroscopy, where loss of a helical signal at 1630 cm^{-1} is accompanied by gain of two distinct helical signals at 1638 cm^{-1} and 1660 cm^{-1} at comparable amplitude (appendix Fig 5A.2). Strikingly, mutation of M2 almost completely abolishes the structural Amide I response of PsbS to low pH (Figure 5.7c). This observation reveals that the lumen-facing amphipatic helix H2 that contains E2 (Figure 5.1) likely represents the site of plasticity that undergoes a pH-dependent structural change and is responsible for the characteristic FTIR signals. This assignment is consistent with the FTIR amplitude of the difference signal in WT PsbS, which corresponds to at least 8 amino acids, which agrees with the length of the H2 helix in the X-ray structure, 9 amino acids[9]. It must be noted that the 1625 cm^{-1} signal is partly compensated by a positive signal at 1638 cm^{-1}, which implies that the number of involved amino acids probably is somewhat larger than 8.

Because E2 is negatively charged at neutral pH, it is expected that at pH 7.5, the polar side of the amphipatic helix H2 will be stabilized at the aqueous environment of the lumen, consistent with the low frequency (1630 cm^{-1}) of the helical element detected at that pH (pD). At pH (pD) 5.0, two populations of helical elements were detected with comparable amplitudes, with frequencies of 1660 and 1638 cm^{-1}. The helical signal at 1660 cm^{-1} clearly indicates a hydrophobic environment. Therefore, in this chapter, it is proposed that protonation of E2 at low pH causes the H2 helix to re-position from the aqueous phase into the membrane phase, as schematically illustrated in Figure 5.8. The 1638 cm^{-1} helical signal detected at pH (pD) 5.0 indicates a remaining degree of solvent exposure, suggesting that a fraction of the H2 helices undergoes incomplete movement into the hydrophobic phase. The observation of this incompletely moving fraction of H2 helix may relate to the less-well defined demarcation between aqueous and hydrophobic phase in detergent micelles as compared to a lipid bilayer environment.

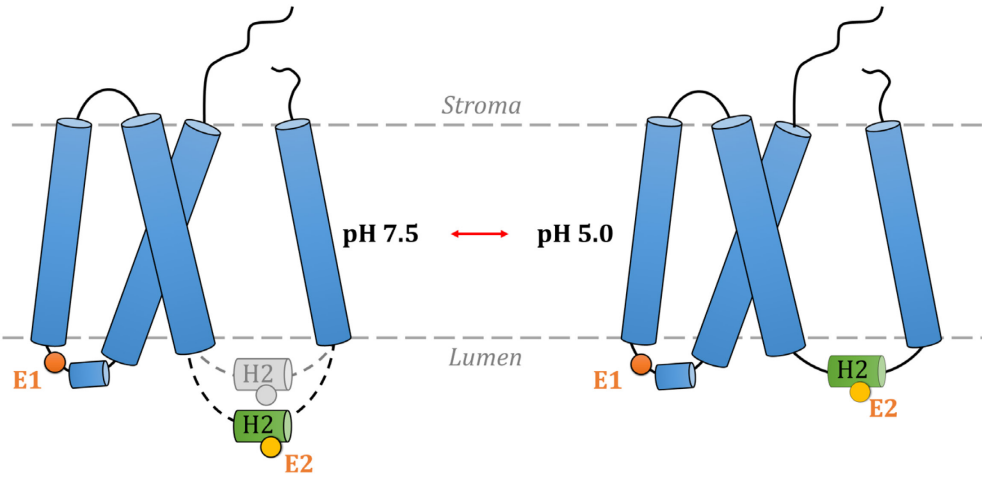

Figure 5.8 A model proposing the repositing of short helix H2 from aqueous phase to membrane phase due to protonation of E2 at low pH

The idea of helix H2 re-positioning into the membrane phase at low pH is consistent with low pH crystal structures obtained from crystals that were soaked with DCCD, a hydrophobic compound that binds to carboxyl groups of protonated amino acids that are shielded from aqueous environments. The DCCD was used to detect protonation sites of PsbS in the crystal structure[9]. The DCCD-soaked structure shows that DCCD binds to E2 (Glu-173 in Spinach-PsbS), indicating that in the low-pH conformation, this Glu residue indeed resides in a hydrophobic environment[9].

Possibly, the displacement of helix H2 causes a change of hydrogen bond interactions with the loop containing E1 that connect TM1 and TM2 (Figure 5.1), which in turn may affect the PsbS monomer/dimer equilibrium. The WT PsbS has somewhat larger dimer content on gel at low pH, which suggests that re-positioning of H2 into the hydrophobic phase strengthens the inter-monomer hydrogen bonding interactions. Results from Chapter 4 suggested that dimer contents of PsbS in detergent solutions changed over time, and in fact it was observed that after several days the dimer content would be larger at neutral pH than at low-pH solutions[11]. Here, the analysis was performed on freshly prepared samples. From molecular-dynamics simulations, it has been proposed that at high pH, hydrogen bonds are formed between E173 and T162 of the adjacent monomer that are destabilized at low pH[19]. In this light, re-positioning of H2 at low pH may strengthen specific hydrogen-bond interactions while weakening others, delicately controlling the stability of PsbS dimers.

In the M2 mutant, the charge at the E2 site is neutralized by the Glu to Gln mutation, which predicts that M2 PsbS will already adopt a low-pH conformation at neutral pH. This is exactly what is observed, since the Amide I FTIR spectrum of M2 at both pH conditions resembles the low-pH spectrum of the WT (Figure 5.7a,c).

The IR spectrum of M1 does not resemble the WT IR spectrum at low or neutral pH, indicating that part of the M1 PsbS mutant adopts a non-native fold. The luminal loop containing E1 contains an additional conserved, second Glu close to TM2 (Glu-76 for Spinach-PsbS and Glu-78 for Patens-PsbS), and for Patens-PsbS, also contains an Asp residue (Asp-69). At neutral pH, those residues will have a negative charge, while in M1 and M3 the E1 site is neutralized by Gln replacement, resulting in a charge distribution along the luminal loop stretch that neither reflect the luminal loop charges of WT PsbS at neutral pH, nor reflects the loop charges of the WT at low pH conditions. This may lead to a non-native fold of the luminal loop stretch in M1 and M3, accounting for the difference in secondary structure compared to the WT. The collective effect of E1 and E2 mutation may produce a moderated PsbS structure, in which the substituted Gln at the E2 helix site is capable of interacting with the modified loop of the adjacent monomer, which could explain why dimers are more stabilized in M3 than in M1.

The question that now arises concerns the relation of the pH-dependent H2 helix displacement with the PsbS functional switch and the next challenge will be to relate the conformational switch to the PsbS function *in vivo* in interaction with key constituents of the thylakoid membrane. PsbS is a member of the LHC family, of which proteins form pH switches (namely PsbS and LHCSR) and/or photoprotective switches that can alternate between fluorescent and excitation-quenched states (namely LHCII and LHCSR). LHCs share a structure in which transmembrane helices are connected via amphipatic short helices at the luminal site[4,21–23]. Responsiveness of the amphipatic helices to changes in pH, hydrophobicity or other alterations in the physico-chemical environment might be a common motif that enables LHCs to operate as molecular controls for regulating photosynthetic light harvesting.

5.4 Conclusion

Summarizing, it was discovered that the two active Glu sites respond non-equivalently to lowering of the pH. The luminal loop containing E1 has an allosteric effect on PsbS dimerization. E2 is responsible for the structural response of PsbS to lowering the pH, most likely by a re-positioning of the amphipatic short helix fragment H2 from the aqueous phase into the membrane phase, thereby becoming less ordered. Single-point mutations of E1 and E2 in PsbS have been reported to severely reduce NPQ activity[6], implicating that both dimerization and flexibility of the amphipathic short helix stretch H2 are important for PsbS function. The M2 mutant represents the low-pH state of PsbS, which is the active state. Reduced NPQ activity of this mutant in plants suggests that not the activation of PsbS, but its ability to switch on and off is crucial for its function. Indeed, PsbS is not only involved in switching on NPQ, but also essential for rapid de-activation and recovery of this process in fluctuating light conditions[20].

5.5 References

1. Bergantino, E. *et al.* Light- and pH-dependent structural changes in the PsbS subunit of photosystem II. *Proceedings of the National Academy of Sciences of the United States of America* **100,** 15265–15270; 10.1073/pnas.2533072100 (2003).
2. Bonente, G., Howes, B. D., Caffarri, S., Smulevich, G. & Bassi, R. Interactions between the photosystem II subunit PsbS and xanthophylls studied in vivo and in vitro. *Journal of Biological Chemistry* **283,** 8434–8445; 10.1074/jbc.M708291200 (2008).
3. Niyogi, K. K., Li, X. P., Rosenberg, V. & Jung, H. S. Is PsbS the site of non-photochemical quenching in photosynthesis? *Journal of Experimental Botany* **56,** 375–382; 10.1093/jxb/eri056 (2005).
4. Li, X. P. *et al.* A pigment-binding protein essential for regulation of photosynthetic light harvesting. *Nature* **403,** 391–395; 10.1038/35000131 (2000).
5. Dominici, P. *et al.* Biochemical properties of the PsbS subunit of photosystem II either purified from chloroplast or recombinant. *Journal of Biological Chemistry* **277,** 22750–22758; 10.1074/jbc.M200604200 (2002).
6. Li, X. P. *et al.* Regulation of photosynthetic light harvesting involves intrathylakoid lumen pH sensing by the PsbS protein. *Journal of Biological Chemistry* **279,** 22866–22874; 10.1074/jbc.M402461200 (2004).
7. Li, X. P., Phippard, A., Pasari, J. & Niyogi, K. K. Structure-function analysis of photosystem II subunit S (PsbS) in vivo. *Functional Plant Biology* **29,** 1131–1139; 10.1071/FP02065 (2002).
8. Li, X.-P., Gilmore, A. M. & Niyogi, K. K. Molecular and global time-resolved analysis of a psbS gene dosage effect on pH- and xanthophyll cycle-dependent nonphotochemical quenching in photosystem II. *The Journal of biological chemistry* **277,** 33590–33597; 10.1074/jbc.M204797200 (2002).
9. Fan, M. *et al.* Crystal structures of the PsbS protein essential for photoprotection in plants. *Nature structural and molecular biology* **22,** 729–735; 10.1038/nsmb.3068 (2015).
10. Barbara Demmig-Adams, Gyozo Garab, William Adams III, Govindjee. *Non-Photochemical Quenching and Energy Dissipation in Plants, Algae and cyanobacteria. Chapter 13 PsbS-Dependent Non-Photochemical Quenching* (Springer US, 2014).
11. Krishnan, M., Moolenaar, G. F., Gupta, Karthick Babu Sai Sankar, Goosen, N. & Pandit, A. Large-scale in vitro production, refolding and dimerization of PsbS in different microenvironments. *Scientific Reports* **7,** 1–11; 10.1038/s41598-017-15068-3 (2017).
12. Jörg H. Kleinschmidt. *Methods in Molecular Biology - Lipid-Protein Interactions. Chapter 9 : Structural Characterization of Membrane Proteins and Peptides by FTIR and ATR-FTIR Spectroscopy* (2013).
13. Micsonai, A. *et al.* Accurate secondary structure prediction and fold recognition for circular dichroism spectroscopy. *Proceedings of the National Academy of Sciences of the United States of America* **112**; 10.1073/pnas.1500851112 (2015).
14. Schaefer, J., Stejskal, E.O., McKay, R.A. & Dixon, W.T. Phenylalanine ring dynamics by solid-state 13C NMR. *Journal of Magnetic Resonance (1969)* **57,** 85–92; 10.1016/0022-2364(84)90236-1 (1984).

15. Gibson, J. M., Popham, J. M., Raghunathan, V., Stayton, P. S. & Drobny, G. P. A solid-state NMR study of the dynamics and interactions of phenylalanine rings in a statherin fragment bound to hydroxyapatite crystals. *Journal of the American Chemical Society* **128,** 5364–5370; 10.1021/ja056731m (2006).

16. Byler, D. M. & Susi, H. Examination of the secondary structure of proteins by deconvolved FTIR spectra. *Biopolymers* **25,** 469–487; 10.1002/bip.360250307 (1986).

17. Susi, H. & Byler, D. M. Resolution-enhanced Fourier transform infrared spectroscopy of enzymes. *Methods in Enzymology* **130,** 290–311 (1986).

18. Reisdorf, W. C. & Krimm, S. Infrared amide I' band of the coiled coil. *Biochemistry* **35,** 1383–1386; 10.1021/bi951589v (1996).

19. Daskalakis, V. & Papadatos, S. The Photosystem II Subunit S under Stress. *Biophysical journal* **113,** 2364–2372; 10.1016/j.bpj.2017.09.034 (2017).

20. Kromdijk, J., Głowacka, K., Leonelli, L., Gabilly, S. T., Iwai, M., Niyogi, K., Long, S. P. Improving photosynthesis and crop productivity by accelerating recovery from photoprotection. *Science* **354,** 857–860 (2016).

21. Wei, X. *et al.* Structure of spinach photosystem II–LHCII supercomplex at 3.2 Å resolution. *Nature* **534,** 69–74; 10.1038/nature18020 (2016).

22. Pan, X. *et al.* Structural insights into energy regulation of light-harvesting complex CP29 from spinach. *Nature structural & molecular biology* **18,** 309–315; 10.1038/nsmb.2008 (2011).

23. Standfuss, J., van Terwisscha Scheltinga, A. C., Lamborghini, M. & Kühlbrandt, W. Mechanisms of photoprotection and nonphotochemical quenching in pea light-harvesting complex at 2.5 A resolution. *The EMBO Journal* **24,** 919–928; 10.1038/sj.emboj.7600585 (2005).

5.6 Appendix 5A

Fig 5A.1 CD spectroscopy of WT, M1, M2 and M3 mutants under pH 7.5 and pH 5.0 conditions at 1 % FC-12.

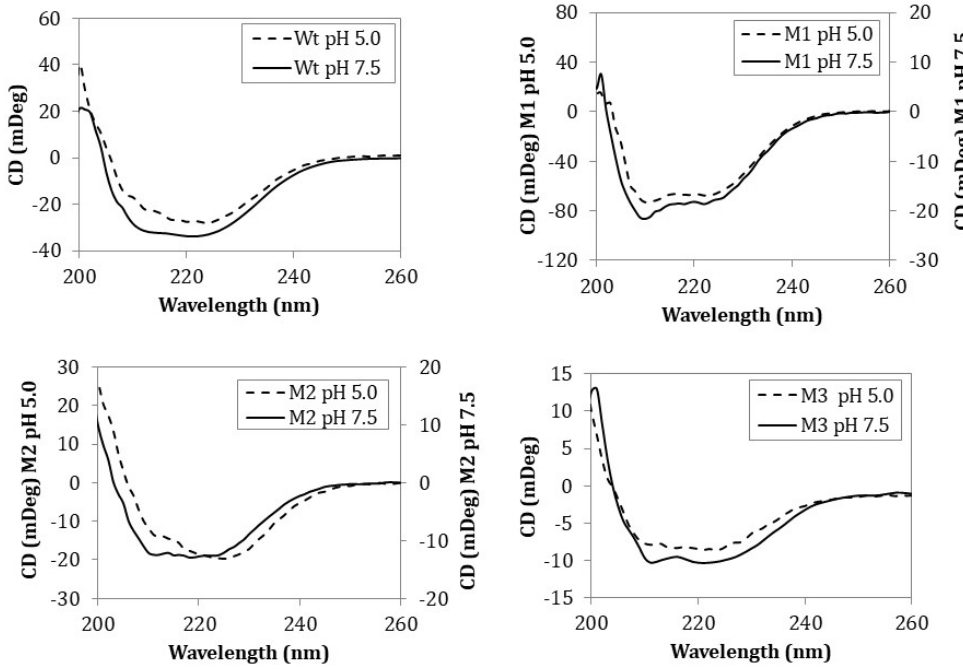

[Results from collaboration with VU Amsterdam]

Fig 5A.2 (a) Steady-state 2DIR correlation spectrum at T=400 fs of WT PsbS in pD 7.5 buffer. (b) pD 5.0 – pD 7.5 difference 2DIR of WT PsbS, thereby scaling the 2DIR spectra on the integrated linear Amide I absorption between 1610 and 1690 cm^{-1} of both samples.

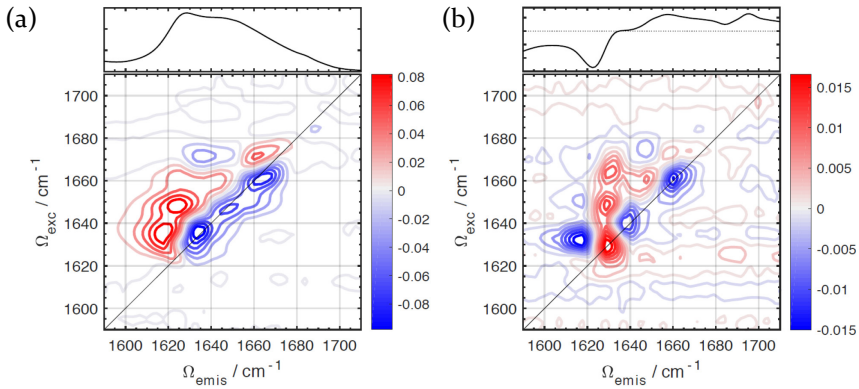

In particular, the negative feature at 1625 cm^{-1} might correspond to either β-sheet or α-helix, and the positive feature at 1660 cm^{-1} could correspond to a helix or a coil/loop. To resolve any ambiguities, two-dimensional IR spectroscopy (2DIR) was applied to PsbS, which has a larger resolving power in this regard.

A quick interpretation of the pD 5.0 minus pD 7.5 difference 2DIR results, considering their frequency, anharmonicity, inhomogeneity, and sign, is as follows:

1. The 1630 cm^{-1} diagonal peak reflects the loss of a single well-ordered helical element in a homogeneous environment and corresponds to the negative signal observed in the difference FTIR spectra.
2. The minor 1638 cm^{-1} diagonal peak represents the gain of a helical element that exhibits a significant degree of conformational disorder.
3. The major 1660 cm^{-1} diagonal peak represents the gain of a helical element with an intermediate degree of conformational disorder.
4. Given that the combined amplitudes of the 1638 and 1660 cm^{-1} diagonal bands are similar to that of the corresponding band at 1630 cm^{-1}, it was concluded that the helical content remains approximately the same at the two pD conditions.

6

Conclusion and Outlook

6.1 Conclusion

PsbS was discovered in 1986[1,2] followed by decades of research to understand its exact role in photoprotection and NPQ. NPQ is PsbS dependent[3] and many models have been proposed for the functional mechanism of PsbS[4,5]. There have been conflicting studies regarding its dimer-monomer transition[4,6,7], localization[8] and interaction with other photosynthetic components[9,10]. Although some insights into the role of PsbS as a photoprotector have been attained[11] from the X-ray crystal structure of Spinach-PsbS[7], the molecular response mechanism of PsbS during the pH lowering still remains unclear.

One of the technical challenges in the structural study of PsbS is the sample preparation for carrying out spectroscopic analyses. Native PsbS is very difficult to isolate and the yield is insufficient for structural characterization. Recombinant PsbS has been produced and refolded[9,12,13] but for spectroscopic techniques like NMR and FTIR, the yields of PsbS expression were low. For carrying out biochemical and spectroscopic studies on PsbS, its production, purification and refolding had to be optimized. As demonstrated in Chapter 3, with the new method, PsbS can be purified with 80 % efficiency as compared to 20 % efficiency by standard protocols that use nickel affinity columns. Particularly while using expensive isotopes for labelling, this purification steps helps in reducing the overall loss and labelling expenditure. In Chapter 3, PsbS was successfully refolded at neutral and low pH conditions using different types of detergents. For refolding of Patens-PsbS, OG and FC-12 were selected as the most suitable detergents for further experiments.

For understanding the molecular mechanism of PsbS, its oligomeric states are important[4]. PsbS has been suggested to be dimeric in alkaline conditions and monomeric in acidic conditions[10,11]. This model was challenged by the crystal structure of dimer PsbS at acidic pH, although the spinach used to isolate and make crystals of PsbS were not grown under high-light stress conditions[7]. In Chapter 4, the oligomeric states of PsbS at neutral and low pH conditions were studied. PsbS under pH 7.5 conditions forms predominantly dimers as compared to pH 5.0 conditions that forms a dimer-monomer equilibrium. Eventually, in both pH conditions, PsbS stabilizes as dimers.

Structural conformational changes in PsbS during pH lowering are hypothesized to be the mechanism of action due to protonation of certain acidic residues at the lumen site of PsbS[14]. HSQC NMR spectra show structural changes of several Gly signals with low pH. A peak of Arg residues appears to be present in the dimer sample and disappears in the monomer sample, suggesting the role of one Arg residue in dimer

formation and to serve as a marker peak in future experiments using NMR spectroscopy.

Mutation of two active Glu residues to Gln (for sake of simplicity, termed as E1 and E2) have shown *in vivo* reduction of NPQ by 60 - 70% [15,16]. To relate pH-dependent conformational changes to the functional mechanism of PsbS, in Chapter 5, three mutants of PsbS were analyzed. The single mutants M1 (E71Q), M2 (E176Q) and double mutant M3 (E71Q, E176Q) of Patens-PsbS were studied. The two Glu residues were proposed to be protonated during pH lowering[14]. Through 1D ^{13}C direct polarization NMR spectroscopy, the protonation of all the titratable Glu and Asp residues were observed. According to the crystal structure of PsbS[7], it is known that the E1 residue resides in the luminal loop that connects the two transmembrane helixes TM1 and TM2, while the E2 resides in an amphipathic short helix between TM3 and TM4 at the water-exposed side towards the lumen. The crystal structure of PsbS also shows that E2 forms hydrogen bonds between its carbonyl and carboxyl group with two backbone amides of amino acids in the adjacent monomer[7]. These hydrogen bonds stabilize the PsbS dimer. From the oligomeric analysis in Chapter 5, the M1 mutant is strongly disabled in dimer formation even though E1 is not residing close to the site of hydrogen bond formation. The highly reduced dimer content in M1, therefore, suggests that there is an allosteric effect of E1 on PsbS dimerization. Mutation of E1 to Gln might re-orient the luminal loop, thereby, disrupting the inter-monomer hydrogen bonds formed by E2.

The M2 mutant, on the other hand, is capable of dimer formation even though it lacks E2 that is involved in inter-monomer hydrogen bond formation. The substituted Gln might be able to form intermonomer hydrogen bonds via the backbone carbonyl and side chain amide. Since the mutant M2 does not show any structural response to pH, it is concluded that the lumen-facing amphipathic helix containing E2 is the site of plasticity that undergoes a pH-dependent structural change. As this glutamate residue is located in the hydrophobic membrane environment in the low-pH crystal structure of PsbS[7], while at neutral pH it resides in the aqueous region due to the negative charges on E2, it is possible that with protonation of E2 at low pH the amphipathic helix could move from water into the membrane phase. The structural conformation of M2 at both neutral and low pH resembles the low-pH conformation of WT PsbS, which is the active state. Reduced NPQ activity of the mutant M2 suggests that the ability to switch on and off during NPQ might be crucial for PsbS function.

The M3 mutant is still capable of forming dimers unlike the M1 mutant while having the same mutation at the E1 site. The FTIR data shows that the conformation of M1 and M3 neither resembles the WT at low pH nor at neutral pH, indicating that

mutation of E1 leads to a non-native fold of PsbS. Mutation of E1, thus, does more than neutralizing charges at the E1 site.

The roles of E1 and E2 in the PsbS response mechanism are non-equivalent. E1 is responsible for dimer formation and E2 brings about conformational changes in PsbS upon pH lowering presumably by a movement of the amphipathic short helix fragment where it is located. As the single mutation of E1 and E2 in PsbS have been reported to severely reduced NPQ activity[15], this implicates that both dimerization and flexibility of the amphipathic short helix stretch are important for the function of PsbS.

6.2 Outlook

The oligomeric state of the recombinant PsbS was explored extensively in Chapter 4 using techniques like SEC, DLS and DOSY NMR. However, the determination of molecular weight or size of membrane proteins like PsbS that are surrounded by detergent micelles is very challenging. SEC combined with multi-angle laser light scattering and a differential refractometer are required for accurate size estimation and analysis of membrane proteins[17]. In an SEC-UV/LS/RI system, the exact molecular weight and the dimerization constant can be determined[18,19]. With the use of these techniques, the pH-dependent oligomerization states of PsbS at neutral and low pH could be determined more accurately in future experiments.

With an NMR chemical shift assignment of the two active Glu residues, it would be possible to resolve their role in the pH-dependent function of PsbS. To assign the two specific peaks of Glu, selective labelling of Glu residues must be carried out. This would reduce the spectral crowding and assignment of the Glu residues would be possible. Alternatively, cell free expression system can be applied to minimize amino acid scrambling during selective labelling.

PsbS interacts with antenna proteins during NPQ and heat dissipation of excess energy takes place[20]. Protein interaction studies in liposomes containing PsbS and LHCII have shown to induce the quenched state of LHCII[12]. Understanding the exact interaction of LHCII and PsbS will help in comprehending the photoprotective function of PsbS in interactions with other membrane components. Reconstitution of isotopic labelled PsbS with unlabelled LHCII protein under varying pH conditions and analysis using NMR spectroscopy could provide a better insight into the interaction of the two proteins.

After characterization of PsbS refolded in detergents[21] (*this thesis*), characterization of PsbS reconstituted in liposomes will be useful to understand how it behaves in a

membrane-like environment. PsbS was reconstituted into liposomes and appeared to be in a monomeric state inside the liposomes, suggesting that the microenvironment is very important for the oligomeric state of PsbS (*Thesis of E. Crisafi*). The next step would be a reconstitution of isotopic labelled PsbS into native thylakoid membrane expressing only LHCII protein (and knocking out major photosynthetic proteins), to carry out NMR studies. This will help in understanding PsbS in its native environment and to understand its function as a photoprotector.

Site-selective mutagenesis studies on PsbS have been carried out to understand which residues are important for its function *in vivo*[15,16]. However, Chapter 5 shows that mutation of one of the active Glu effects the overall structural conformation of PsbS. Thus, it is important to realize that site-selective mutations might result in an improperly folded protein. *In vitro* structural studies as performed in this thesis can be used to test and validate whether PsbS mutants retain their overall fold.

Lastly, it will be important to validate the structural analyses of recombinant PsbS by comparing with analyses from the native PsbS. Sufficient amounts of native PsbS from plants is challenging to isolate. The yields might be difficult to achieve for NMR spectroscopy, but could be achieved for structural characterization by IR or CD spectroscopy.

6.3 References

1. Ghanotakis, D. F. & Yocum, C. F. Purification and properties of an oxygen-evolving reaction center complex from photosystem II membranes. *FEBS Letters* **197,** 244–248; 10.1016/0014-5793(86)80335-0 (1986).

2. Ljungberg, U., Akerlund Hans-Erik & Andersson Bertil. Isolation and characterization of the 10-kDa and 22-kDa polypeptides of higher plant photosystem 2. *European Journal of Biochemistry* **158,** 477–482; 10.1111/j.1432-1033.1986.tb09779.x (1986).

3. Barbara Demmig-Adams, Gyozo Garab, William Adams III, Govindjee. *Non-Photochemical Quenching and Energy Dissipation in Plants, Algae and cyanobacteria. Chapter 13 PsbS-Dependent Non-Photochemical Quenching* (Springer US, 2014).

4. Bergantino, E. *et al.* Light- and pH-dependent structural changes in the PsbS subunit of photosystem II. *Proceedings of the National Academy of Sciences of the United States of America* **100,** 15265–15270; 10.1073/pnas.2533072100 (2003).

5. Niyogi, K. K., Li, X. P., Rosenberg, V. & Jung, H. S. Is PsbS the site of non-photochemical quenching in photosynthesis? *Journal of Experimental Botany* **56,** 375–382; 10.1093/jxb/eri056 (2005).

6. Dominici, P. *et al.* Biochemical properties of the PsbS subunit of photosystem II either purified from chloroplast or recombinant. *Journal of Biological Chemistry* **277,** 22750–22758; 10.1074/jbc.M200604200 (2002).

7. Fan, M. *et al.* Crystal structures of the PsbS protein essential for photoprotection in plants. *Nature structural and molecular biology* **22,** 729–735; 10.1038/nsmb.3068 (2015).

8. Funkapb, C., Schriider, W. P., Greena, B. R., Rengerb, G. & Anderssona, B. The intrinsic 22 kDa protein is a chlorophyll-binding photosystem II subunit of **342,** 261–266 (1994).

9. Bonente, G., Howes, B. D., Caffarri, S., Smulevich, G. & Bassi, R. Interactions between the photosystem II subunit PsbS and xanthophylls studied in vivo and in vitro. *Journal of Biological Chemistry* **283,** 8434–8445; 10.1074/jbc.M708291200 (2008).

10. Correa-Galvis Viviana & Gereon Poschmann , Michael Melzer, Kai Stühler and Peter Jahns. PsbS interactions involved in the activation of energy dissipation in Arabidopsis. *Nature Plants* **2,** 15225–15232; 10.1038/nplants.2015.225 (2016).

11. Sacharz, J., Giovagnetti, V., Ungerer, P., Mastroianni, G. & Ruban, A. V. The xanthophyll cycle affects reversible interactions between PsbS and light-harvesting complex II to control non-photochemical quenching. *Nature Plants* **3**; 10.1038/nplants.2016.225 (2017).

12. Wilk, L., Grunwald, M., Liao, P.-N., Walla, P. J. & Kühlbrandt, W. Direct interaction of the major light-harvesting complex II and PsbS in nonphotochemical quenching. *Proceedings of the National Academy of Sciences of the United States of America* **110,** 5452–5456; 10.1073/pnas.1205561110 (2013).

13. Aspinall-O'Dea, M. *et al.* In vitro reconstitution of the activated zeaxanthin state associated with energy dissipation in plants. *Proceedings of the National Academy of Sciences* **99,** 16331–16335; 10.1073/pnas.252500999 (2002).

14. Niyogi, K. K. & Truong, T. B. Evolution of flexible non-photochemical quenching mechanisms that regulate light harvesting in oxygenic photosynthesis. *Current Opinion in Plant Biology* **16,** 307–314; 10.1016/j.pbi.2013.03.011 (2013).

15. Li, X. P., Phippard, A., Pasari, J. & Niyogi, K. K. Structure-function analysis of photosystem II subunit S (PsbS) in vivo. *Functional Plant Biology* **29,** 1131–1139; 10.1071/FP02065 (2002).

16. Li, X. P. *et al.* Regulation of photosynthetic light harvesting involves intrathylakoid lumen pH sensing by the PsbS protein. *Journal of Biological Chemistry* **279,** 22866–22874; 10.1074/jbc.M402461200 (2004).

17. Bowman, G. R. *et al.* Oligomerization and higher-order assembly contribute to sub-cellular localization of a bacterial scaffold. *Molecular microbiology* **90,** 776–795; 10.1111/mmi.12398 (2013).

18. Yernool, D., Boudker, O., Folta-Stogniew, E. & Gouaux, E. Trimeric subunit stoichiometry of the glutamate transporters from Bacillus caldotenax and Bacillus stearothermophilus. *Biochemistry* **42,** 12981–12988; 10.1021/bi030161q (2003).

19. Kapoor, N. *et al.* Nucleobindin 1 is a calcium-regulated guanine nucleotide dissociation inhibitor of G{alpha}i1. *The Journal of biological chemistry* **285,** 31647–31660; 10.1074/jbc.M110.148429 (2010).

20. Gerotto, C., Franchin, C., Arrigoni, G. & Morosinotto, T. In vivo Identification of Photosystem II Light Harvesting Complexes Interacting with Photosystem II subunit S. *Plant Physiology* **168,** 1747–1761; 10.1104/pp.15.00361 (2015).

21. Krishnan, M., Moolenaar, G. F., Gupta, Karthick Babu Sai Sankar, Goosen, N. & Pandit, A. Large-scale in vitro production, refolding and dimerization of PsbS in different microenvironments. *Scientific Reports* **7,** 1–11; 10.1038/s41598-017-15068-3 (2017).

Summary

Several decades of research on the membrane protein PsbS and PsbS-dependent NPQ have been carried out, yet the exact role of PsbS in qE remains unresolved. Due to conflicting data on dimer-monomer transition, localization, interaction with other components and many unanswered questions about its exact mechanism of action and dynamics, many models are proposed for the role and mechanism action of PsbS during qE. Although the crystal structure of *S. oleracea* PsbS has given more insights about this mysterious thylakoidal membrane protein, the structural dynamics of PsbS is still unclear. This thesis outlines the production of recombinant PsbS followed by several biochemical and spectroscopic techniques to understand the structural dynamics and mechanism of PsbS during pH change due to light stress conditions.

In Chapter 2, the production of PsbS using a cell free expression system is documented. PsbS was produced as both pellet and soluble fraction. Purification of cell free synthesized PsbS was followed by refolding in β-DM detergent that corresponded well with the PsbS produced from *E. coli* shown in Chapter 3.

In Chapter 3, the production of PsbS using *E. coli* was successfully achieved. The overexpression of PsbS was optimized giving a yield of 125 mg/L and additionally using minimal media to label either ^{13}C or ^{15}N in PsbS. Since PsbS was produced as inclusion bodies in *E. coli*, purification steps had to optimized carefully to achieve minimal losses. An urea buffer wash method was developed to achieve 80 % efficiency as compared to 20 % efficiency from nickel affinity columns. Refolding of PsbS from *P. patens*, *A. thaliana* and *S. oleracea* using several detergents like OG, β-DM, Brij-78, FC-12, DHPC and NG were explored to determine the appropriate environmental conditions for right structural refold of PsbS. OG and Fc-12 detergent proved to be the best refolding conditions for *P. patens* PsbS under pH 7.5 and pH 5.0 conditions to carry out biochemical and spectroscopic studies on PsbS.

In Chapter 4, experiments to understand the oligomeric state of PsbS during pH fluctuations were carried out. It was concluded that PsbS under pH 7.5 conditions forms predominantly dimers as compared to pH 5.0 conditions that forms a dimer-monomer equilibrium. However, in both conditions PsbS stabilizes as a dimer after sufficient amount of time. DLS and DOSY NMR was carried out to determine the diameter size of PsbS, that was estimated to be in the range of 10 - 12 nm. HSQC NMR on PsbS showed structural changes of some of the Gly residues at low pH. Additionally, NMR signals of Arg residues disappeared in PsbS monomers. This suggests the role of one of Arg residue in dimer formation.

In Chapter 5, a mutational approach using NMR and FTIR spectroscopy was implemented to understand the role of Glu-71 and Glu-176 residues in PsbS from *P. patens*, that are proposed to be protonated at low pH. The double mutant M3 (E71Q, E176Q) appears to form a loose structure as compared to the wild-type under neutral pH from the DOSY NMR analysis. In the mutant M1 (E71Q), the dimer formation is destabilized as compared to the WT. This suggests that Glu-71, which located in the loop at the luminal side of the membrane, has clearly an important role in dimer formation. Meanwhile the importance of Glu-176 to bring about pH-dependent conformational changes was observed using FTIR spectroscopy. Contrasting to the previous belief, the two glutamate residues Glu-71 and Glu-176 have a different response upon lowering of pH. In additional to this information, protonation of all the glutamate and aspartate residues were observed by both NMR and FTIR spectroscopy.

Samenvatting

Na decennia van onderzoek aan de membraan eiwitten PsbS en PsbS-afhankelijk NPQ is de exacte rol van PsbS bij qE nog altijd onbekend. Dankzij conflicterende data over de dimeer-monomeer transitie, de lokalisatie en interactie met andere componenten, is een groot aantal modellen voorgesteld voor de rol en werking van PsbS bij qE. Ondanks dat de kristalstructuur van *S. oleracea* PsbS meer inzicht geeft in dit mysterieuze eiwit uit het thylakoïde membraan, is de structurele dynamiek nog onduidelijk. Dit proefschrift beschrijft de productie van recombinant PsbS en de karakterisatie door middel van biochemische en spectroscopische technieken. Om zodoende, de structurele dynamiek en werking van PsbS te begrijpen bij pH veranderingen veroorzaakt door licht stress.

In hoofdstuk 2 wordt de productie van PsbS beschreven aan de hand van een cel vrij expressie systeem. Zodoende werd PsbS in oplosbare en geaggregeerde vorm geproduceerd. Cel vrij geproduceerd PsbS is gezuiverd en hervouwen in aanwezigheid van β-DM detergens. De integriteit van het hervouwen PsbS is in goede overeenkomst met recombinant PsbS geproduceerd in *E. coli*.

In hoofdstuk 3 is de recombinante productie van PsbS in *E. coli* beschreven. De overexpressie is geoptimaliseerd en resulteerde in 125 mg/L PsbS. Minimaal media werden gebruikt om ^{13}C of ^{15}N gelabeled PsbS te produceren. De productie van PsbS in inclusion bodies vereiste zorgvuldige optimalisatie om verlies van eiwit te voorkomen. Een ureum buffer wasmethode werd ontwikkeld met een efficiëntie van 80 % in verhouding tot 20 % efficiëntie verkregen met traditionele nikkel kolom zuivering. Hervouwing van PsbS van *P. patens, A. thaliana* en *S. oleracea* is onderzocht in aanwezigheid van verschillende detergenten zoals OG, β-DM, Brij-78, Fc-12, DHPC en NG. De detergenten OG en FC-12 resulteerde bij pH 7.5 en pH 5. in de beste condities voor hervouwing van *P. patens* PsbS voor biochemisch en spectroscopisch onderzoek.

In hoofdstuk 4 zijn experimenten uitgevoerd om de oligomerisatie toestand van PsbS te begrijpen. Uit deze experimenten is geconcludeerd dat PsbS bij pH 7.5 voornamelijk dimeren vormt en dat er bij pH 5.0 een dimeer-monomeer evenwicht ontstaat. In beide gevallen stabiliseerde PsbS als dimeer na verloop van tijd. DLS en DOSY NMR werden gebruikt om de diameter van de PsbS dimeer te bepalen. Een diameter in de orde van grootte van 10-12 nm werd vastgesteld. HSQC NMR met PsbS toonde structurele veranderingen van enkele van de glycine residuen bij lage pH. Verder verdwenen de NMR signalen van Arg residuen in PsbS monomeren, wat duidt op de betrokkenheid van Arg bij de formatie van PsbS dimeren.

In hoofdstuk 5 werden mutaties van PsbS in combinatie met NMR en FTIR spectroscopie gebruikt om de rol van Glu-71 en Glu-176 in *P. patens* PsbS te bepalen. Het is voorgesteld dat deze residuen geprotoneerd zijn bij lage pH. Uit de DOSY NMR analyse bij neutrale pH bleek de dubbel mutant M3 (E71Q, E176Q) een flexibelere structuur te hebben ten opzichten van het wild-type. PsbS dimeer formatie is bij de mutant M1 (E71Q) belemmerd in vergelijking met het wild-type. Dit wijst er op dat Glu-71, welke gelokaliseerd is in het thylakoïde lumen een belangrijke rol vervult in de formatie van PsbS dimeren. Met behulp van FTIR spectroscopie werd daarnaast het belang van Glu-176 om pH-afhankelijke conformatie veranderingen te weeg te brengen geobserveerd. In tegenstelling tot voorgaand onderzoek, blijkt dat de beide glutamaat residuen Glu-71 en Glu-176 een verschillende respons geven bij verlaging van de pH. Tevens werd protonering van alle glutamaat en aspertaat residuen waargenomen met behulp van NMR en FTIR spectroscopie.

Acknowledgements

Lastly, at the very end of this long and beautiful journey, here comes my long list of acknowledgements. By enlarge I want to acknowledge everyone (mentioned here or not) who made me into the person I am today.

Firstly I would like to remember Late Prof Simon De Vries from TU Delft, who was my track mentor during my master studies. It was his encouragement that helped me take up this challenging project on membrane proteins.

When I think about how I started with this project, I always get back to the memory of my first meeting with Dr. Anjali Pandit in her office (from the old building). You explained to me the project with so much enthusiasm and humbleness that I fell in love with the project topic. Later you tailored the project to fit my love of biology and were very understanding that I was new to NMR technique. Anjali, you have always been very welcoming to my questions and to me knocking at your door. Thank you for your support during the past four years.

I met Prof Huub de Groot on the day of my interview and you made a profound impression on me. Soon after, I took an NMR class given by you, where you were full of enthusiasm, this made me appreciate NMR much more. I would always remember and cherish our "solar panel" discussions during the lunchtime. I would like to thank the rest of the SSNMR group for their cheerful presence and support during my time as a PhD student in the group.

Dear Geri, I began in my first year, first day under your supervision in the CPF and slowly we have developed to this wonderful friendship now. It was very motivating to work with you. I will always remember your Stroopwaffles and I follow your traditional "coffee break" at 11 am!.. Dear Nora, you are my role model, always very smiling, approachable, concern to my problems. I loved to chat with you whether it is DNA repair or Indian culture. I know many students have said this to you but you are an amazing teacher.

Dear Fons, I can never forget that you helped me put up the curtains in my first house as I had no experience or tools for it. It is very pleasant to see you in the NMR facility always ready to help us. Dear Liesbeth, you are the best secretary and a wonderful person who goes beyond boundaries to help every student. We feel so welcomed by your smiling face. SSNMR department is lucky to have you. Dear Vidya, you are a joy to the group and are a wonderful friend to me. Always compassionate, thoughtful and supportive. I remember you showing me the labs on day 1, it has been a long way from that day to today. I miss all your vegan cakes, yaar! I am grateful to have you as a colleague and now as a dear friend in my life.

Let me now describe the EE 2.11 office that had at some point Rubin, Emanuela, Fatemeh and myself as 'inmates'. You all made every day so much fun, supporting me whenever necessary and putting up with me during my hard and dark days 😊. Thank you all for making my time so pleasant and bearing with me during my broken hip :P. Dear Rubin, still holding the fort, I would cherish our intellectuals talks, coffee breaks and chess games. I know one day you will make an amazing professor. "*Mera naam roshan karo*". Dear Emanuela, we took our time to become friends, but I am grateful that we did. We have been through a lot, supporting each

other and finally almost graduating together too! This makes me so happy! You will always be for me – "the spinach queen" with a lovely Italian accent. Thank you for teaching me how to make-up :P. Dear Fatemeh, you were a part of my journey and supported me as not just a colleague but as a dear friend. I would miss all our "game nights" and dinner gatherings 😊.

Dear Karthick (& family), how shall I began to express gratitude for all your time and effort during my PhD phase. I can never forget your 'greed' for more protein :P. Without your help, I would have never managed any of the NMR experiments. Thank you for teaching me, supporting me and for becoming a very dear friend of mine.

Dear Kassi, thanks for being such a lovely friend during our time at CPF and later on. Your happy face is always very welcoming. Additionally, I would like to thank Antonella, Kim, Soumya, Ramon, other members of Prot Chem group for being welcoming colleagues and helping me whenever required. I thank also my students who made me a better teacher, especially Floris who worked very hard on Cell-free expression of PsbS. I would like to recall the group of MedBio during the 2014-2016 who worked alongside in the CFP lab with me and had many coffee breaks, birthday cakes, and celebrations.

I consider myself very lucky to have a wonderful extended family back in India who have always cherished and loved me. Arvind, I don't have words to explain how important you are and have been in my life. You have always supported me and been the big worrying brother that I always wanted. Parth, you are the big motivator and joy in my life. Knowing that you are always willing to listen to me and guide me assured me that I can do and achieve goals in life. Ranjitha, Teju, Priya, Rashmi, Arun, Gaurav you all have unknowing been a great support in my time as a PhD student.

Already before I realised it, my mom knew that I loved biology a lot. That's what mother's do! You helped me choose biotechnology as a major during my bachelor, which today has lead to the completion of PhD in a similar field. For this and much more support & love that you have always given me, I am grateful. Appa, you trusted and supported me in my decision to travel so far away from home to pursue my career, without which I would not be standing here. So this thesis is dedicated to you and Amma.

The best thing that came out of my PhD journey was falling in love with my husband, Dominik. You have brought such joy to my life, all the while supporting me during my good and bad times. You took care of me during my broken hip phase and even married me :P. It means a lot to me and without your support, I would not have survived my PhD time. You are the sweetest, caring, inspiring, logical person I know. I find myself very blessed to have such a loving and understanding partner in life.

Maithili Krishnan-Schmieden
Leiden, September 2019

Curriculum Vitae

09-12-1988	Born in Bhilai, India
1999- 2006	High school diploma, India
2006 – 2010	B.Tech Biotechnology Jawaharlal Nehru Technological University, Hyderabad, India
2012 – 2014	MSc Life science and Technology (Honours) Delft University of Technology, Delft, Netherlands
2014 – 2018	PhD research Biophysical Organic Chemistry group, Leiden Institute of Chemistry, Leiden University, Netherlands
2019 – present	Postdoc research Macromolecular Biochemistry group, Leiden Institute of Chemistry, Leiden University, Netherlands

List of Publications

1. Maithili Krishnan, Geri F. Moolenaar, Karthick B. S. S. Gupta, Nora Goosen, and Anjali Pandit, *Large-scale in vitro production, refolding and dimerization of PsbS in different microenvironments*, Scientific reports, 2017, DOI: 10.1038/s41598-017-15068-3

2. Maithili Krishnan, Anjali Pandit, *Cell- free expression of the membrane protein PsbS*, Protein Expression and Purification, 2019, DOI: 10.1016/j.pep.2019.02.010

3. Maithili Krishnan, Patrick Konold, John T.M. Kennis, Anjali Pandit, *The two active glutamates of the plant stress sensor PsbS contribute non-equivalently to its pH-activated molecular response mechanism*, In preparation

4. Emanuela Crisafi, Maithili Krishnan, Anjali Pandit, *Time-resolved fluorescence analysis of LHCII in the presence of PsbS at neutral and low pH*, BBA – Bioenergetics, In revision